My Moffat w Orh

NOLTR 73-209

NOLTR 73-209

NOL TECHNICAL REPORT

PREDICTION OF NORMAL FORCE, PITCHING MOMENT, AND YAWING FORCE ON BODIES OF REVOLUTION AT ANGLES OF ATTACK UP TO 50 DEGREES USING A CONCENTRATED VORTEX FLOW-FIELD MODEL

M < 0.9

BY
Andrew B. Wardlaw, Jr.

24 OCTOBER 1973

NAVAL ORDNANCE LABORATORY
WHITE OAK, SILVER SPRING, MD. 20910

- Approved for Public Release; Distribution unlimited

NAVAL ORDNANCE LABORATORY
WHITE OAK, SILVER SPRING, MARYLAND 20910

UNCLASSIFIED

SECURITY CLASSIFICATION OF THIS PAGE (When Data Entered)

REPORT DOCUMENTATION PAGE

READ INSTRUCTIONS BEFORE COMPLETING FORM

1. REPORT NUMBER: NOLTR 73-209	2. GOVT ACCESSION NO.
3. RECIPIENT'S CATALOG NUMBER	
4. TITLE (and Subtitle): PREDICTION OF NORMAL FORCE, PITCHING MOMENT, AND YAWING FORCE ON BODIES OF REVOLUTION AT ANGLES OF ATTACK UP TO 50 DEGREES USING A CONCENTRATED VORTEX FLOW-FIELD MODEL	5. TYPE OF REPORT & PERIOD COVERED
	6. PERFORMING ORG. REPORT NUMBER
7. AUTHOR(s): Andrew B. Wardlaw, Jr.	8. CONTRACT OR GRANT NUMBER(s)
9. PERFORMING ORGANIZATION NAME AND ADDRESS: Naval Ordnance Laboratory, Silver Spring, Maryland 20910	10. PROGRAM ELEMENT, PROJECT, TASK AREA & WORK UNIT NUMBERS: Air Task No. A320-0000/ WF32-322-202
11. CONTROLLING OFFICE NAME AND ADDRESS: Naval Air Systems Command, Department of the Navy, Washington, D. C. 20361	12. REPORT DATE: 24 October 1973
	13. NUMBER OF PAGES: 110
14. MONITORING AGENCY NAME & ADDRESS (if different from Controlling Office)	15. SECURITY CLASS. (of this report): UNCLASSIFIED
	15a. DECLASSIFICATION/DOWNGRADING SCHEDULE

16. DISTRIBUTION STATEMENT (of this Report)

Approved for public release; distribution unlimited

17. DISTRIBUTION STATEMENT (of the abstract entered in Block 20, if different from Report)

18. SUPPLEMENTARY NOTES

19. KEY WORDS (Continue on reverse side if necessary and identify by block number)

High angle of attack
Induced yaw forces
Vortex shedding
Side force

20. ABSTRACT (Continue on reverse side if necessary and identify by block number)

A method initially proposed by Bryson is extended to include asymmetric shedding. This method employs the impulsive flow analogy, and models each wake vortex using a single-point vortex. Free parameters inherent in the problem formulation are determined empirically. Normal force, pitching moment and yawing force coefficients are predicted for slender bodies with a nose fineness ratio greater than four and at a Mach number

less than 0.9. For models with smaller nose fineness ratios, and at higher Mach numbers, accuracy deteriorates and side force predictions are too high.

NOLTR 73-209 24 October 1973

PREDICTION OF NORMAL FORCE, PITCHING MOMENT, AND YAWING FORCE ON BODIES OF REVOLUTION AT ANGLES OF ATTACK UP TO 50 DEGREES USING A CONCENTRATED VORTEX FLOW-FIELD MODEL

This work was performed at the Naval Ordnance Laboratory for the Naval Air Systems Command under Task Number A320-0000/WF32-322-202.

Acknowledgement is made of the assistance given by Mr. G. Pick of the Naval Ship Research and Development Center in providing wind-tunnel models and supplementary data.

ROBERT WILLIAMSON II
Captain, USN

L. H. Schindel
L. H. SCHINDEL
By direction

TABLE OF CONTENTS

Illustrations (continued)

TABLE

INTRODUCTION

As a body of revolution is exposed to an increasing angle of attack, the flow on its leeward side separates and rolls up to form vortices. Under these conditions, normal force and pitching moment can no longer be predicted by slender body theory. For relatively small angles of attack ($\alpha < \tan^{-1}(4.5/\ell)$) two symmetric vortices form as shown in Figure 1a. At larger angles of attack wake vortices grow unsymmetrically and break away or are shed from the leeward side, as illustrated in Figure 1b. The resulting flow-field asymmetries induce a yawing force and moment.

The analysis of bodies of revolution at angles of attack has been approached by many workers with varying degrees of rigor. Simple engineering calculations can be used to determine normal forces and pitching moments (Refs. (1)-(3)), but extensive numerical computations must be employed if detailed flow-field information is desired (Refs. (4), (5)). The objective of this report is to predict the yawing force component. Since this force arises from asymmetries in the vortex wake, the appropriate level of analysis must be sufficiently rigorous to provide an approximate wake description. Engineering level calculations do not generally provide this description and, therefore, are not amenable to these ends. While detail flow-field calculations can, in principle, achieve this purpose, they have only been applied up to very moderate angles of attack (10-15 degrees), too low for yawing forces to occur. Semi-empirical methods, such as those by Bryson (Ref. (6)), Schindel (Ref. (7)), and Angelucci (Ref. (8)), provide an approximate wake description, but assume a symmetric vortex wake and are not capable of predicting yawing forces. Also, normal forces and pitching moments can only be calculated up to moderate angles of attack (20-30 degrees).

The theory developed in this paper extends the model originally proposed by Bryson (Ref. (6)) by removing the symmetric wake assumption. This allows the side forces to be predicted, and increases angle of attack for which the theory is valid to about 50 degrees. In the current theory, the flow field is approximated using the impulsive flow analogy. This analogy assumes that the crossflow field is swept down the length of the body at the rate $U\cos\alpha$. At each axial station the flow field is taken to be analogous to flow about a cylinder in crossflow, whose radius is equal to the body radius at that axial location. The developing crossflow field is thus similar to flow about an impulsively started cylinder in crossflow. The development of the viscous flow field is modeled by superimposing point vortices on the potential flow solution for flow about a cylinder. Analysis is limited to ogive cylinders with sharp or blunt nose tips.

Using experimental data for a body with a laminar boundary layer ($2.5 < Re/ft \times 10^{-6} < 5.6$) and covering a range in Mach number from 0.5 to 1.1, free parameters inherent in the model are determined.

Calculated force and moment values are compared to experiment and computed vortex paths are compared to those determined from schlieren photographs. This type of approach allows conclusions to be drawn concerning the validity of the current problem formulation.

SYMBOLS

C_{DC}	local drag coefficient, $\frac{\pi}{2} \frac{r}{\sin^2\alpha} \frac{dC_N}{dx}$
C_M	pitching moment coefficient, $\frac{M_Y}{Dq_\infty \pi r^2}$, referenced to model nose
C_M'	yawing moment coefficient, $\frac{M_z}{Dq_\infty \pi r^2}$
C_N	normal force coefficient, $\frac{F_N}{q_\infty \pi r^2}$
C_Y	yawing force coefficient, $\frac{F_Y}{q_\infty \pi r^2}$
D	diameter of body of revolution
F_N	normal force
F_Y	yawing force
k	number of vortices in wake
L	body length
L_N	nose length
ℓ	body fineness ratio
ℓ_n	nose fineness ratio
M	Mach number
M_c	crossflow Mach number, $M\sin\alpha$
M_Y	pitching moment
M_z	yawing moment
n	frequency for shedding vortices of like sign

q_∞	free-stream dynamic pressure
R_n	nose tip radius of curvature
r	local body radius
r_0	maximum body radius
Δr	difference in the radial location of the two initial vortices at which the first vortex will be shed.
r_n	the distance from the separation point, measured along the feed sheet at which nascent vortices are introduced
Re	Reynolds number
Δr_I	perturbation in the radial location of the first two vortices
S	Strouhal number
t	time
U	free-stream velocity
$W(\zeta)$	crossflow plane velocity at ζ, $\frac{d\overline{\phi}(\zeta)}{d\zeta}$
w	dimensionless crossflow plane velocity, W/Usinα
w_j	dimensionless crossflow plane velocity at the location of the jth vortex. The influence of the jth vortex is neglected.
x	distance along missile body (see Fig. 1)
Δx	x distance between points where successive vortices are shed.
y,z	crossflow plane coordinates (see Fig. 2)
y_j, z_j	y and z coordinates of the jth vortex
α	angle of attack
Γ	vortex circulation
δ	rate of radius change as a function of x, $\frac{dr}{dx}$
ζ	complex crossflow plane coordinate, y + iz
ζ_{0_1}, ζ_{0_2}	crossflow plane separation points (see Fig. 2)

θ_{0_1}, θ_{0_2}	crossflow plane separation angles (see Fig. 2)
λ	dimensionless circulation, $\frac{\Gamma}{2\pi r \sin\alpha U}$
λ_n	dimensionless circulation of newly introduced vortice
$\Delta\lambda_I$	initial vortex strength
ϕ	crossflow velocity potential
ϕ_N	nose roll angle
$\tilde{\phi}$	dimensionless crossflow velocity potential, $\phi/U\sin\alpha$

LITERATURE SURVEY

The complete analysis of a body of revolution at angle of attack is a three-dimensional problem involving the solutions to the Navier-Stokes equations. This problem may be approached numerically in its entirety requiring an extensive computational effort. For relatively small angles of attack (12 degrees), numerical solutions have been obtained for cones using an approximate set of Navier-Stokes equations (Ref. (4)).

The device most commonly used to simplify the problem formulation is the impulsive flow analogy. This reduces the complete problem to a two-dimensional time varying analysis of a viscous fluid. By this analogy, the crossflow field is equivalent to that about an impulsively started, expanding cylinder, where t = x/Ucos. The expanding cylinder represents the increase in cross-sectional radius which occurs along the length of the body. Often the additional assumption is made that the flow about an impulsively started cylinder is incompressible. Throughout the remainder of this report the term impulsive flow analogy will be assumed to imply this assumption.

On the most rigorous level, the impulsive flow analogy allows the crossflow drag to be deduced from a numerical solution to the Navier-Stokes equations for flow over an impulsively started cylinder in crossflow. Several examples of this type of procedure are available for cylinders of constant radius (Refs. (9), (10)). For direct application to a body at angle of attack Walitt and Trulio (Ref. (5)) have carried out this analysis with a cylinder of varying radius in compressible flow. However, the computational requirements are prohibitive and solutions have only been obtained for angles of attack of 15 degrees.

A less rigorous analysis of impulsively started flow over a cylinder involves superposition of a large number of point vortices on the potential solution for incompressible flow about a cylinder. Typically, several hundred discrete vortices may be used. After formation, each point vortex is assumed to drift with the local fluid velocity. The schemes for predicting rate of vorticity

formation differ extensively. Although many such studies have been carried out, most are restricted to bodies of fixed cross-sectional dimensions (Refs. (11), (12) and (13)). However, Angelucci (Ref. (8)) has made a direct application to bodies at angle of attack, assuming a symmetric vortex wake. Good agreement is obtained for normal forces and moments.

A somewhat simpler method uses a single vortex to describe each wake vortex. In a procedure originally proposed by Bryson (Ref. (6)), vortex motion is determined by a balance of forces on a vortex and its feeding sheet. The model was originally limited to circular bodies with a wake pattern containing two symmetric vortices. This approach has been extended by Schindel (Ref. (7)) to bodies of elliptic cross section using conformal mapping techniques. In addition, changes in empirical parameters allow laminar and turbulent boundary effects to be accounted for. Results compare well with experimental data for normal forces. However, agreement of the pitching-moment calculation with experimental data is not as good. Range of validity for the results is $\alpha < \tan^{-1}(5/\ell)$. Davis (Ref. (14)) has extended Bryson's methods to a cylinder in crossflow with an asymmetric wake. But this formulation is valid only for cylinders of fixed radius and, therefore, cannot be directly applied to a body at angle of attack.

The most approximate theories available consider forces on a body at angle of attack to be made up of a viscous and an inviscid contribution which are additive. Initial attempts along these lines were by H. J. Allen (Ref. (1)). The inviscid force expression applied is similar to that obtained from slender body theory. The viscous contribution at each axial station is computed by applying the steady-state drag force for a cylinder in crossflow. This report was followed by that of Kelly (Ref. (2)) who attempted to improve the method by using drag data of an impulsively started cylinder in crossflow. His results were somewhat better than those of Allen, giving a better prediction of the pitching moment. Kelly's method has been refined by others, most recently by Thomson (Ref. (15)) to include angles of attack up to 90 degrees. In this work advantage is taken of impulsive flow data obtained by Sarpkaya (Ref. (16)). Correction tables allow Mach number, end effects, nose shapes, and the transition from laminar to turbulent flow to be taken into consideration. In addition, an experimental wake description is developed which allows side forces to be estimated. In a slightly different vein, L. H. Jorgensen (Ref. (3)) in an extension of Allen's work, presents a method of estimating normal forces on bodies at an angle of attack varying from 0 to 180 degrees and Mach numbers varying from subsonic to hypersonic.

BRYSON'S METHOD FOR IMPULSIVELY STARTED CYLINDERS IN INCOMPRESSIBLE FLOW

As pointed out above, our analysis is essentially that of an impulsively started cylinder in incompressible, viscous flow. Such flow can be simulated by superimposing point vortices on the potential solution for flow about a cylinder. In the present approach, a single point vortex is used to simulate each wake vortex. To satisfy the boundary conditions on a cylinder, each vortex in the wake is required to have a corresponding image vortex. The resulting configuration is shown in Figure 2 and the complex velocity potential is given as follows:

$$\phi(\zeta) = U\left[-\left(\zeta - \frac{r^2}{\zeta}\right)i - \frac{i}{2\pi}\sum_{j=1}^{k} \Gamma_j \ln\left\{\frac{(\zeta-\zeta_j)}{(\zeta - r^2/\bar{\zeta}_j)}\right\} + \frac{r}{\tan\alpha}\frac{dr}{dx}\ln(\zeta)\right] \tag{1}$$

The term, $-(\zeta - \frac{r^2}{\zeta})i\ U$, is the velocity potential solution for flow over a cylinder. Each of the logarithic terms within the summation represent the velocity potential for a vortex and its image within the cylinder. The remaining term, which is the expression for a source, takes into account the changing cylinder radius.

The equations governing the motion of the vortices remain to be determined. Each logarithmic term within the summation in Equation (1) is a double valued function and has a branch line which connects the described vortex to its image. The portion of the branch line of physical importance is the part which crosses the flow field. It is considered to extend from the vortex location to the nearer of the points, ζ_{0_1} and ζ_{0_2}, which are on the cylinder surface (see Fig. 2). These two points correspond to the position where flow is assumed to separate from the cylinder surface. The branch line of a growing vortex ($d\Gamma/dt \neq 0$) is known as a feeding sheet. Across it, a pressure jump of $\frac{\rho(d\Gamma/dt)}{\text{unit length}}$ occurs, which can be determined from the momentum conservation equation. The total force on the feeding sheet is $i\rho(\zeta_k - \zeta_{0_k})\frac{d\Gamma}{dt}$. This force on the feeding sheet is balanced by a lift force on the vortex of $-i\rho\Gamma(\frac{d\zeta_k}{dt} - W_k)$ given by the Kutta-Joukowski theorem. Here $(\frac{d\zeta_k}{dt} - W_k)$ is the vortex velocity with

respect to the local fluid velocity. Thus, the motion of each vortex is governed by the equation

$$\frac{d\zeta_j}{dt} + \frac{(\zeta_j - \zeta_{0j})}{\Gamma_j}\frac{d\Gamma_j}{dt} = W_j \tag{2}$$

The vortex circulations are determined by applying the Kutta conditions at the crossflow separation points:

$$W(\zeta_{01}) = W(\zeta_{02}) = 0 \tag{3}$$

This allows the circulation of two different vortices at a time to be specified. This does not preclude the existence of other vortices in the flow whose circulations are known.

Left undetermined by the Bryson method are the crossflow separation points, ζ_{01} and ζ_{02}, and boundary conditions in t. The boundary conditions in t include the points where vortices are introduced and shed. Also, the location of vortices in the crossflow plane and their strengths must be specified when they are introduced.

In applying the Bryson method the boundary conditions in t must be specified in such a manner that the resulting wake conforms to observations. When the wake behind the cylinder is assumed to become asymmetric, the following type of procedure appears to be required. Initially, two vortices are introduced. Using the governing equations the growth and the motion of these vortices are traced numerically. At some point, to be empirically determined, the circulation of one of these vortices is fixed and this vortex is considered to be shed. A new vortex is then introduced on the same side of the cylinder that the shed vortex originally emanated from. This shedding process is repeated at later points in time, vortices being shed from alternate sides of the cylinder.

APPLICATION OF THE BRYSON METHOD TO A MISSILE AT ANGLE OF ATTACK

The impulsive flow analogy implies the relations $x = U\cos\alpha t$ and $W(\infty) = U\sin\alpha$. Using these expressions and the definitions $\Gamma = 2\pi U r \sin\alpha\lambda$ and $W_j = w_j U\sin\alpha$, Equation (2) becomes

$$\frac{d\zeta_j}{dx} + \frac{(\zeta_j - \zeta_{0j})}{\lambda_j}\frac{d\lambda_j}{dx} = \tan\alpha\, w_j - \frac{(\zeta_j - \zeta_{0j})}{r}\frac{dr}{dx}\ ;\ j = 1,2 \quad \text{growing vortices}$$

$$\frac{d\zeta_j}{dx} = \tan\alpha\, w_j\ ;\ j = 3,4\cdots K \quad \text{shed vortices}$$

(4)

The Kutta condition for a cylinder whose radius may be expanding becomes:

$$\frac{1}{U\sin\alpha}\,\frac{\overline{d\phi}(\sigma_{01})}{d\sigma} = \omega\,(\sigma_{01}) = \frac{r}{\tan\alpha}\,\frac{dr}{dz}\,\frac{1}{\bar{\sigma}_{01}} \tag{5}$$

$$\frac{1}{U\sin\alpha}\,\frac{\overline{d\phi}(\sigma_{01})}{d\sigma} = \omega\,(\sigma_{02}) = \frac{r}{\tan\alpha}\,\frac{dr}{dz}\,\frac{1}{\bar{\sigma}_{02}}$$

Substituting Equation (1) into Equations (5), it becomes evident that λ_1 and λ_2 are determined by solving two simultaneous equations. It is also evident in this formulation that satisfaction of the inviscid boundary condition on the cylinder is sufficient to ensure that both λ_1 and λ_2 are real.

In solving Equations (4) subject to conditions (5), λ_1 and λ_2 have been eliminated from (4) reducing the number of equations involved. The actual derivation is shown in Appendix A.

The formulated method is applied in the following manner. Near the nose of the missile two nascent vortices are introduced. The x coordinate of introduction is determined by satisfying the relation $\frac{2}{3}\sin\theta\tan\alpha = \tan\delta$. This relationship moves the point of vortex introduction toward the nose of the model with increasing angle of attack. In cases where this relation places the starting point in front of the nose, the problem is automatically started at the nose. This relationship was derived by Bryson (Ref. (6)) by considering a cone. The slope δ represents the half angle of the largest cone for which vortex separation occurs. The two vortices are each assumed to be located along the directions $\theta_{0_1} + \pi/3$ and $\theta_{0_2} - \pi/3$ from their respective separation points δ_{0_1} and δ_{0_2}. This criterion is also due to Bryson and was determined by the analysis of the trajectory of a vortex near the crossflow separation point.

Asymmetry is introduced at this point by slightly perturbing the radial location* of the two vortices. The initial strengths of the two vortices, as well as the magnitude of the perturbation applied, are free parameters which are empirically determined. They will be discussed in more detail later.

As the numerical solution to the governing equations progresses, the asymmetry in the problem grows. When the difference in radial location of the two vortices reaches a specified value, the outermost vortex is shed and a new vortex is introduced on the same

*the radial location of the jth vortex is defined to be $\sqrt{y_j^2 + z_j^2}$

side of the body. In order to introduce a new vortex whose circulation is other than zero, the existing vortex pattern must be perturbed. This is accomplished by reducing the circulation of the shed vortex a few percent. It can be shown that this procedure will always lead to a new vortex with a circulation of the correct sign. The new vortex is assumed to be located along the feeding sheet of the vortex to be shed. Its initial strength is uniquely determined by its crossflow field location and the decrease in circulation ascribed to the shed vortex.

Subsequent vortices are shed at intervals specified by the Strouhal frequency. Initial conditions for succeeding vortices are identical to those just described.

Application of the method described above requires specification of the following free constants:

1. Initial vortex strength (λ_I)

2. Initial radial perturbation (Δr_p)

3. The difference in radial location of the two initial vortices at which the first vortex is shed (Δr)

4. The distance from the separation point, measured along the feeding sheet of the shed vortex, at which a nascent vortex is introduced (r_n)

5. Circulation reduction of the shed vortex ($\Delta\lambda_n$)

6. Crossflow separation angles (θ_{0_1} and θ_{0_2})

7. Strouhal number (S)

The Strouhal number is determined experimentally using schlieren photographs of a tangent ogive cylinder at angle of attack. Although measured values showed a large degree of fluctuation, an average value of .17 was established.

The crossflow separation angle can also be determined in the wind tunnel, however, use of measured values leads to unstable numerical results. This may be due to the approximate nature of the flow field model. Simulation of a wake vortex using a single point vortex may not be giving an accurate flow field description in the vicinity of the separation points. To circumvent this problem, the lead of Bryson is followed and the separation angle is set near 45 degrees.

There is no direct way of readily determining the remaining parameters. However, it should be pointed out that the numerical solution is much less sensitive to these remaining parameters. Their actual values were established by a comparison with experimental measurements of normal forces and schlieren pictures of the leeward flow field.

NORMAL AND YAWING FORCES

The forces acting on any section of a body can be determined by enclosing it in a cylindrical control volume and balancing the momentum flux through the volume. Such a procedure is adequately discussed elsewhere (Ref. (17)) and results in the following expression:

$$C_N + i C_Y = 2 \sin\alpha \cos\alpha \left(\frac{r}{r_0}\right)^2 \left[1 + 2 \sum_{j=1}^{k} \lambda_j \left\{ \frac{\zeta_j}{r} - \frac{r}{\bar{\zeta}_j} \right\} \right]$$

The first term in the above equation reduces to the slender body theory result of 2α at small angles of attack. The second term represents the crossflow drag due to the presence of the vortices, or the viscous contribution.

EVALUATION OF THE PROBLEM FORMULATION

The validity of the current formulation hinges on several points which are difficult to resolve in a conclusive manner. First and foremost, is the validity of the impulsive flow analogy. This analogy cannot be justified in its entirety. However, for inviscid flow about a slender body at small angle of attack, it is a consequence of slender body theory. At low Mach numbers where the flow is approximately incompressible, the restriction on small angle of attack can be relaxed. This does not, of course, shed any light on the validity of the impulse flow analogy for fluid flows in which viscous effects are important. All that can really be said in these cases is that the observed development of a vortex wake on the leeward side of a body at angle of attack bears at least a qualitative relation to the wake which develops behind a cylinder in crossflow (Ref. (18)).

Another point of question in the current problem formulation is the practice of simulating viscous flow by superimposing point vortices on inviscid, potential flow solutions. Even though this is an ad-hoc problem formulation, previous success in studies for cylinders in crossflow using a large number of point vortices indicate that this manner of approach provides an accurate wake description - in one case, good enough to predict the shedding frequency (Ref. (11)). The use of a single-point vortex to describe each wake vortex, as is done in this report, is more questionable. Such an approach is only capable of describing the gross flow-field features. Pressure calculations around the circumference of a cylinder using this type of description show an unrealistic peak near each point vortex. Despite this shortcoming, previous studies using this approach indicate that the integrated circumferential pressure distribution gives a good approximation of the normal forces at low angles of attack (Refs. (6), (7)).

The present approach is thus the extension of other studies which have proved to be accurate at lower angles of attack. Free parameters available in the current model allow adjustments to be made for effects which are not directly accounted for.

NUMERICAL CALCULATIONS

The governing equations are integrated using an Adams-Moulton predictor-corrector scheme which adjusts step size based on estimated error. This routine is started using the Runge-Kutta technique. The adjustable step size feature is extremely important in reducing running time. Small step sizes are required near the model nose where the local radius is small and at points at which new vortices are introduced. A listing of the program is provided in Appendix B.

Correct use of the outlined method requires the determination of a set of free parameter values that not only give a correct qualitative description of the wake, but also produce realistic forces and moments. There does not appear to be a unique set of parameters that best satisfy these requirements. However, certain sets of parameter values produce unacceptable results in that the computed crossflow wake does not develop into a Karman vortex street type of pattern. In some instances newly introduced vortices may move with diminishing circulation toward the cylinder surface. In any event, unless an orderly wake is formed, point vortices eventually approach one another resulting in numerical instability.

Numerical results were initially calculated for an impulsively started cylinder in crossflow. Suitable results were obtained using the set of parameters shown in Table 1. As indicated in this table, calculations were carried out assuming a symmetric wake containing two vortices, an unsymmetric wake still containing only a vortex pair, and an asymmetric wake in which vortices were periodically shed. In Figure 3 the calculated drag curves are plotted as a function of dimensionless time. Also shown in this graph is the experimental drag curve determined on an impulsively started cylinder

Table 1

FREE PARAMETER VALUES

Parameter	Cylinder in Crossflow			Missile at angle of attack Mach no. taken into account
	Symmetric Vortex Pair	Asymmetric Vortex Pair no shedding	Asymmetric wake with vortex shedding	
S	-	-	.1666	.1666
θ_{0_1}, θ_{0_2}	←	$\begin{cases} 40^\circ & \text{if } \frac{u_t}{r} < 10.2 \\ 44.6^\circ - 4.6\,e^{-.7(\frac{u_t}{r} - 10.2)} & \text{if } \frac{u_t}{r} \geq 10.2 \end{cases}$	→	$42^\circ + 7.5(F)^\circ$
λ_I	.08	.08	.08	.04
$\Delta r_p/D$	0.0	.006	.006	.006
$\Delta r_s/D$	-	∞	.1	.1 + .05(F)
$\Delta\lambda_n$	-	-	-2.5%	-2.5%
r_n/D			.075	.075

$$F = -.835 + 1.67M - .244 \sin\left[\frac{\pi}{6}(M - .5)\right] \qquad .5 \leq M \leq 1.1$$

in crossflow by Sarpkaya (Ref. (16)). Only the calculation which provides for vortex shedding is comparable to experimental results over wide ranges in dimensionless time. The accompanying wake development is illustrated in Figure 4.

In our initial attempt to apply this method to a body at angle of attack, the same set of free parameter values used for the impulsively started cylinder was assumed. Results were compared to experimental tests on a tangent ogive cylinder ($\ell = 12$ and $\ell_n = 4$). These tests are further described in Appendix C. The only adjustment to the set of free parameter values concerned the crossflow separation angles. As can be seen in Table 1 for the cylinder in crossflow, the separation angles are decreased at the dimensionless time $\frac{Ut}{r} = 10.2$. In application to the ogive cylinder at angle of attack, the point in the computation where this decrease occurs must be adjusted, since the change in radial dimensions at the missile nose disturbs the time sequence of the flow development. It is found that the point at which $\frac{Ut}{r} = 10.2$ occurs two-thirds of the distance in time between the point where the first and second vortices are shed. This criterion is used to determine where θ_{0_1} and θ_{0_2} will be decreased. As suggested by Schindel (Ref. (7)), the smooth transition from one separation angle to another is achieved by solving the equation:

$$\frac{d\theta_{oj}}{dx} = \frac{.7}{r} \tan\alpha \,(44° - \theta_{oj}) \quad ; \quad j = 1, 2 \tag{6}$$

and subject to the boundary condition: $x \to \infty$ as $\theta_{0_j} \to 48°$. In the special case of a cylinder in crossflow, r is constant and the solution to 16 reduces to that shown in Table 1 for a cylinder in crossflow.

The calculated forces and pitching moments are compared to experimental results in Figures 5 and 6. In each of these figures experimental data for a range in Mach number from .5 to 1.1 are shown. The computed normal force coefficient (Fig. 5) compares well to the experimental data being closest to the curve generated at Mach .9. The calculated pitching moment coefficient (Fig. 6) is slightly high, matching best with the Mach 1.1 curve. The predicted yawing force coefficient, shown in Fig. 7, is somewhat larger than those measured and is closest to the Mach .5 curve.

The current theory is independent of Mach number. However, as can be seen from experimental data in Figures 5, 6, and 7, force and moment data is Mach number dependent. In order to include a Mach number effect in the theory, the set of free constants is assumed to be a weak function of Mach number. The relation between Mach number and free constant value is determined empirically by adjusting the set of constants to give the measured normal force curve at each Mach number. In addition, the sets of

free parameter values are modified somewhat to obtain better correspondence between observed and calculated vortex trails. The final set of constants is shown in the right-hand column of Table 1. These constant values yield stable vortex streets up to angles of attack near 50 degrees. The upper limit in each case is dependent on the actual nose configuration. Generally, the upper limit on angles of attack increases with decreasing nose fineness.

Computations using the Mach number dependent set of constants are compared to experiment in Figures 8 through 19. The close agreement between experimental and computed normal force coefficients are shown in Figure 8 while the pitching moment results are compared in Figure 9. The computed yawing force coefficient is compared to experimental measurements at Mach .5, .7, .9, and 1.1, in Figures 10, 11, 12, and 13, respectively. In each of these graphs four different yawing force coefficient curves are shown. They were generated by rolling the model nose. From these graphs it is evident that the yawing force coefficient is reasonably well predicted for Mach numbers less than .9. For larger Mach numbers the measured magnitudes of the yaw force coefficients decreases. This trend is not followed by the computed results. At the highest Mach number tested, 1.1, the yawing force coefficient is over-estimated by a factor of four.

In Figures 14 through 19, comparisons between the computed and observed vortex wakes are shown for angles of attack varying from 20 degrees to 45 degrees and Mach numbers of .5 and .9. It is evident from these pictures that the wake is qualitatively well reproduced. More consistent agreement is obtained at lower Mach numbers. At an angle of attack of 45 degrees and a Mach number of .9, the wake width is clearly over-estimated.

In order to assess the general applicability of this model, a comparison is made between calculated and experimental results for differently shaped ogive cylinders. Results at Mach .5 are shown in Figures 20 through 22. Good agreement is obtained for normal force. Although the pitching moment coefficient comparison is not as good as the normal force comparison, the experimental trend is followed. Figure 22 reveals that the decreasing yawing force coefficient observed on blunter bodies is not predicted by the theory.

Comparison between experimental and calculated results on differently shaped bodies at Mach 1.1 (Figures 23 through 25) shows that general trends found in experimental data for normal force and pitching moments are followed. However, agreement is not as close as in the case of lower Mach numbers. Also the side forces (Fig. 26) are consistently over-estimated and do not follow experimental trends.

SUMMARY AND CONCLUSIONS

The flow field surrounding an ogive cylinder at high angles of attack is simulated using an extension of the method initially proposed by Bryson (Ref. (6)). This method employs the impulsive flow analogy and models each wake vortex using a single point vortex. Free parameters inherent in the problem formulation are initially determined by comparison to drag force coefficient data on an impulsively started cylinder in crossflow.

Final parameter values are obtained by matching the normal force measured on a tangent ogive cylinder ($\ell n = 4.0$, $\ell = 12$) over a range in Mach number of .5 to 1.1. These parameter values are made weakly Mach number dependent to reflect the experimental data. The resulting pitching moments compare well in trend with experiment. The calculated yaw force coefficient is of the correct magnitude at Mach numbers less than .9, but is too large at higher Mach numbers.

At a Mach number of .5 calculated and experimental results are compared for ogive cylinders with different nose fineness ratios. Predicted normal force and pitching moment coefficients are in good agreement with experimental results. On ogive cylinders with small slenderness ratios ($\ell n \lesssim 3$) yawing force calculations over-estimated the experimental results.

The same type of comparison is carried out at a Mach number of 1.1. Agreement between calculated normal force and pitching moment coefficients was not as good as at Mach .5. The yawing force coefficient was consistently lower than predicted.

The current results indicate that on slender bodies and at low Mach numbers, the impulsive flow analogy combined with the Bryson method can be used to predict normal force, pitching moment and yawing force. For nose fineness ratios less than 4 and at Mach numbers near unity, accuracy deteriorates markedly and side forces are over-estimated.

Apparently the separation parameters are sensitive to Mach number in the transonic range. A more thorough investigation of this effect would be required to improve the accuracy of side force predictions in this regime.

REFERENCES

(1) Allen, H. J., "Estimation of the Forces and Moments on Induced Bodies of Revolution of High Fineness Ratio," NACA RM A9I26, 1949

(2) Kelly, H. R., "The Estimation of Normal Force, Drag, and Pitching Moment Coefficients for Blunt Based Bodies of Revolution at Large Angles of Attack," Journal of Aeronautical Science, Vol. 21, No. 8, Aug 1954

(3) Jorgensen, L. H., "Prediction of Static Aerodynamic Characteristics for Space-Shuttle-Like and Other Bodies at Angles of Attack from 0° to 180°," NASA TN D-6996, Jan 1973

(4) Lubard, S. C., Helliwell, W. S., "Calculation of the Flow on a Cone at High Angle of Attack," AIAA Paper No. 73-636, Jul 1973

(5) Walitt, L., and Trulio, J. G., "A Numerical Method for Computing Three-Dimensional Viscous Supersonic Flow Field About Slender Bodies," NASA-CR-1963, Nov 1971

(6) Bryson, A. E., "Symmetric Vortex Separation on Circular Cylinders and Cones," Journal of Applied Mechanics, Vol. 26, pp. 643-648, Dec 1959

(7) Schindel, L. H., "Effects of Vortex Separation on the Lift Distribution on Bodies of Elliptic Cross Section," Journal of Aircraft, Vol. 6, No. 6, pp. 537-542, 1969

(8) Angelucci, S. B., "A Multivortex Method for Axisymmetric Bodies at Angle of Attack," Journal of Aircraft, Vol. 8, No. 12, pp. 959-966, 1971

(9) Jordan, S. K., and Fromm, J. E., "Oscillatory Drag, Lift, and Torque on a Circular Cylinder in Uniform Flow," Vol. 15, No. 3, pp. 371-376, 1972

(10) Thoman, D. C., and Szewczyk, A. A., "Time Dependent Viscous Flow Over a Circular Cylinder," Phys. Fluids, Suppl. II, pp. II 76-II 86, 1969

(11) Gerrard, J. H., "Numerical Computation of the Magnitude and Frequency of Lift on a Circular Cylinder," Phil. Trans. Roy. Soc., Vol. 261, pp. 137-162, Jan 1967

(12) Laird, A. D. K., "Eddy Formation Behind Circular Cylinders," Journal of the Hydraulics Division, Proceedings of the American Society of Civil Engineers, Jun 1971

(13) Sarpkaya, T., "An Analytic Study of Separated Flows About Circular Cylinders," Journal of Basic Engineering, Transactions of the ASME, Dec 1968

(14) Davis, M. D., "An Analytic Study of Separated Flow About a Circular Cylinder," Masters thesis, Naval Postgraduate School, Dec 1969

(15) Thomson, K. D., "The Estimation of Viscous Normal Force, Pitching Moment, Side Force and Yawing Moment on Bodies of Revolution at Incidences Up to 90°," WRE-Report-782 (WR&D), Oct 1972

(16) Sarpkaya, T., "Separated Flow About Lifting Bodies and Impulsive Flow About Cylinders," AIAA Journal, Vol. 4, No. 3, pp. 414-420, 1966

(17) Schindel, L. H., "Effects of Vortex Separation on Lifting Bodies of Elliptic Cross Section," TR 118, Massachusetts Institute of Technology Aerophysics Laboratory, 1965

(18) Thomson, K. D., and Morrison, D. F., "The Spacing, Position and Strength of Vortices in the Wake of Slender Cylindrical Bodies at Large Incidence," J. Fluid Mech, Vol. 50, Part 4, pp. 751-783, 1971

(19) Pick, G., Unpublished data, Naval Ship Research and Development Center, Washington, D. C.

(20) Pick, G., "Investigation of Side Forces on Ogive-Cylinder Bodies at High Angles of Attack in the M = 0.5 to 1.1 Range," AIAA Paper No. 71-570, Jun 1971

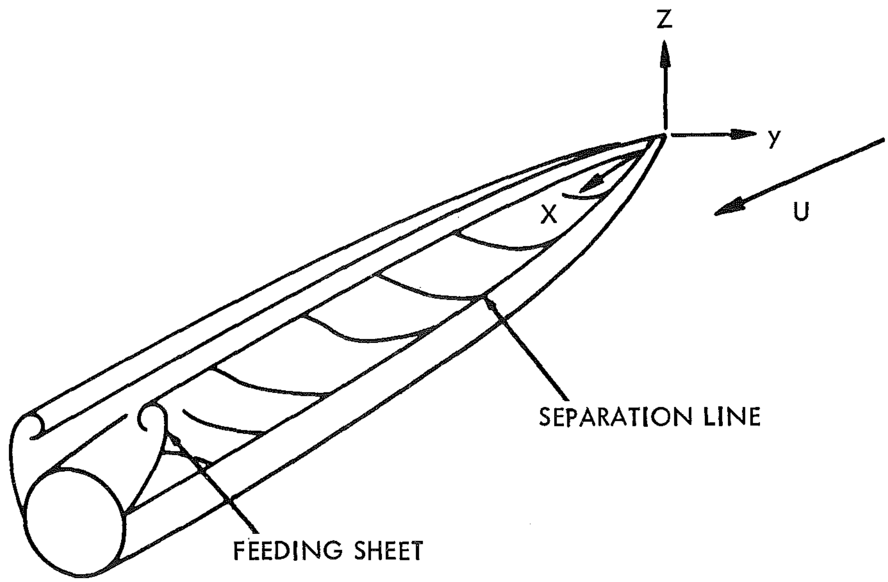

(a) SYMMETRICAL VORTEX SHEDDING

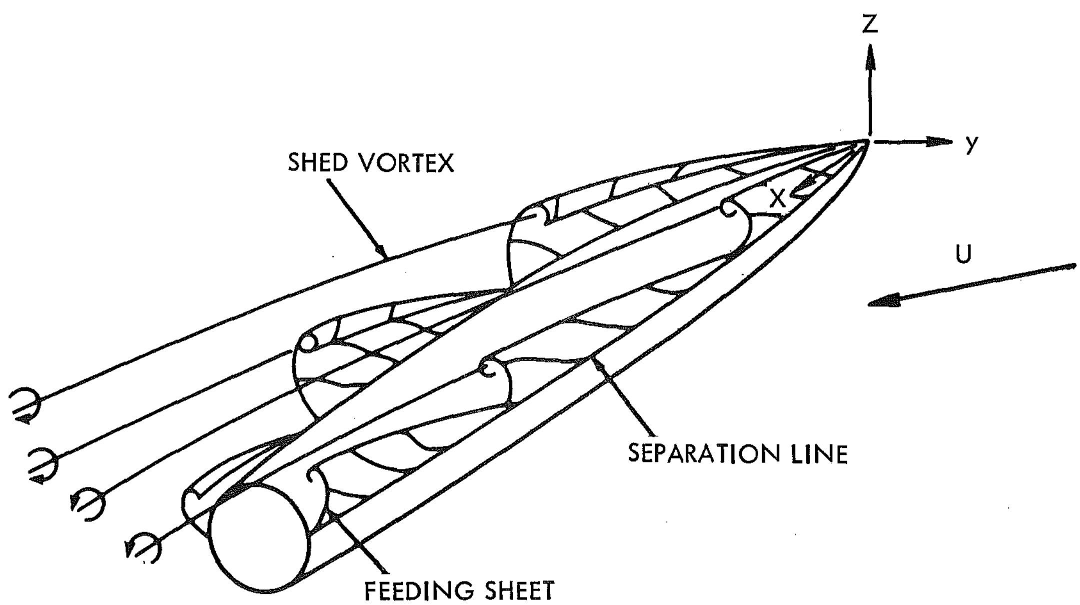

(b) ASYMMETRICAL VORTEX SHEDDING

FIG. 1 VORTEX FORMATION ON A BODY OF REVOLUTION AT ANGLE OF A ATTACK

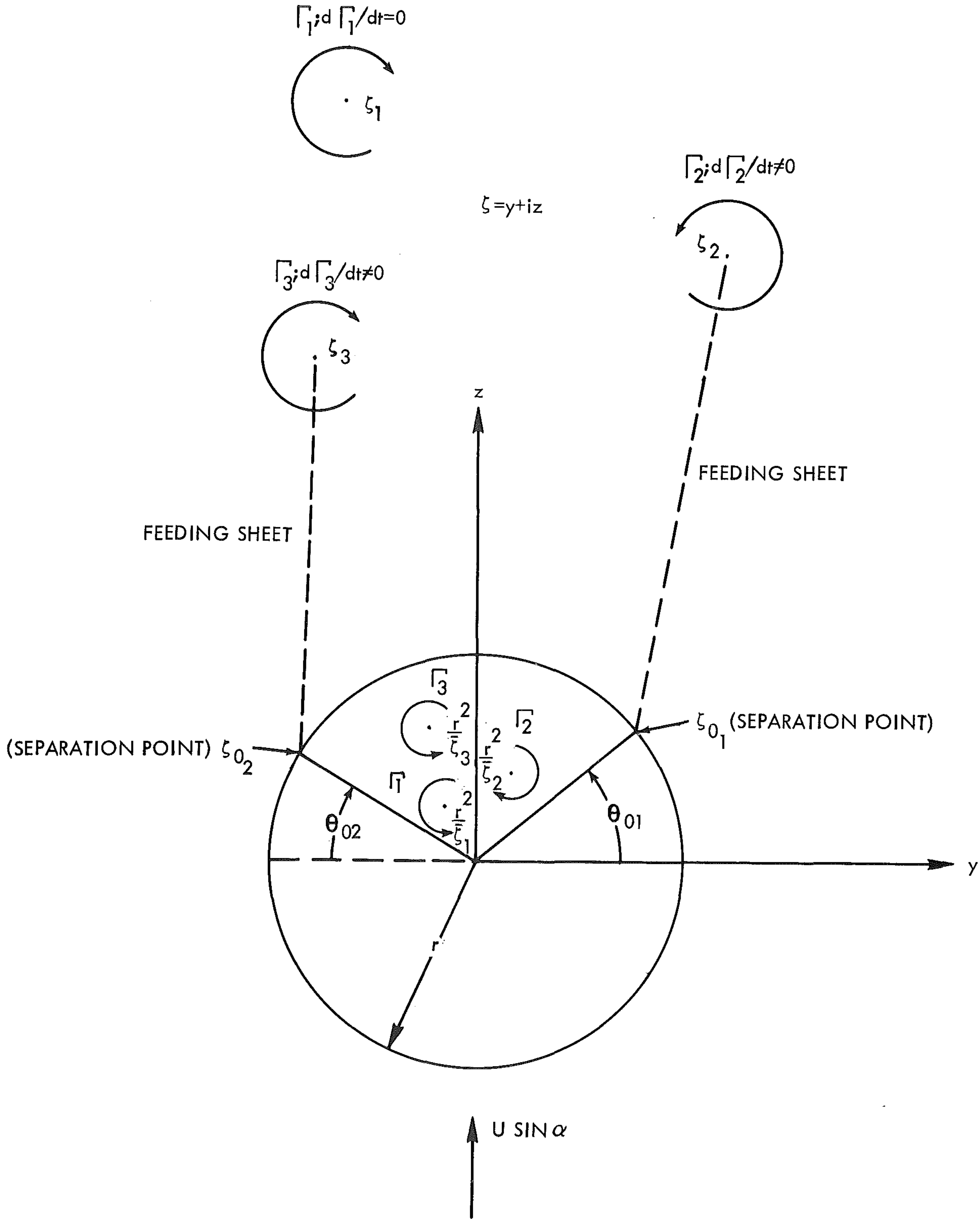

FIG. 2 DIAGRAM OF THE CROSSFLOW PLANE.

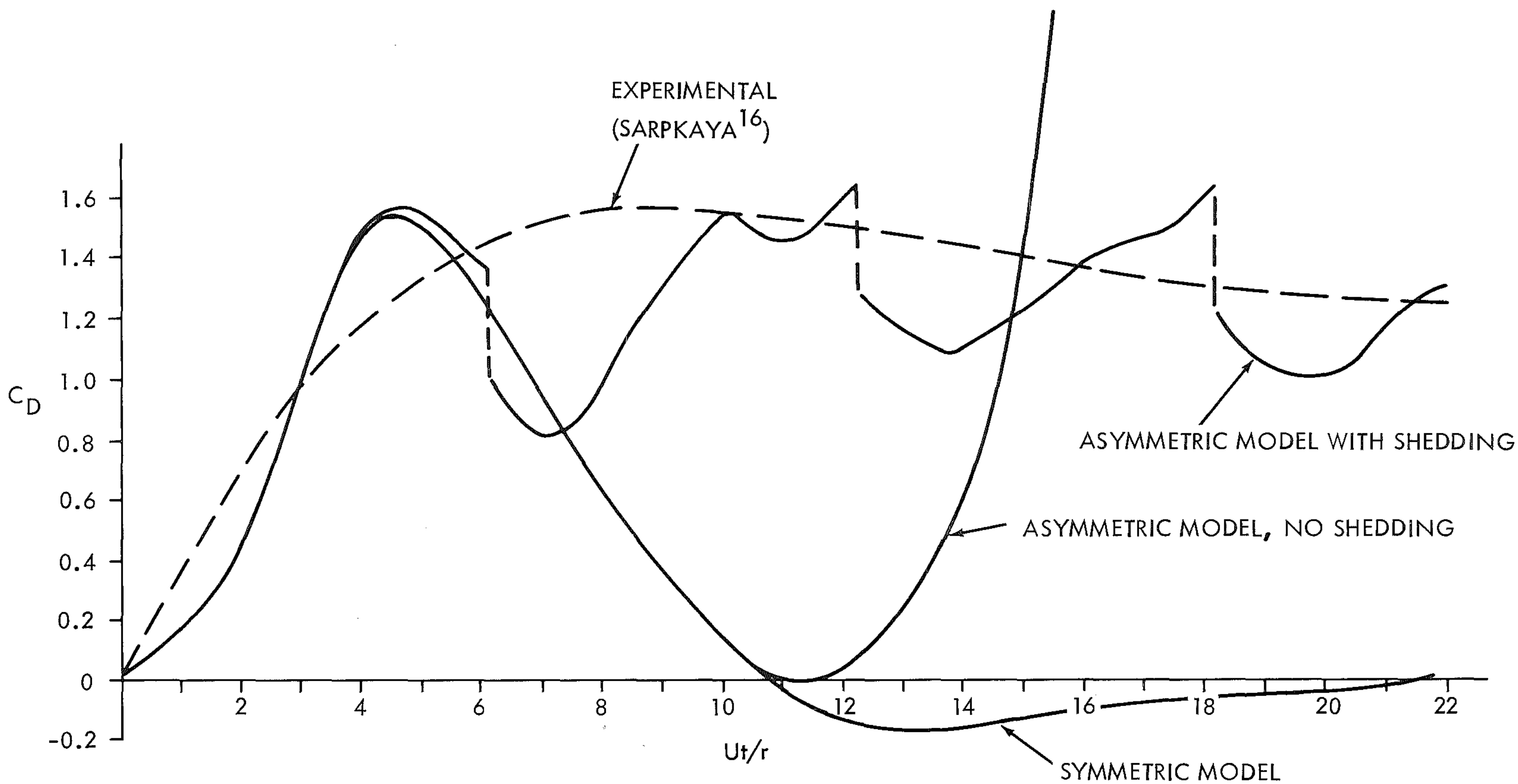

FIG. 3 DRAG FORCE COEFFICIENT AS A FUNCTION OF DIMENSIONLESS TIME FOR AN IMPULSIVELY STARTED CYLINDER IN CROSSFLOW.

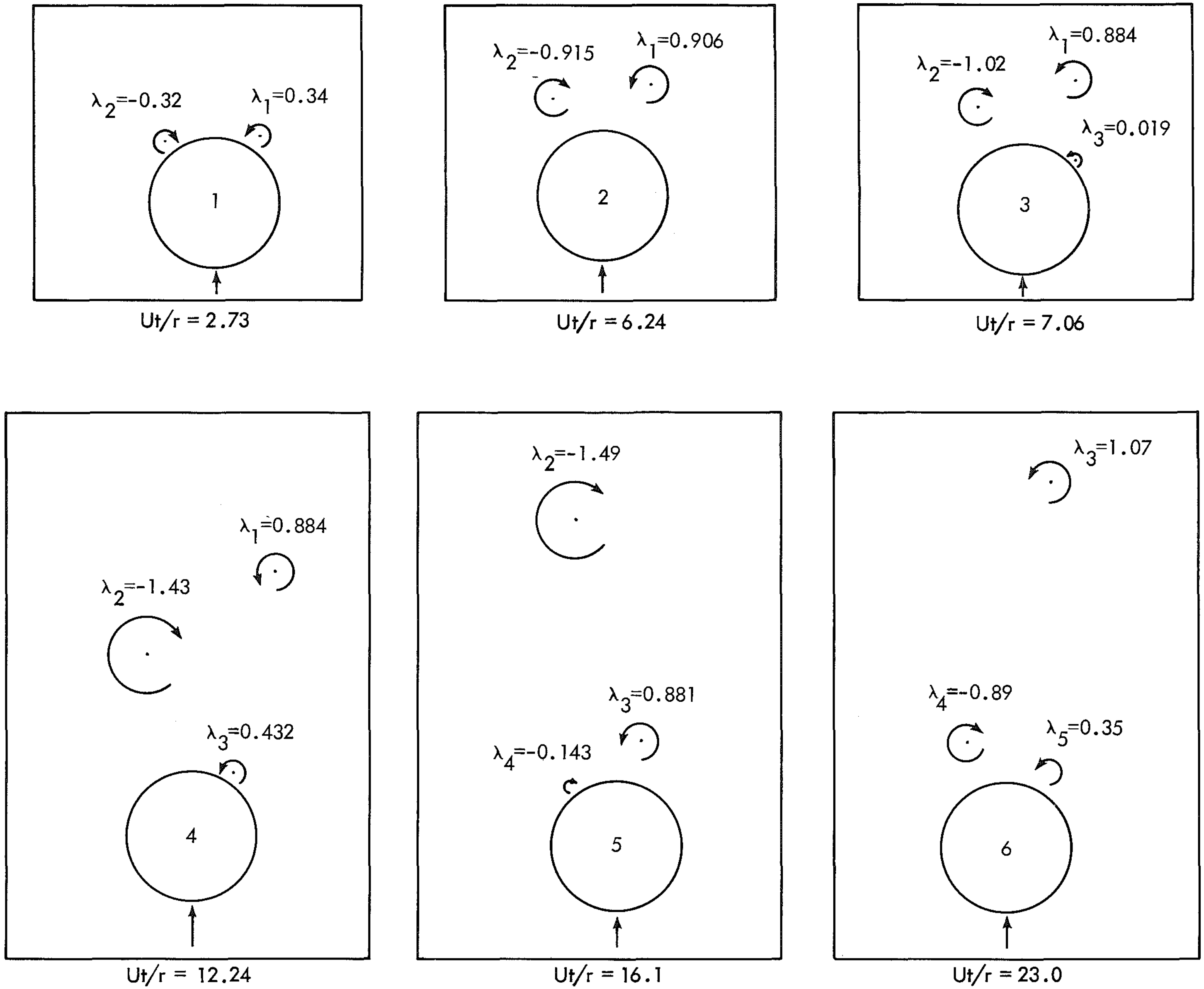

FIG. 4 DEVELOPMENT OF THE FLOW FIELD BEHIND AN IMPULSIVELY STARTED CYLINDER IN CROSSFLOW.

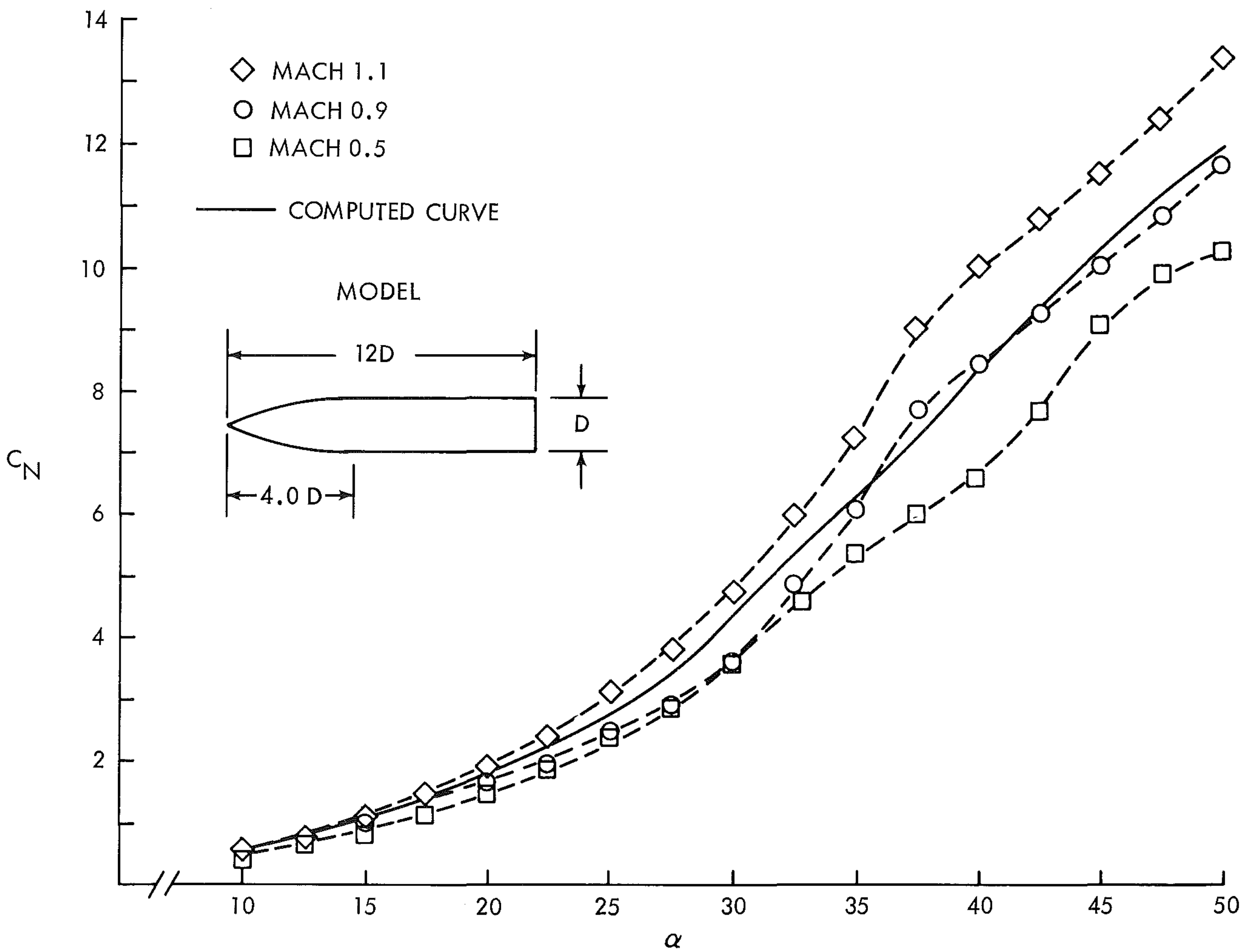

FIG. 5 NORMAL FORCE COEFFICIENT AS A FUNCTION OF ANGLE ATTACK. COMPUTED CURVE BASED ON FREE PARAMETER VALUES USED FOR A CYLINDER IN CROSSFLOW.

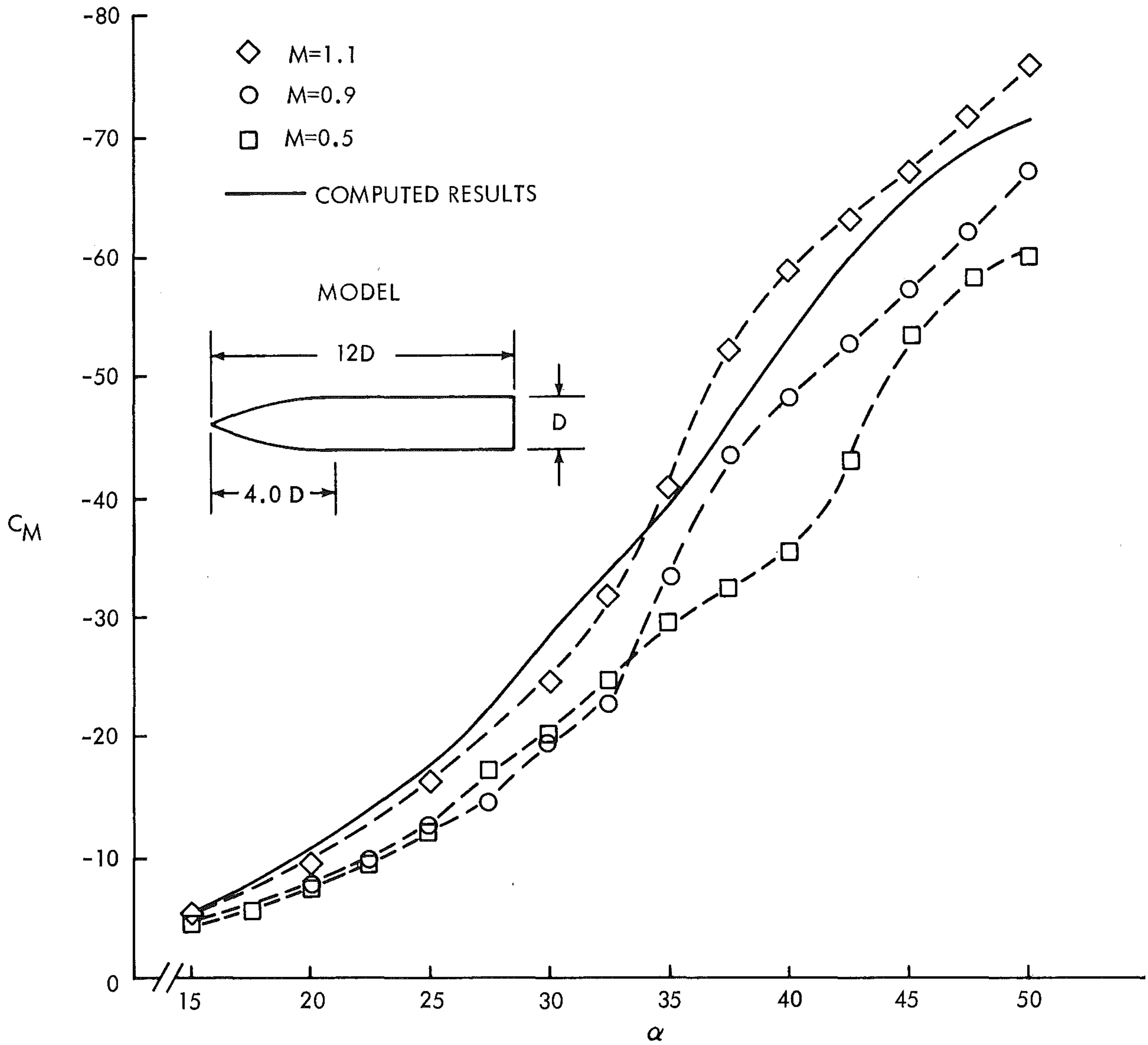

FIG. 6 PITCHING MOMENT COEFFICIENT AS A FUNCTION OF ANGLE OF ATTACK. COMPUTED CURVE BASED ON FREE PARAMETER VALUES USED FOR A CYLINDER IN CROSSFLOW.

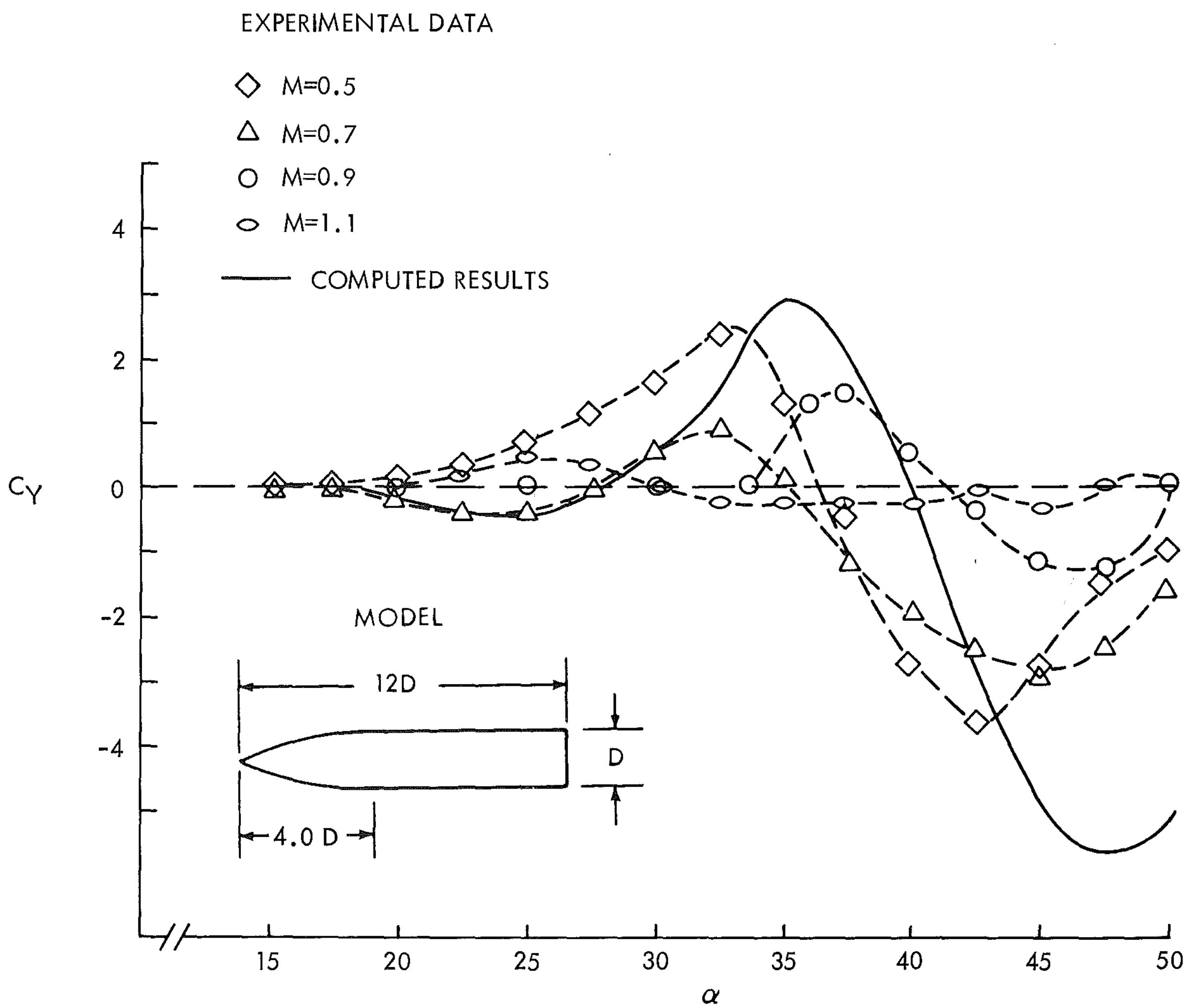

FIG. 7 YAWING FORCE COEFFICIENT AS A FUNCTION OF ANGLE OF ATTACK. COMPUTED CURVE BASED ON THE FREE PARAMETER VALUES USED FOR A CYLINDER IN CROSSFLOW.

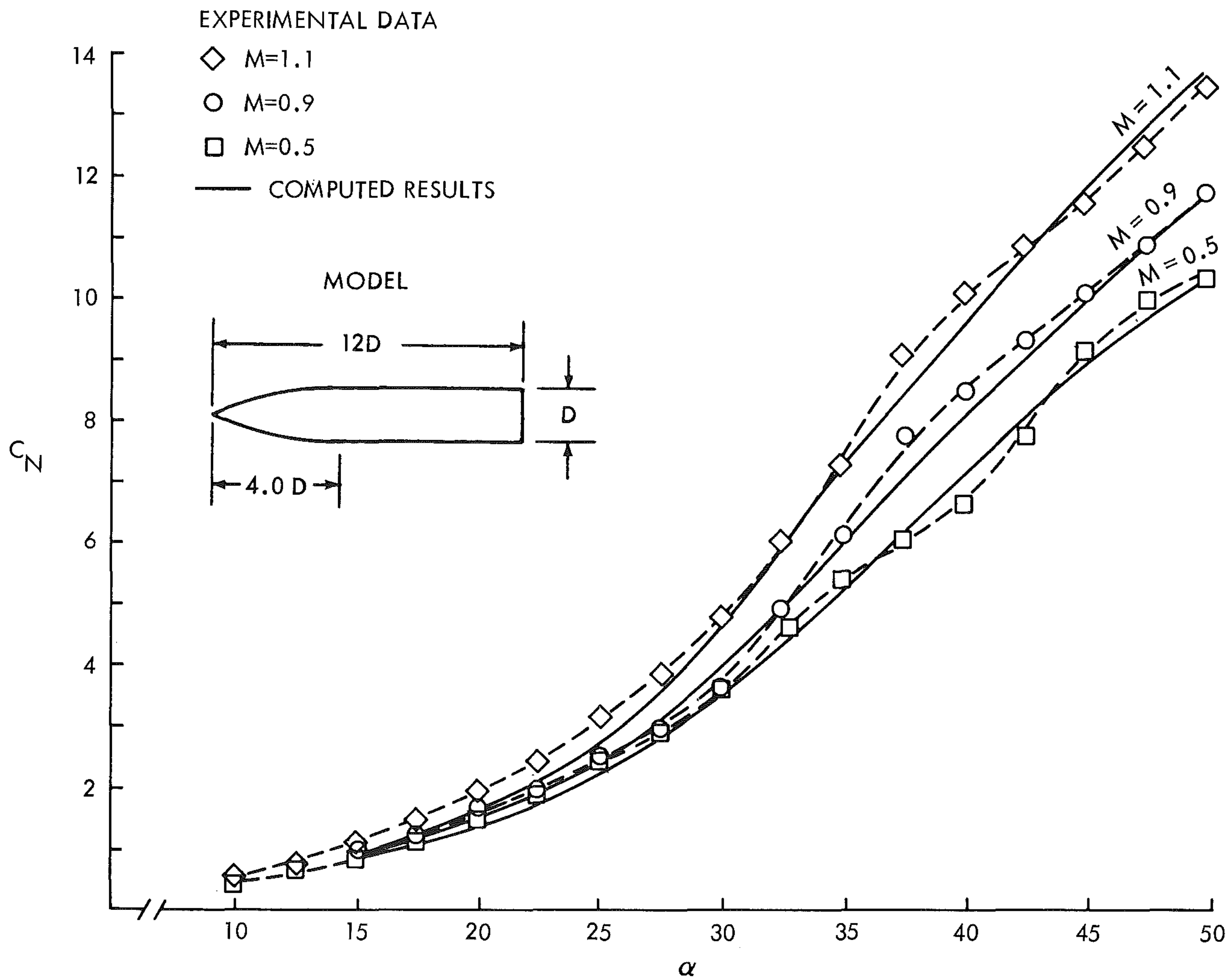

FIG. 8 NORMAL FORCE COEFFICIENT AS A FUNCTION OF ANGLE OF ATTACK. COMPUTED CURVES ARE BASED ON A SET OF PARAMETER VALUES WHICH ARE MACH NUMBER DEPENDENT.

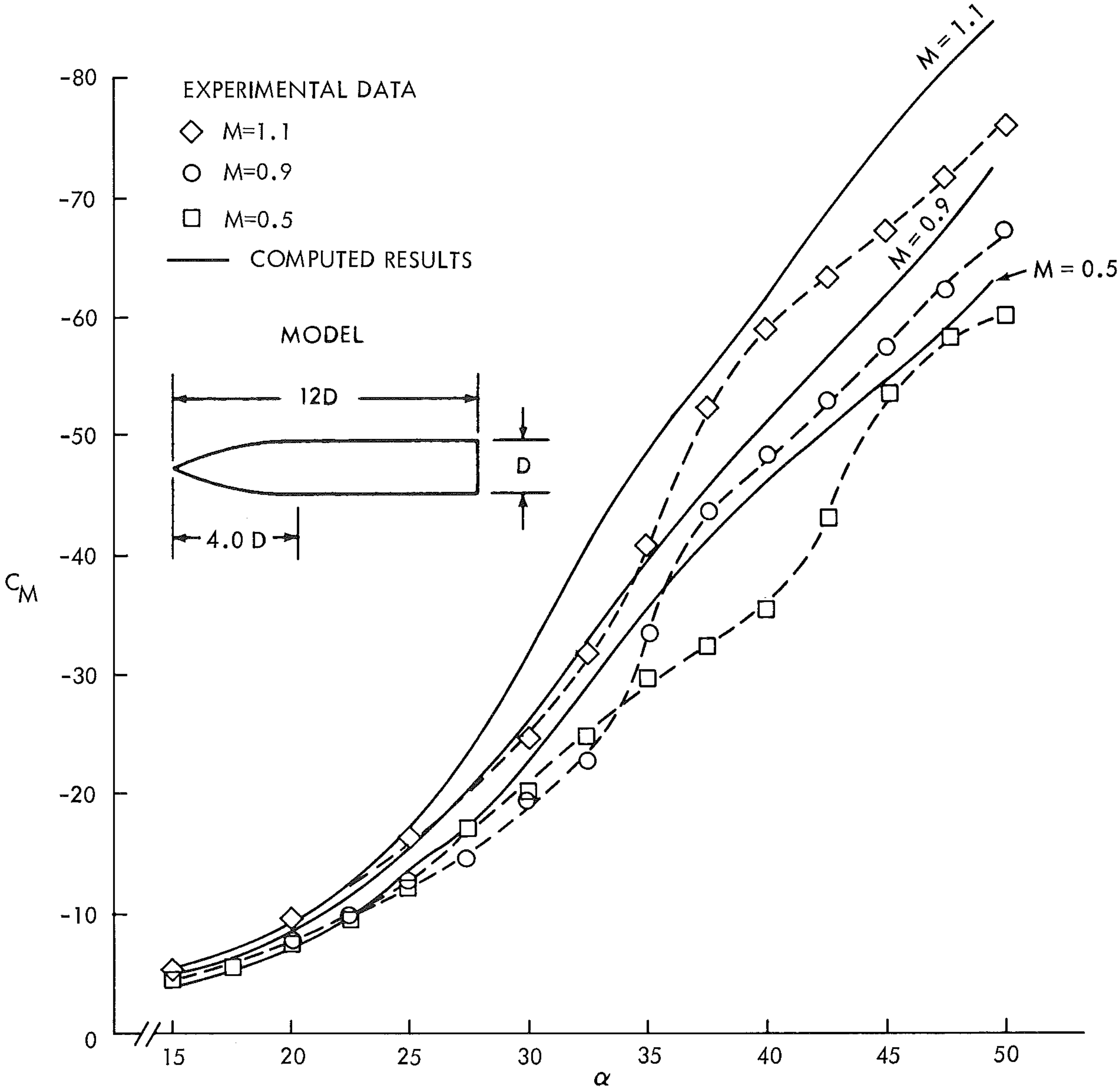

FIG. 9 PITCHING MOMENT COEFFICIENT AS A FUNCTION OF ANGLE OF ATTACK. COMPUTED CURVES ARE BASED ON A SET OF PARAMETER VALUES WHICH ARE MACH NUMBER DEPENDENT.

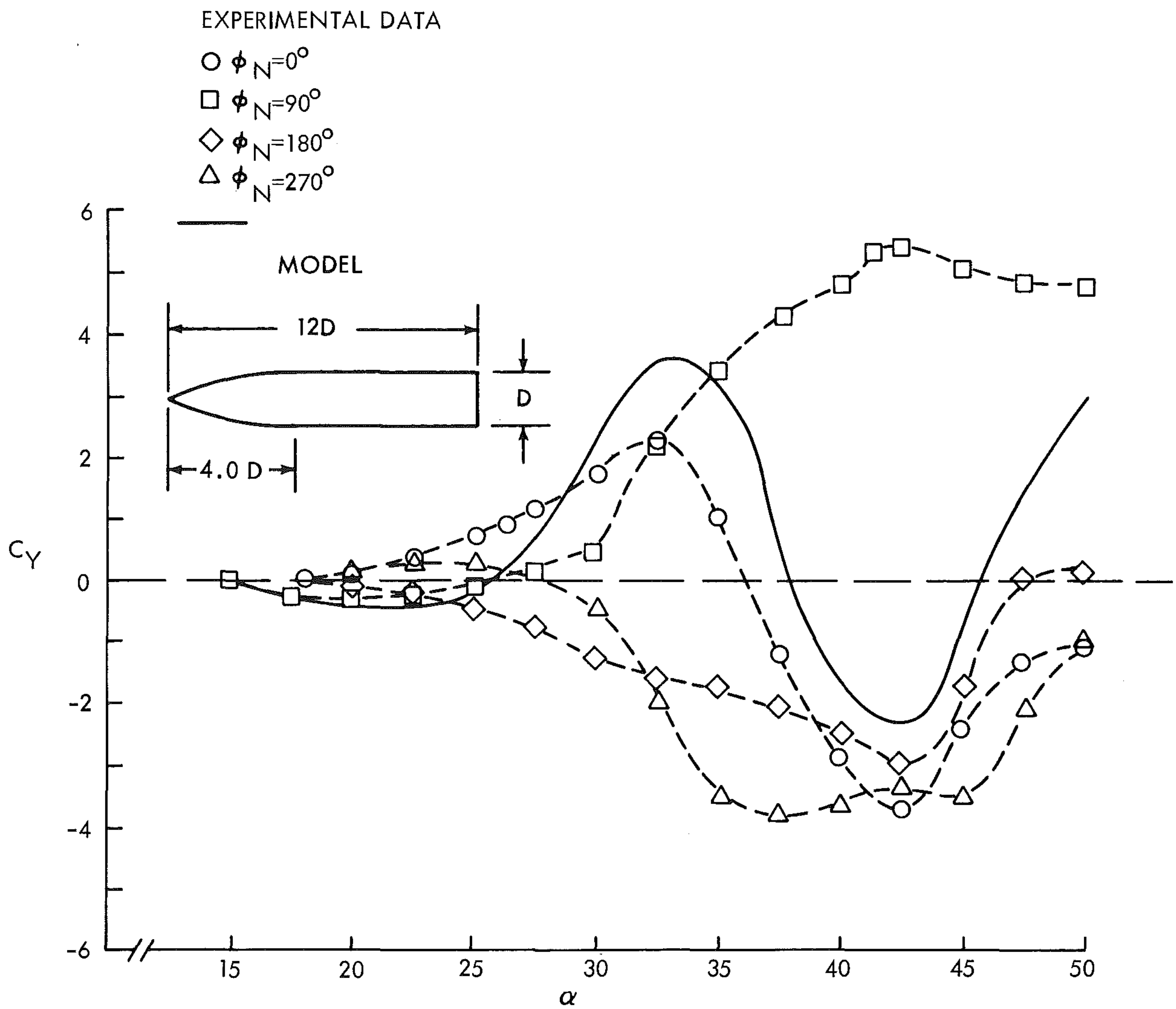

FIG. 10 YAW FORCE COEFFICIENT AS A FUNCTION OF ANGLE OF ATTACK FOR M=0.5. COMPUTED CURVES BASED ON FREE PARAMETER VALUES WHICH ARE MACH NUMBER DEPENDENT.

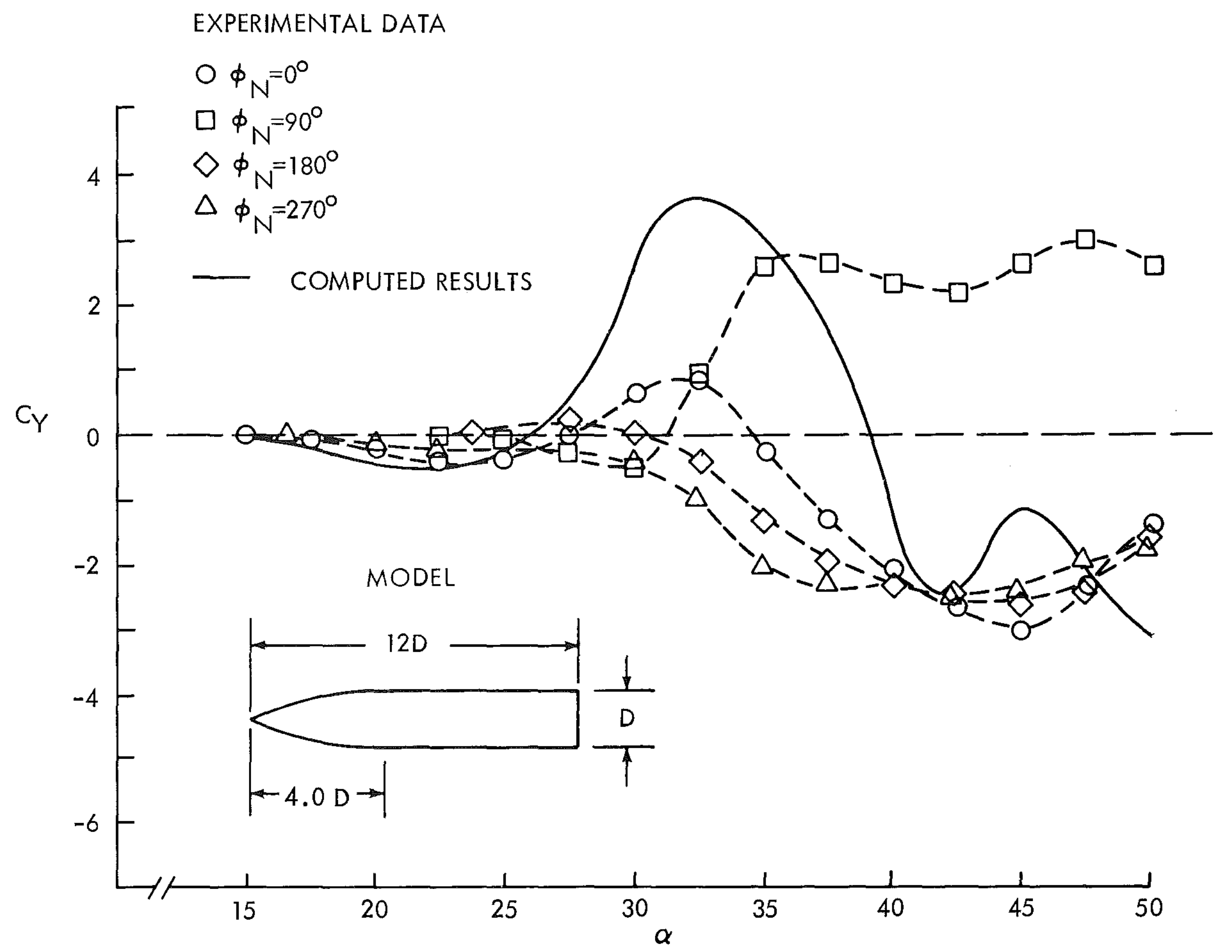

FIG. 11 YAW FORCE COEFFICIENT AS A FUNCTION OF ANGLE OF ATTACK FOR M=0.7. COMPUTED CURVE BASED ON FREE PARAMETER VALUES WHICH ARE MACH NUMBER DEPENDENT.

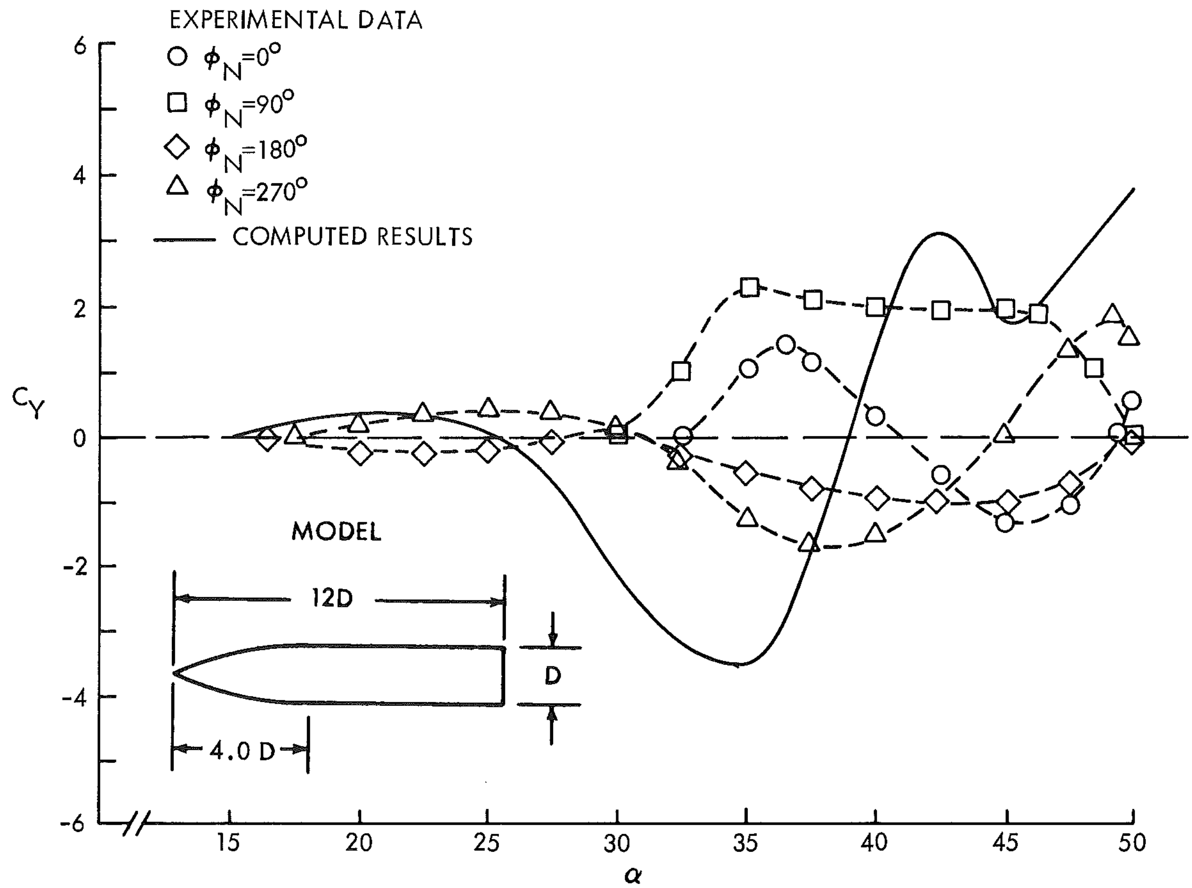

FIG. 12 YAW FORCE COEFFICIENT AS A FUNCTION OF ANGLE OF ATTACK FOR M=0.9. COMPUTED CURVE BASED ON FREE PARAMETER VALUES WHICH ARE MACH NUMBER DEPENDENT.

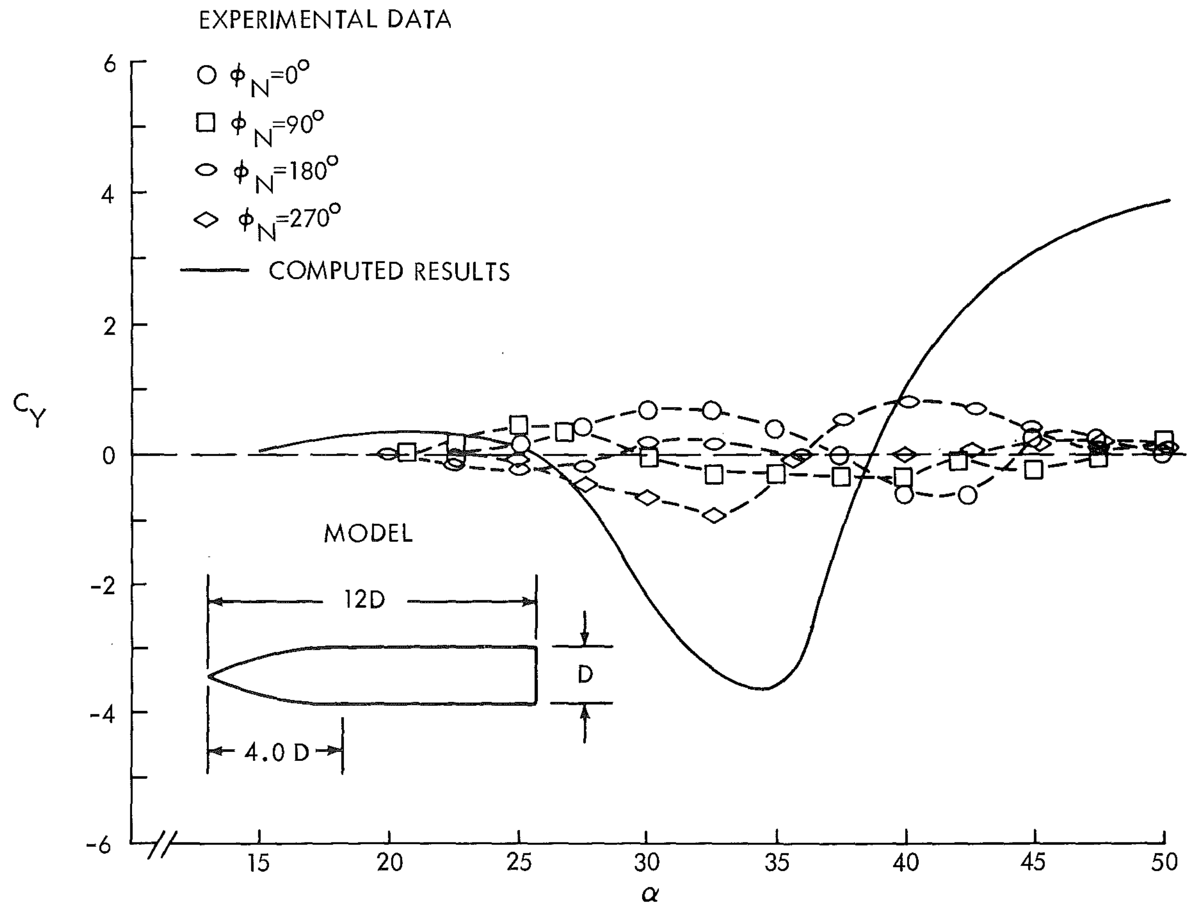

FIG. 13 YAW FORCE COEFFICIENT AS A FUNCTION OF ANGLE OF ATTACK FOR M=1.1. COMPUTED CURVE BASED ON FREE PARAMETER VALUES WHICH ARE MACH NUMBER DEPENDENT.

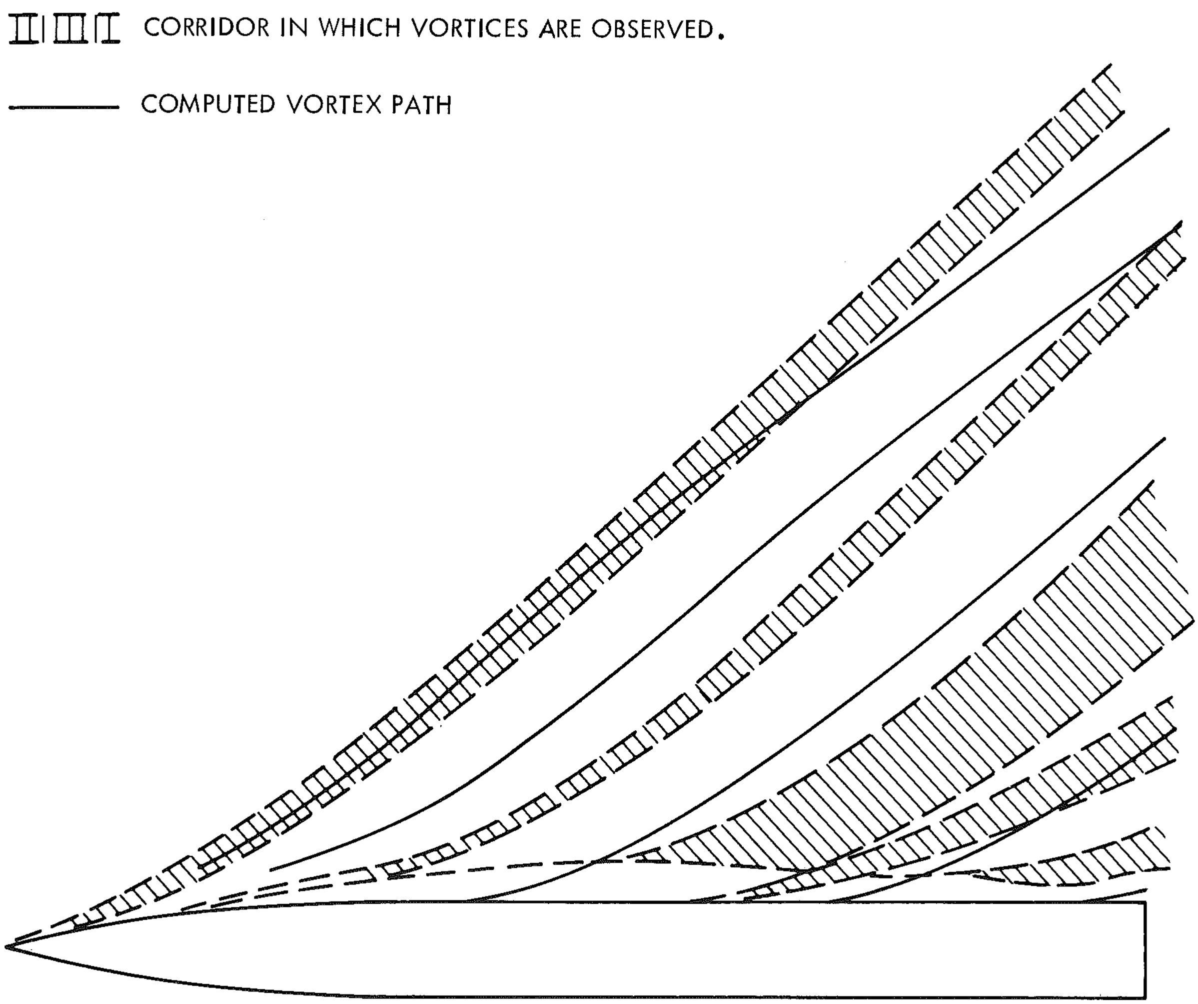

FIG. 14 COMPARISON OF OBSERVED AND COMPUTED VORTEX PATHS. α=45° MACH=0.5

CORRIDOR IN WHICH VORTICES ARE OBSERVED.

COMPUTED VORTEX PATH.

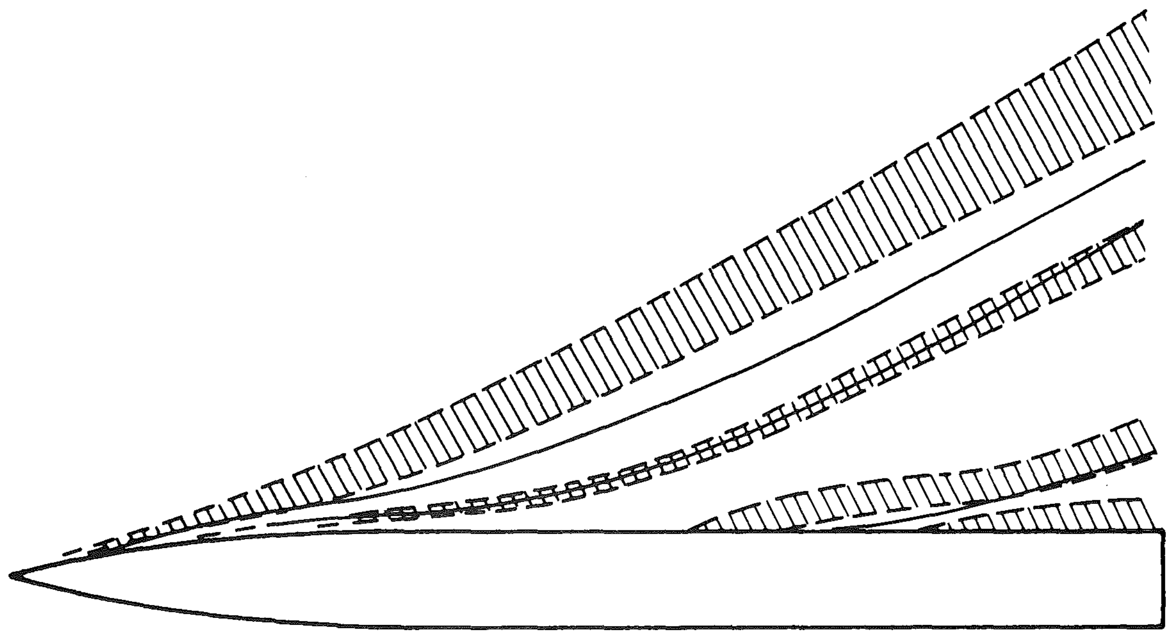

FIG. 15 COMPARISON OF OBSERVED AND COMPUTED VORTEX PATHS.
$\alpha = 35°$ MACH = 0.5

OBSERVED VORTEX PATH.

COMPUTED VORTEX PATH.

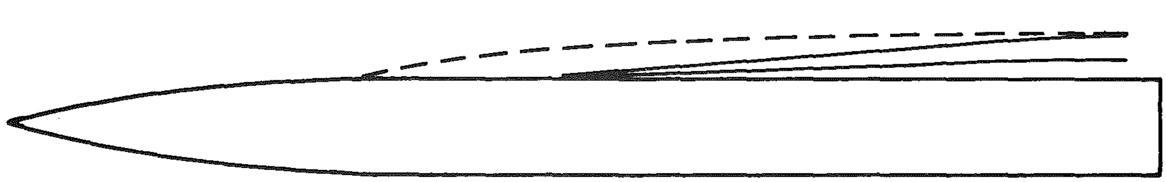

FIG. 16 COMPARISON OF OBSERVED AND COMPUTED VORTEX PATHS.
$\alpha = 20°$ MACH = 0.5

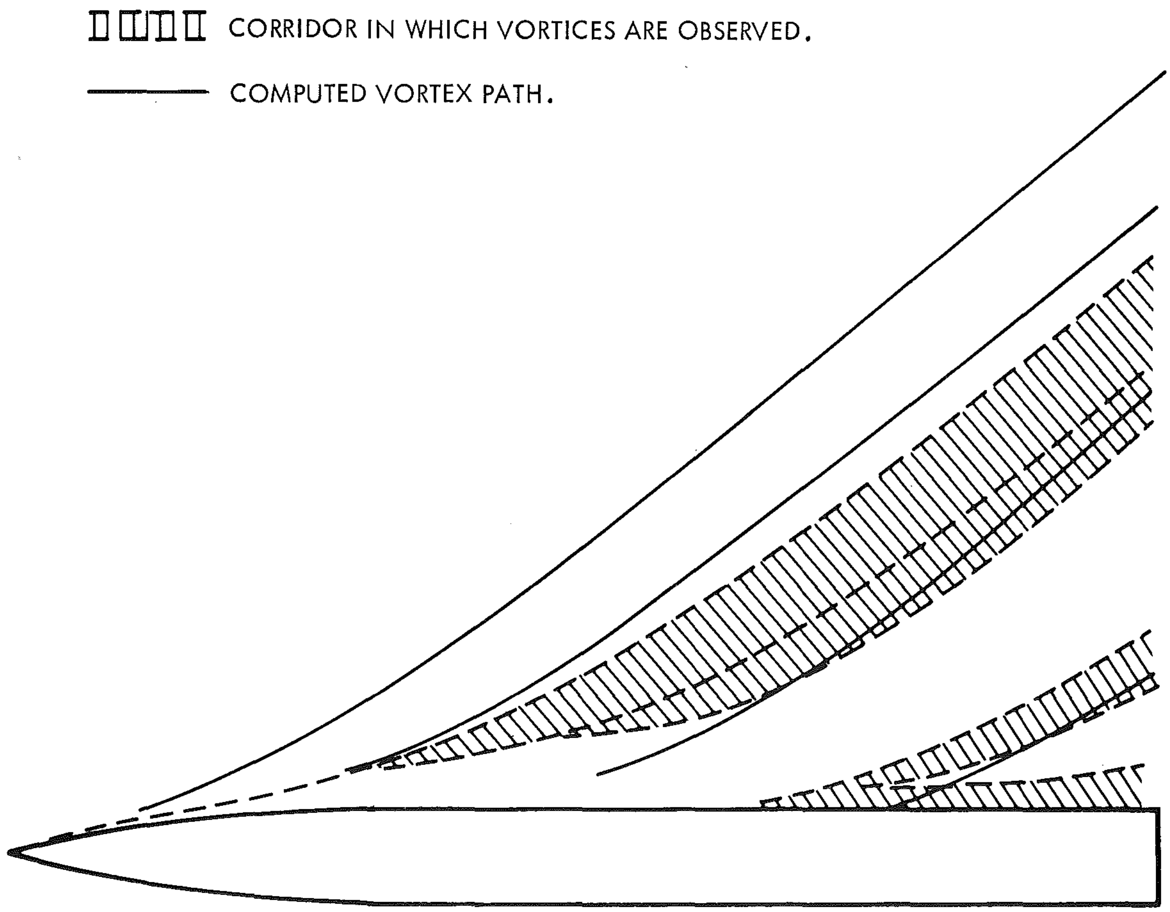

FIG. 17 COMPARISON OF OBSERVED AND COMPUTED VORTEX PATHS.
$\alpha = 45°$ MACH = 0.9

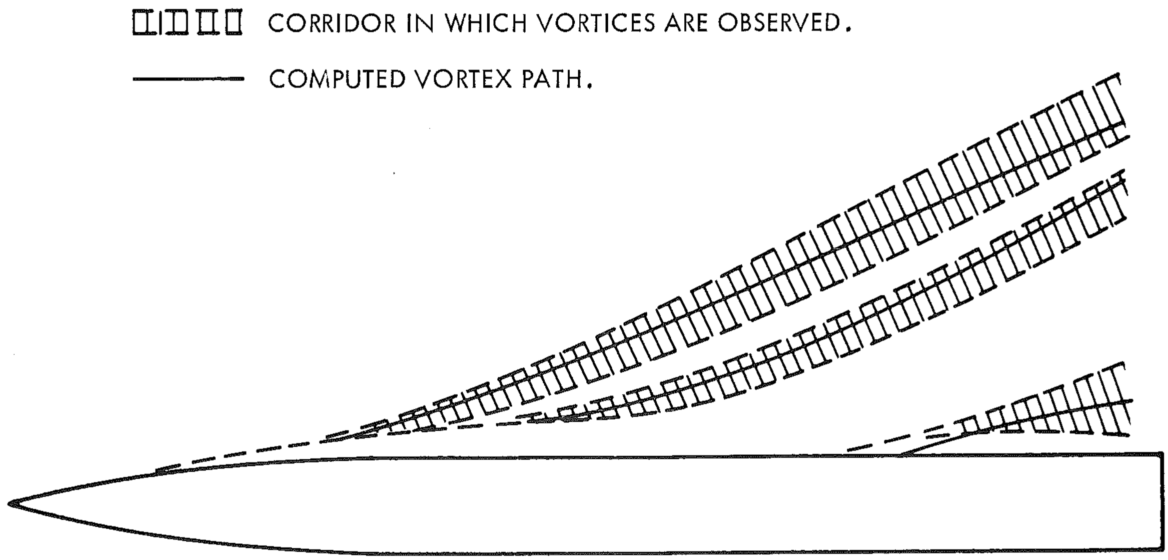

FIG. 18 COMPARISON OF OBSERVED: AND COMPUTED VORTEX PATHS.
$\alpha = 35°$ MACH = 0.9

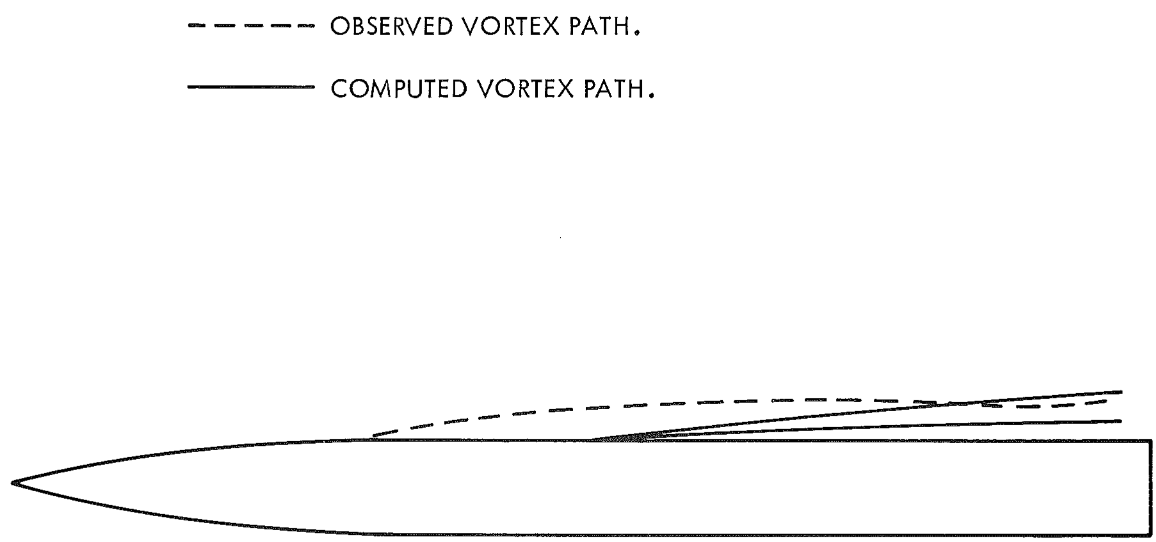

FIG. 19 COMPARISON OF OBSERVED AND COMPUTED VORTEX PATHS.
$\alpha = 20°$ MACH = 0.9

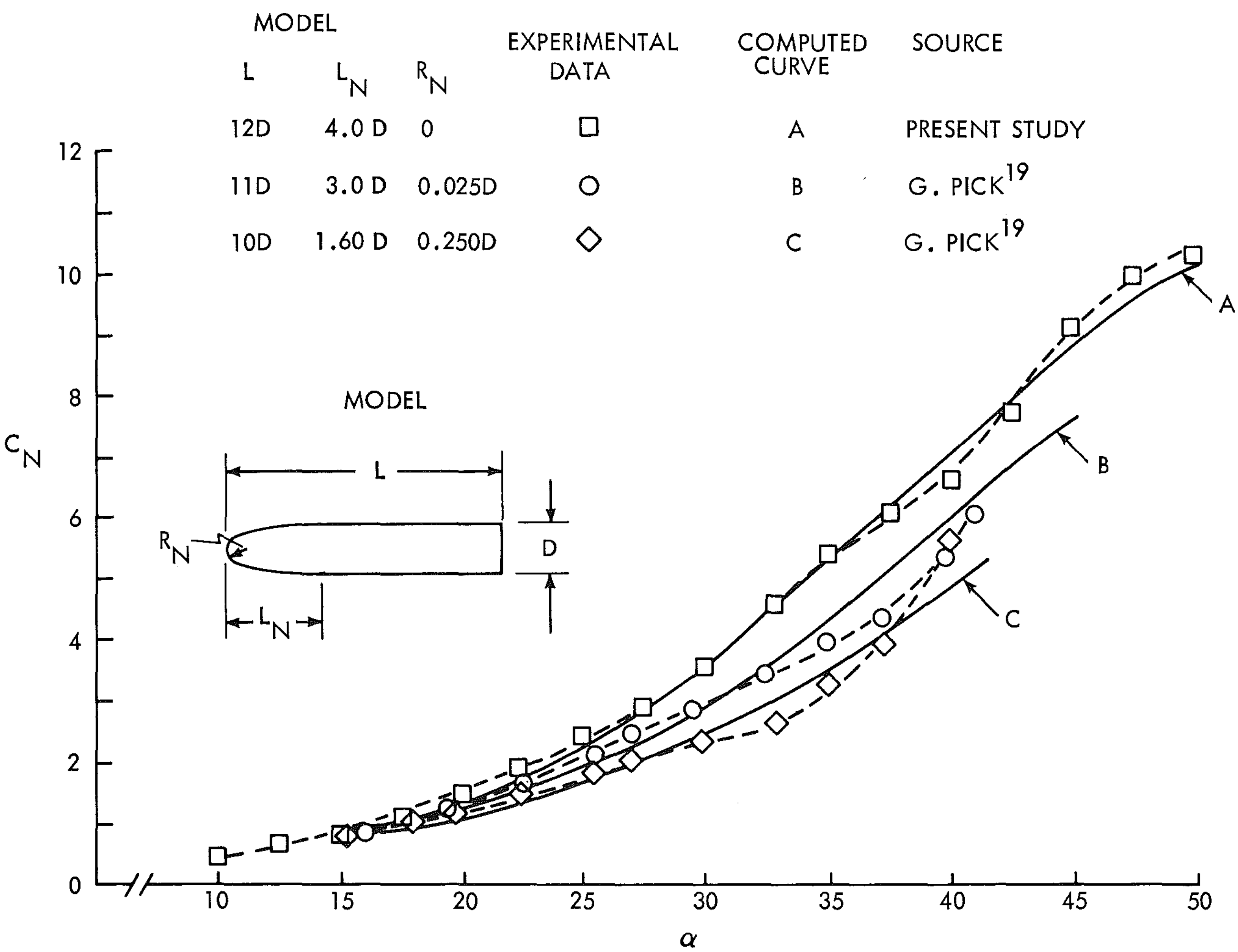

FIG. 20 NORMAL FORCE COEFFICIENT AS A FUNCTION OF ANGLE OF ATTACK FOR SEVERAL DIFFERENT MODELS, M = 0.5

MODEL			EXPERIMENTAL DATA	COMPUTED CURVE	SOURCE
L	L_N	R_N			
12D	4.0 D	0	□	A	PRESENT STUDY
11D	3.0 D	0.025D	○	B	G. PICK[19]
10D	1.60 D	0.250D	◇	C	G. PICK[19]

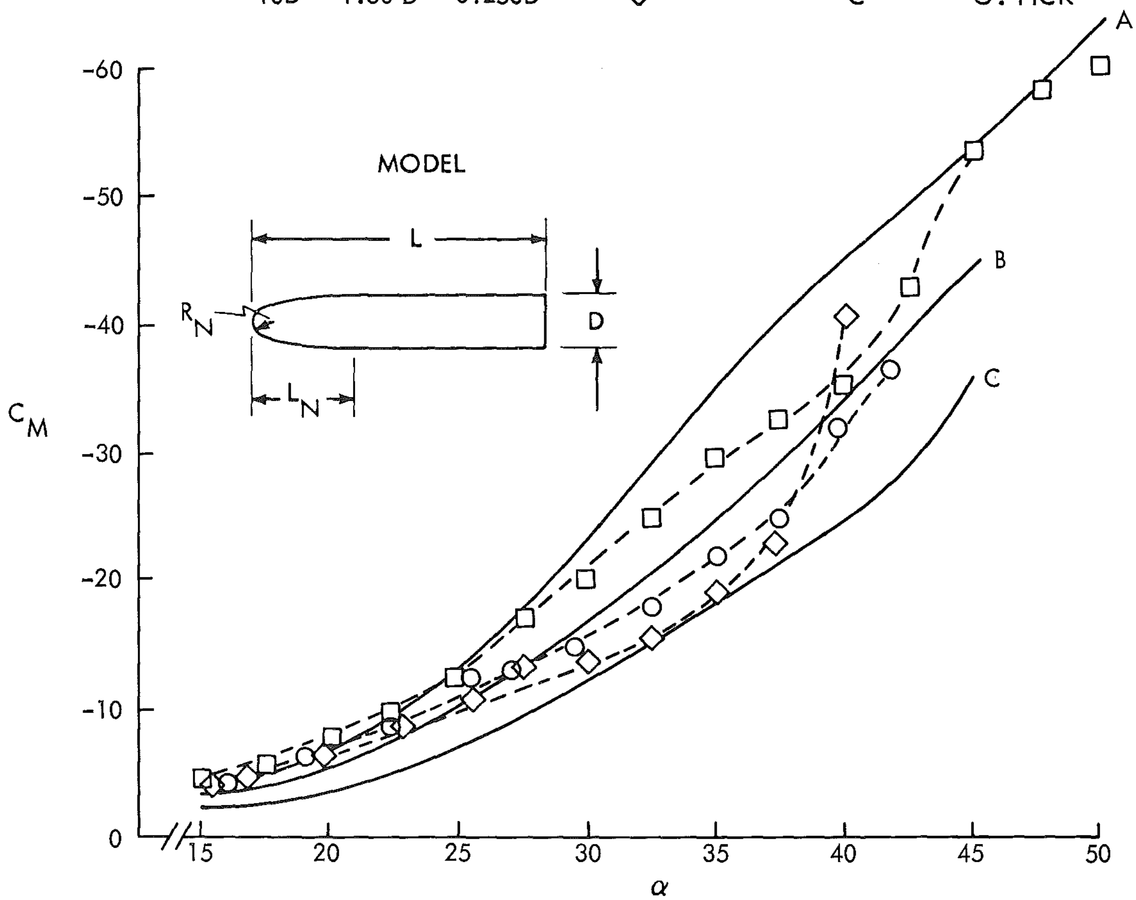

FIG. 21 PITCHING MOMENT COEFFICIENT AS A FUNCTION OF ANGLE OF ATTACK FOR SEVERAL DIFFERENT MODELS, M = 0.5.

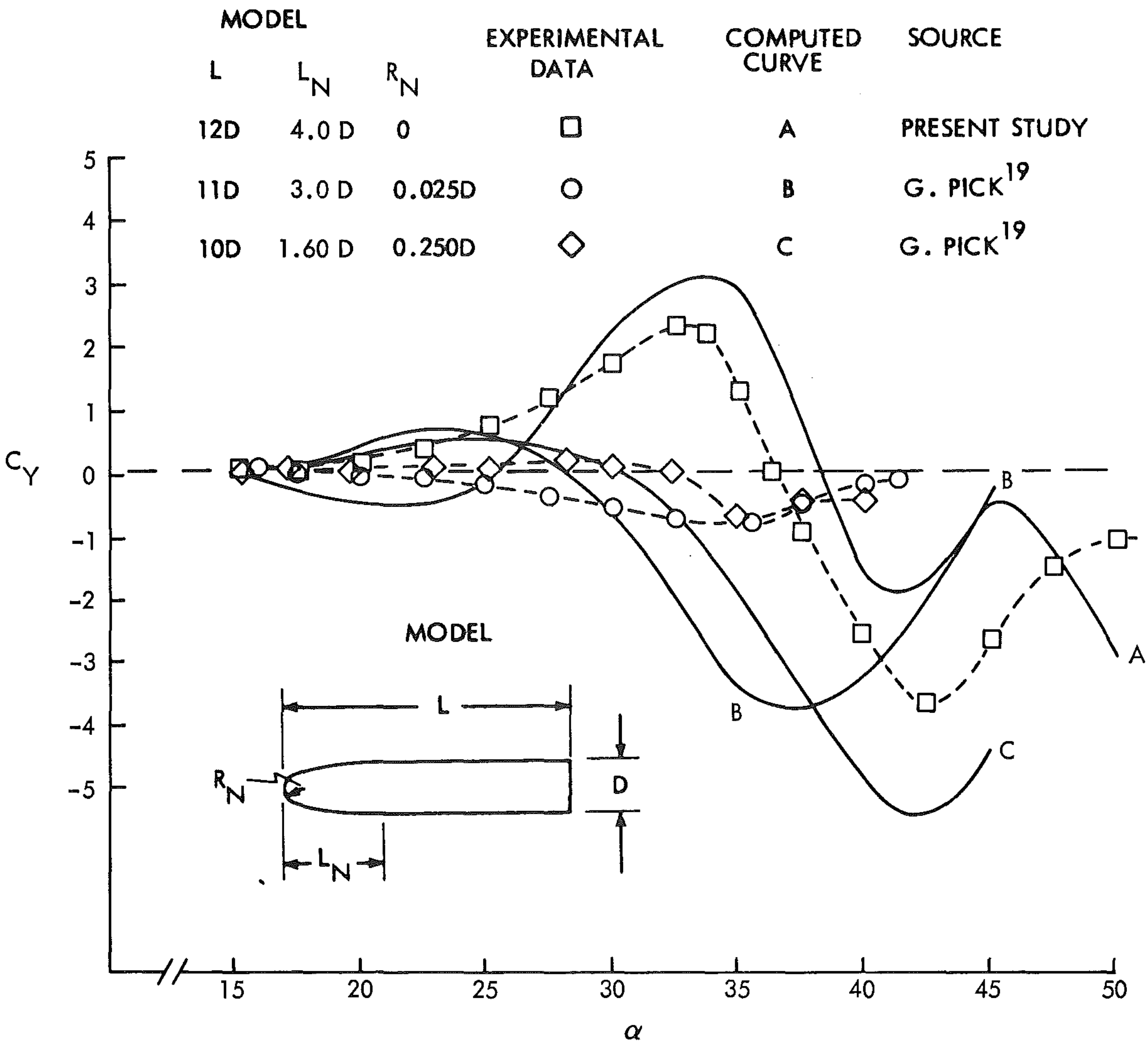

FIG. 22 YAW FORCE COEFFICIENT AS A FUNCTION OF ANGLE OF ATTACK FOR SEVERAL DIFFERENT MODELS, M = 0.5.

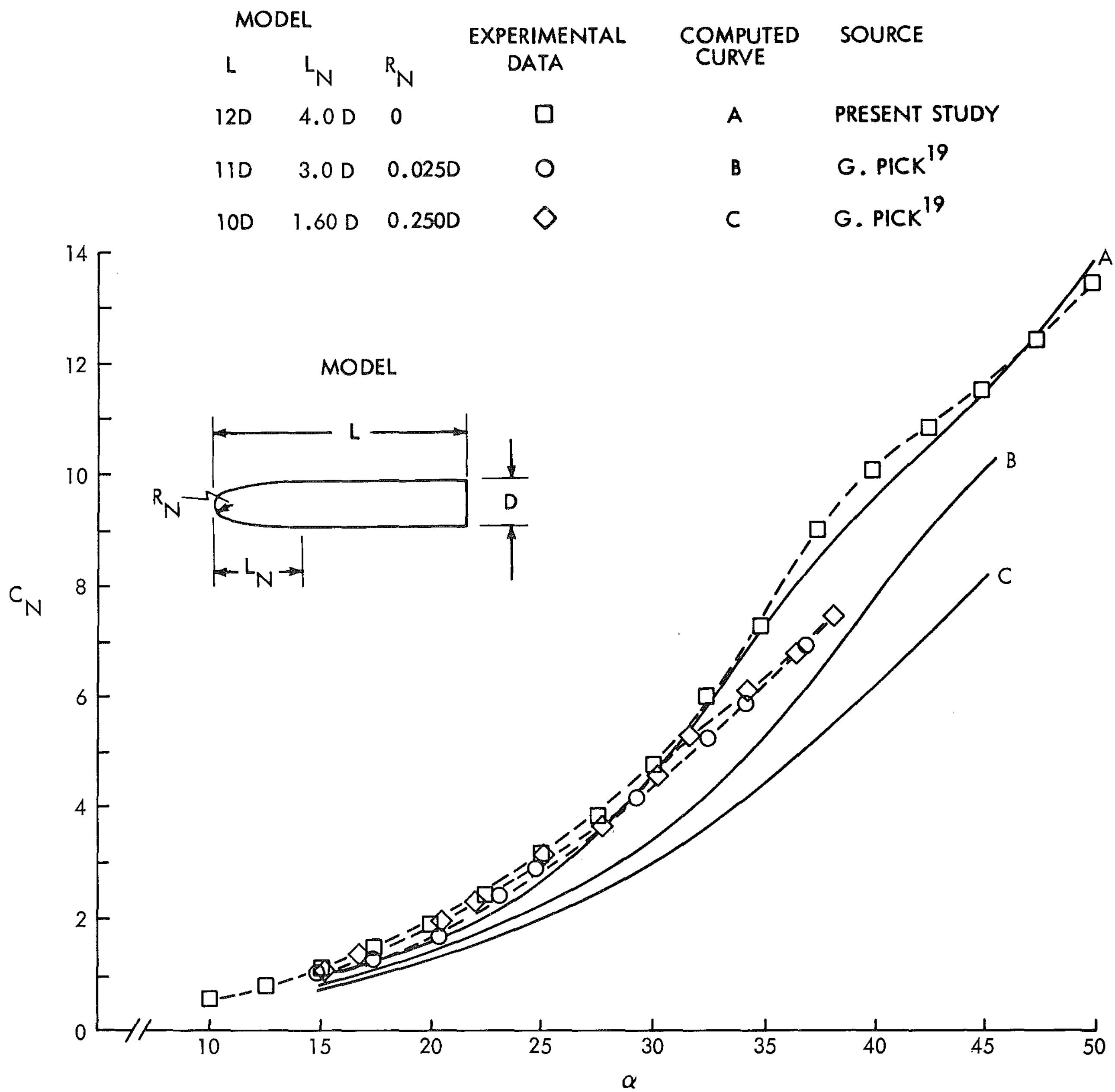

FIG. 23 NORMAL FORCE COEFFICIENT AS A FUNCTION OF ATTACK FOR SEVERAL DIFFERENT MODELS, M = 1.1.

MODEL L	L_N	R_N	EXPERIMENTAL DATA	COMPUTED CURVE	SOURCE
12D	4.0 D	0	□	A	PRESENT STUDY
11D	3.0 D	0.025D	○	B	G. PICK[19]
10D	1.60 D	0.250D	◇	C	G. PICK[19]

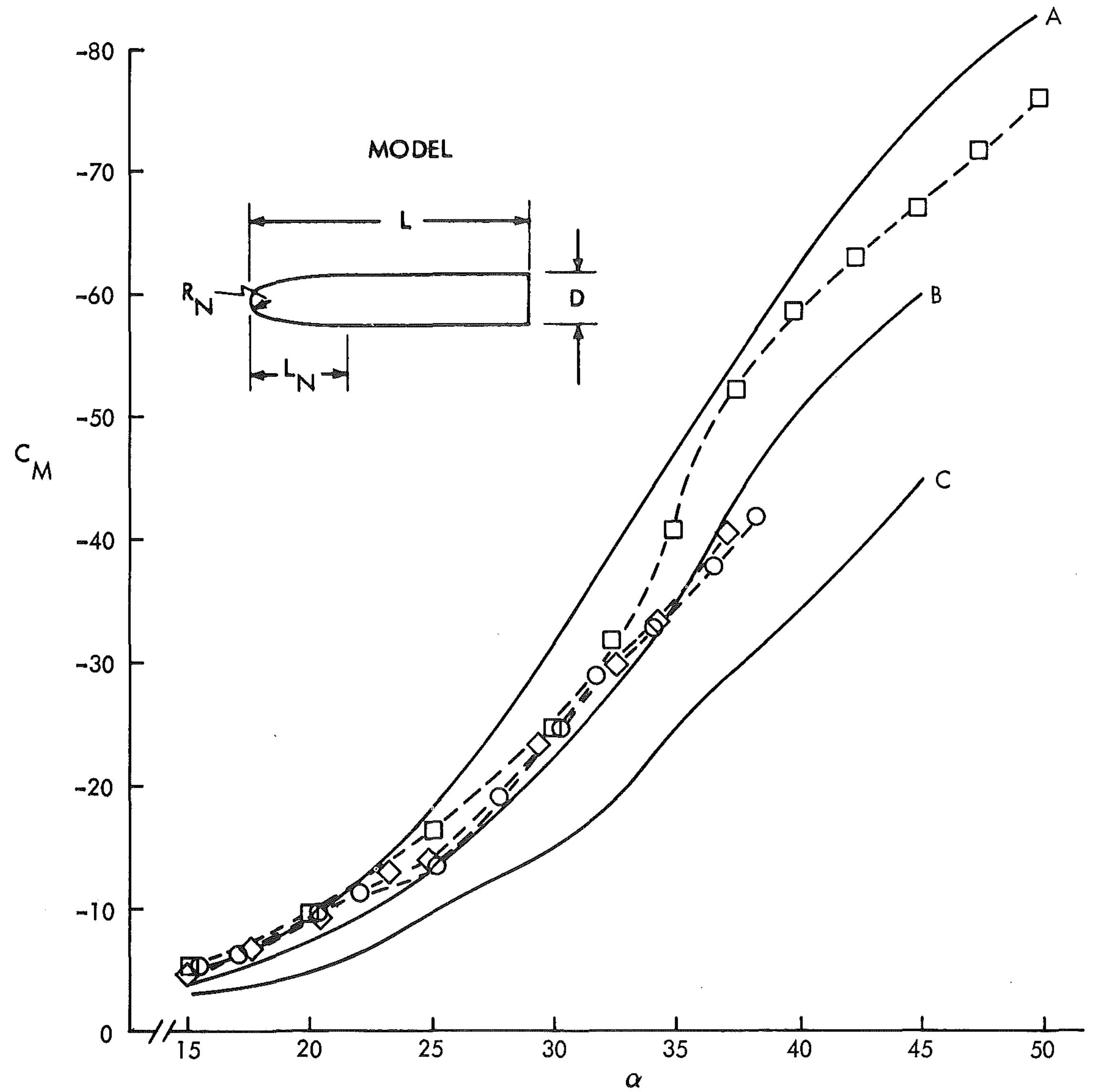

FIG. 24 PITCHING MOMENT COEFFICIENT AS A FUNCTION OF ANGLE OF ATTACK FOR SEVERAL DIFFERENT MODELS, M = 1.1

MODEL L	L_N	R_N	EXPERIMENTAL DATA	COMPUTED CURVE	SOURCE
12D	4.0 D	0	□	A	PRESENT STUDY
11D	3.0 D	0.025D	○	B	G. PICK[19]
10D	1.60 D	0.250D	◇	C	G. PICK[19]

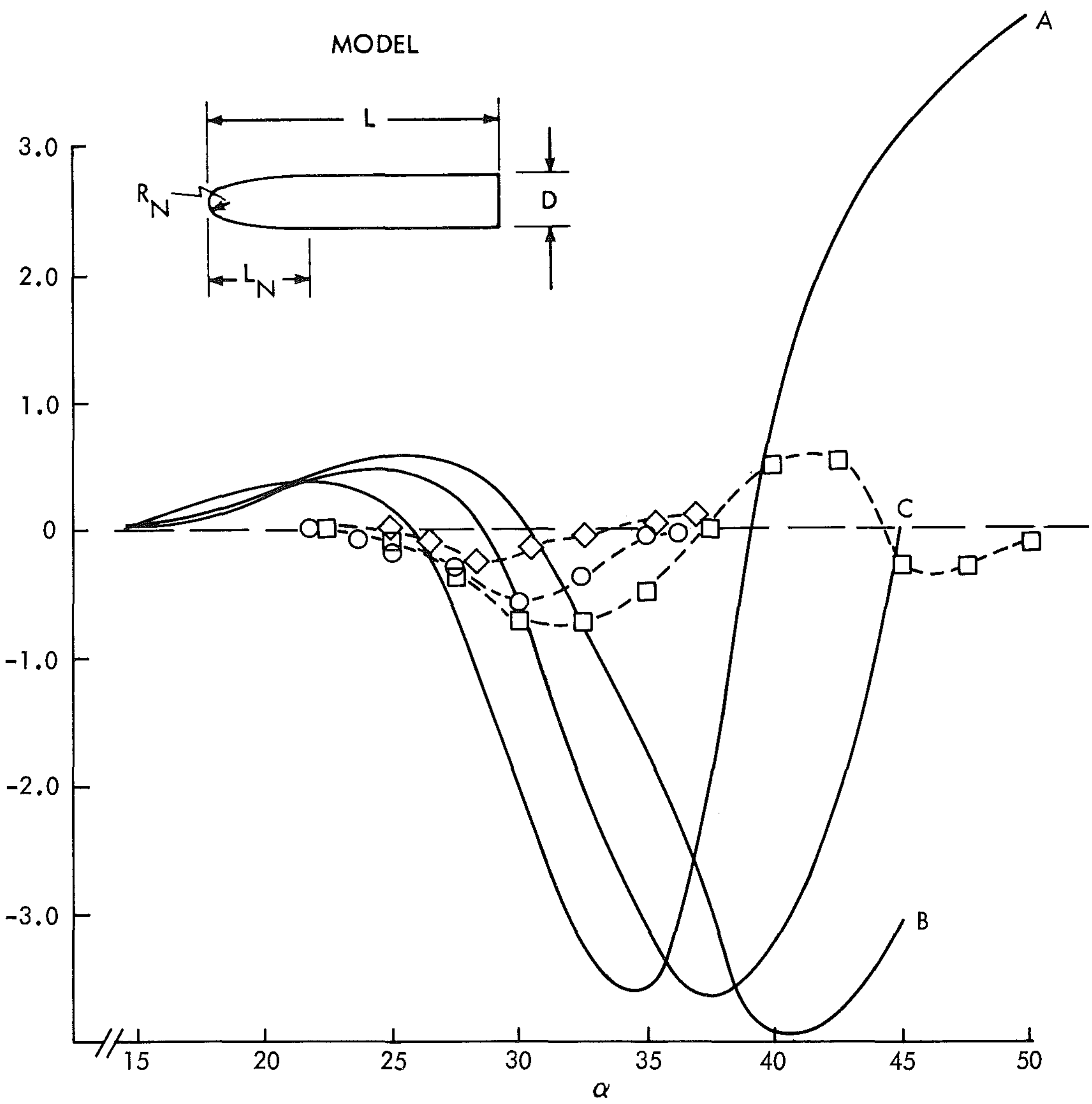

FIG. 25 YAW FORCE COEFFICIENT AS A FUNCTION OF ANGLE OF ATTACK FOR SEVERAL DIFFERENT MODELS, M = 1.1

APPENDIX A

DERIVATION OF PROGRAMMED EQUATIONS

The governing equations are:

$$\left.\begin{aligned}
\frac{d\zeta_1}{dx} + \frac{(\zeta_1 - \zeta_{01})}{\lambda_1}\frac{d\lambda_1}{dx} &= \tan\alpha\, \omega_1 - \frac{(\zeta_1 - \zeta_{01})}{r}\frac{dr}{dx} \\
\frac{d\zeta_2}{dx} + \frac{(\zeta_2 - \zeta_{02})}{\lambda_2}\frac{d\lambda_2}{dx} &= \tan\alpha\, \omega_2 - \frac{(\zeta_2 - \zeta_{02})}{r}\frac{dr}{dx}
\end{aligned}\right\} \text{growing vortices}$$

$$\frac{d\zeta_j}{dx} = \tan\alpha\, \omega_j \qquad j = 3, 4 \cdots k \qquad \text{shed vortices} \tag{A-1}$$

In order to define λ_1 and λ_2 the above equation must be augmented by the constraint that the fluid velocity be zero at the stagnation points relative to the changing radius:

$$\omega(\zeta_{01}) = \frac{r}{\tan\alpha}\frac{dr}{dz}\frac{1}{\bar{\zeta}_{01}} \qquad \omega(\zeta_{02}) = \frac{r}{\tan\alpha}\frac{dr}{dz}\frac{1}{\bar{\zeta}_{02}} \tag{A-2}$$

The dimensionless velocity potential, $\tilde{\phi}$, is defined as follows:

$$\tilde{\phi}(\zeta) = -\left(\zeta - \frac{r^2}{\zeta}\right)i - ir\sum_{j=1}^{k} \lambda_j \ln\left[\frac{(\zeta - \zeta_j)}{(\zeta - r^2/\bar{\zeta}_j)}\right] + \frac{r}{\tan\alpha}\frac{dr}{dz}\ln(\zeta) \tag{A-3}$$

Differentiating Equation (A-3), the dimensionless velocity is determined.

$$\omega = \text{CONJUGATE}\left| -i\left(1 + \frac{r^2}{\zeta^2}\right) - ir\sum_{j=1}^{k}\lambda_j\left\{\frac{1}{(\zeta - \zeta_j)} - \frac{1}{(\zeta - r^2/\bar{\zeta}_j)}\right\} + \frac{r}{\tan\alpha}\frac{dr}{dz}\frac{1}{\zeta}\right| \tag{A-4}$$

To simplify manipulations, the following functions are defined

$$a(\zeta, \zeta_j) = \left\{ \frac{1}{(\zeta - \zeta_j)} - \frac{1}{(\zeta - r^2/\bar{\zeta}_j)} \right\} \tag{A-5a}$$

$$b(\zeta) = \left(\frac{1}{r} + \frac{r}{\zeta^2} \right) + \sum_{j=3}^{K} \lambda_j a(\zeta, \zeta_j) \tag{A-5b}$$

Substituting Equations (A-5) into Equation (A-4):

$$\omega = -ir \text{ CONJUGATE} \left| b(\zeta) + \lambda_1 a(\zeta, \zeta_1) + \lambda_2 a(\zeta, \zeta_2) + \frac{i}{\tan\alpha} \frac{dr}{dz} \frac{1}{\zeta} \right| \tag{A-6}$$

Substituting Equation (A-6) into constraints (A-2):

$$\begin{aligned} \lambda_1 a(\zeta_{01}, \zeta_1) + \lambda_2 a(\zeta_{01}, \zeta_2) &= -b(\zeta_{01}) \\ \lambda_1 a(\zeta_{02}, \zeta_1) + \lambda_2 a(\zeta_{02}, \zeta_2) &= -b(\zeta_{02}) \end{aligned} \tag{A-7}$$

Solving the above:

$$\begin{aligned} \lambda_1 &= \frac{b(\zeta_{02})a(\zeta_{01}, \zeta_2) - b(\zeta_{01})a(\zeta_{02}, \zeta_2)}{a(\zeta_{01}, \zeta_1)a(\zeta_{02}, \zeta_2) - a(\zeta_{02}, \zeta_1)a(\zeta_{01}, \zeta_2)} \equiv \frac{A1}{C} \\ \lambda_2 &= \frac{b(\zeta_{01})a(\zeta_{02}, \zeta_1) - b(\zeta_{02})a(\zeta_{01}, \zeta_1)}{a(\zeta_{01}, \zeta_1)a(\zeta_{02}, \zeta_2) - a(\zeta_{02}, \zeta_1)a(\zeta_{01}, \zeta_2)} \equiv \frac{B1}{C} \end{aligned} \tag{A-8}$$

Differentiating the above and substituting into the governing equations produces differential equations for z_j and y_j. The algebra involved is simplifed by defining the following functions.

$$T(\zeta, \zeta_j) = \left[\frac{1}{(\zeta - r^2/\bar{\zeta}_j)^2} - \frac{1}{(\zeta - \zeta_j)^2} \right]$$

$$E(\zeta, \zeta_j) = (\zeta - \zeta_j)^{-2}$$

$$H(\zeta, \zeta_j) = \frac{-2r}{\bar{\zeta}_j(\zeta - r^2/\bar{\zeta}_j)^2} \frac{dr}{dx}$$

$$XF(\zeta, \zeta_j) = \frac{r^2}{\bar{\zeta}_j^2(\zeta - r^2/\bar{\zeta}_j)^2}$$

$$G(\rho) = -\frac{2r}{\rho^3} + \sum_{j=3}^{K} \lambda_j T(\rho, \rho_j)$$

$$P(\rho) = \frac{dr}{dz}\left(\frac{1}{\rho^2} - \frac{1}{r^2}\right) + \sum_{j=3}^{K} H(\rho, \rho_j)\lambda_j$$

$$C1 = [-a(\rho_{02}, \rho_2)E(\rho_{01}, \rho_1) + a(\rho_{01}, \rho_2)E(\rho_{02}, \rho_1)]/C$$

$$C2 = [-a(\rho_{02}, \rho_2)XF(\rho_{01}, \rho_1) + a(\rho_{01}, \rho_2)XF(\rho_{02}, \rho_1)]/C$$

$$C3 = [-a(\rho_{01}, \rho_1)E(\rho_{02}, \rho_2) + a(\rho_{02}, \rho_1)E(\rho_{01}, \rho_2)]/C$$

$$C4 = [-a(\rho_{01}, \rho_1)XF(\rho_{02}, \rho_2) + a(\rho_{02}, \rho_1)XF(\rho_{01}, \rho_2)]/C$$

$$C5 = [-a(\rho_{02}, \rho_2)T(\rho_{01}, \rho_1) + a(\rho_{02}, \rho_1)T(\rho_{01}, \rho_2)]/C$$

$$C6 = [-a(\rho_{01}, \rho_1)T(\rho_{02}, \rho_2) + a(\rho_{01}, \rho_2)T(\rho_{02}, \rho_1)]/C$$

$$C7 = [a(\rho_{02}, \rho_1)H(\rho_{01}, \rho_2) + a(\rho_{01}, \rho_2)H(\rho_{02}, \rho_1) - a(\rho_{01}, \rho_1)H(\rho_{02}, \rho_2) - a(\rho_{02}, \rho_2)H(\rho_{01}, \rho_1)]/C$$

$$K11 = C1(\rho_1 - \rho_{01}) + 1.$$

$$K12 = C2(\rho_1 - \rho_{01})$$

$$K13 = \left[C3 - \frac{E(\rho_{02}, \rho_2)b(\rho_{01})}{A1} + \frac{b(\rho_{02})E(\rho_{01}, \rho_2)}{A1}\right](\rho_1 - \rho_{01})$$

$$K14 = \left[C4 - \frac{XF(\rho_{02}, \rho_2)b(\rho_{01})}{A1} + \frac{b(\rho_{02})E(\rho_{01}, \rho_2)}{A1}\right](\rho_1 - \rho_{01})$$

$$K15 = \left[C5 - \frac{a(\rho_{02}, \rho_2)G(\rho_{01})}{A1} + \frac{b(\rho_{02})T(\rho_{01}, \rho_2)}{A1}\right](\rho_1 - \rho_{01})$$

$$K16 = \left[C6 - \frac{a(\rho_{01}, \rho_2)G(\rho_{02})}{A1} + \frac{T(\rho_{02}, \rho_2)B(\rho_{01})}{A1}\right](\rho_1 - \rho_{01})$$

$$KL(\rho_j) = [-a(\rho_{02}, \rho_2)E(\rho_{01}, \rho_j) + a(\rho_{01}, \rho_2)E(\rho_{02}, \rho_j)](\rho_1 - \rho_{01})/A1$$

$$KM(\rho_j) = [-a(\rho_{02}, \rho_2)XF(\rho_{01}, \rho_j) + a(\rho_{01}, \rho_2)XF(\rho_{02}, \rho_j)](\rho_1 - \rho_{01})/A1$$

$$K19 = [C7 - \{b(\zeta_{01})H(\zeta_{02},\zeta_2) + a(\zeta_{02},\zeta_2)P(\zeta_{01}) - b(\zeta_{02})H(\zeta_{01},\zeta_2) - a(\zeta_{01},\zeta_2)P(\zeta_{02})\}/A1](\zeta_1 - \zeta_{01})$$

$$K21 = \left[C1 - \frac{b(\zeta_{02})E(\zeta_{01},\zeta_1)}{B1} + \frac{b(\zeta_{01})E(\zeta_{02},\zeta_1)}{B1}\right](\zeta_2 - \zeta_{02})$$

$$K22 = \left[C2 - \frac{b(\zeta_{02})XF(\zeta_{01},\zeta_1)}{B1} + \frac{b(\zeta_{01})XF(\zeta_{02},\zeta_1)}{B1}\right](\zeta_2 - \zeta_{02})$$

$$K23 = C3(\zeta_2 - \zeta_{02}) + 1.$$

$$K24 = C4(\zeta_2 - \zeta_{02})$$

$$K25 = \left[C5 - \frac{b(\zeta_{02})T(\zeta_{01},\zeta_2)}{B1} + \frac{a(\zeta_{02},\zeta_1)G(\zeta_{01})}{B1}\right](\zeta_2 - \zeta_{02})$$

$$K26 = \left[C6 - \frac{b(\zeta_{01})T(\zeta_{02},\zeta_1)}{B1} + \frac{a(\zeta_{01},\zeta_1)G(\zeta_{02})}{B1}\right](\zeta_2 - \zeta_{02})$$

$$KN(\zeta_j) = [-E(\zeta_{02},\zeta_j)a(\zeta_{01},\zeta_j) + E(\zeta_{01},\zeta_j)a(\zeta_{02},\zeta_1)](\zeta_2-\zeta_{02})/B1$$

$$KO(\zeta_j) = [-XF(\zeta_{02},\zeta_j)a(\zeta_{01},\zeta_j) + XF(\zeta_{01},\zeta_j)a(\zeta_{02},\zeta_1)](\zeta_2-\zeta_{02})/B1$$

$$K29 = [C7 - \{b(\zeta_{02})H(\zeta_{01},\zeta_1) + a(\zeta_{01},\zeta_1)P(\zeta_{02}) - b(\zeta_{01})H(\zeta_{02},\zeta_1) - a(\zeta_{02},\zeta_1)P(\zeta_{01})\}/B1](\zeta_2 - \zeta_{02})$$

Using the above, explicit expressions for all derivatives can be obtained in the following form:

$$\frac{dy_j}{dx} = \mathrm{Real}[\omega_j] \qquad \text{(A-9a)}$$

$$j = 3, 4 \cdots\cdots k$$

$$\frac{dz_j}{dx} = \mathrm{Imag.}[\omega_j] \qquad \text{(A-9b)}$$

$$\begin{Bmatrix} \frac{dy_1}{dx} \\ \frac{dz_1}{dx} \\ \frac{dy_2}{dx} \\ \frac{dz_2}{dx} \end{Bmatrix} = [D]^{-1}\{Q\} \qquad \text{(A-9c)}$$

The matrices D and Q are defined as follows:

$D(1,1) = \text{Real}[K11 + K12]$

$D(1,2) = \text{Imag.}[K12 - K11]$

$D(1,3) = \text{Real}[K13 + K14]$

$D(1,4) = \text{Imag.}[K14 - K13]$

$D(2,1) = \text{Real}[K11 + K12]$

$D(2,2) = \text{Imag.}[K11 - K12]$

$D(2,3) = \text{Real}[K13 + K14]$

$D(2,4) = \text{Imag.}[K13 - K14]$

$D(3,1) = \text{Real}[K21 + K22]$

$D(3,2) = \text{Imag.}[K22 - K21]$

$D(3,3) = \text{Real}[K23 + K24]$

$D(3,4) = \text{Imag.}[K24 - K23]$

$D(4,1) = \text{Real}[K21 + K22]$

$D(4,2) = \text{Imag.}[K21 - K22]$

$D(4,3) = \text{Real}[K23 + K24]$

$D(4,4) = \text{Imag.}[K23 - K24]$

$Q(1) = \text{Real}(L_1)$

$Q(2) = \text{Imag}(L_1)$

$Q(3) = \text{Real}(L_2)$

$Q(4) = \text{Imag}(L_2)$

APPENDIX B

COMPUTER PROGRAM FOR A BODY OF REVOLUTION AT ANGLE OF ATTACK UP TO 50 DEGREES

The program listing and a sample run are included in this section. The program was developed on the CDC 6400. Running time is on the order of a minute. The sample run is for a sharp nose tangent ogive body of revolution at an angle of attack of 45 degrees.

The program is written to describe an ogive body of revolution with a sharp or blunt nose. If a sharp nose is to be specified, variables listed by the caption "nose tip dimensions" can be neglected. Allowable geometries for the blunted nose tip are restricted to ogive shapes of which a circle is a special case.

To use the program the following input is required.

	Card	Variables	Format
	1	N	I5
These cards must be repeated for each case	2	A	F10.0
	3	XL, r_{max}, ZM2, TL, OLAP, XL1, R_N, ZM1	7F10.0
	4	XTR, AKT, AKL, λ_I, XST, S, $\Delta r_p/D$	7F10.0
	5	M, NE, NGB, G, Y(N+2)	3I5, 2F10.0
	6	$\Delta r_s/D$, GS, r_n/D, $\Delta\lambda_n$, NNE	4F10.0, I5

where:

N - number of cases to be run

A - angle of attack (degrees)

XL, r_{max}, ZM2 — ogive dimensions

TL — total missile length

OLAP, XL1, R_N, ZM1 — nose tip dimensions

these parameters are defined in the accompanying figure

XTR	fractional distance from missile nose to the point where transition from one separation angle to another takes place
AKT	final separation angle (radians)
AKL	initial separation angle (radians)
λ_I	initial vortex strength. If not specified, the value of .04 is assumed.
XST	nearest point to missile nose that integration is allowed to start. If not specified, the value of .1D is assumed.
S	Strouhal number
Δr_p	initial radial perturbation
M	number of integration steps between printing
NE	error bound. Step size is adjusted to keep estimated error between 10^{-NE} and $10^{-(NE+3)}$.
NGB	NGB-1 is the number of consecutive steps to be printed at the start or restart of integration.
G	initial step size
Y(N+2)	applies when M=0. It is the approximate distance in x between printing.
Δr_s	first vortex is shed when the radial location of the first two vortices, multiplied by r_{max}, differs by more than this amount.
r_n	this parameter, multiplied by r, represents the distance between the flow separation point, ζo_j, and a newly introduced vortex. This distance is taken along the feeding sheet of the shed vortex.
$\Delta\lambda$	percent decrease in the circulation of a shed vortex
NNE	error bound in effect after first vortex is shed

Values for the parameters listed on this page which are used in the current study are found in the right-hand column of Table 1.

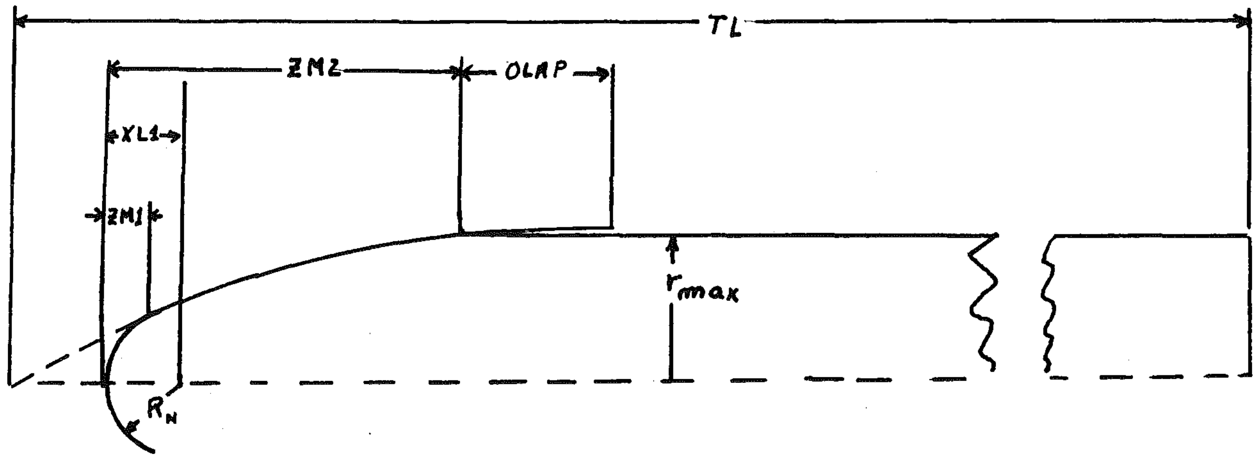

The symbols on the output page have the following meanings.

x	distance along body axis
R	local body radius
THETA0	θ_{0_1}, θ_{0_2}

VORTEX NUMBER - identification number for vortex

LAM	circulation strength, λ	
RADIUS / ANGLE	polar coordinates of vortex see accompanying figure	
Y / Z	cartesian coordinates of vortex see accompanying figure	
CL	linear portion of normal force	C_N = CL+CN
CN	nonlinear portion of normal force	
CML	linear portion of pitching moment	C_M = CML+CMN
CMN	nonlinear portion of pitching moment	

CD local normal force coefficient, $\frac{C_{DC}}{dx}$

CY yaw force coefficient, C_Y

CYM yawing moment coefficient, C_M'

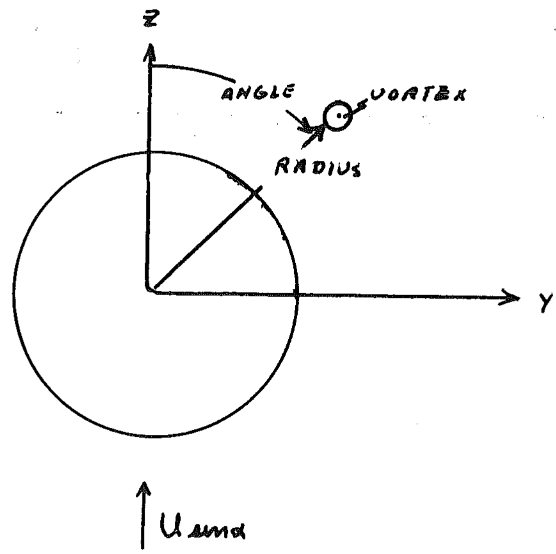

```
      PROGRAM VORT(INPUT,OUTPUT,TAPE5=INPUT,TAPE6=OUTPUT)
C.....MAIN PROGRAM
      COMPLEX XC
      DIMENSION Y(35),D(35),XL(15),XC(15),ERROR(31)
      COMMON/GAMM/WRAD,ZM,FLEN,CR,TL,TSL,WRAD2,ZM2,FLEN2,CR2,OLAP
      COMMON/BG/N,DRT,PRAD,PRTU,TOP,XLP,PERR,STR,SHED,XAKT,XAKL,XXTR
      COMMON/GARB/XL,R,DR,XC,TAL,FVORT
      COMMON/STA/A,NGB
      COMMON/VEL/U,IE
      COMMON/XLIF/MC,M,CDMN,CDML,XS,CYM,CDCL,CDCN,CY
      COMMON/TRAN/XTR,X,AKT,AKL,ISD
      EXTERNAL DERIV,OUT,TERM2,TERM3
      CONVR=57.2957795
      READ(5,1005)NDS
      DO 21 KT=1,NDS
      READ (5,1000)A
      WRITE(6,2000)A
      ZM2=0.0
      READ(5,1000)FLEN,WRAD,ZM,TL,OLAP,FLEN2,WRAD2,ZM2
      A=A/CONVR
      TAL=TAN(A)
      ISEC=0
      IF(FLEN2.GT.0.0)ISEC=1
      WRITE(6,2001)WRAD,FLEN,ZM,TL
      CR2=(WRAD2*WRAD2+FLEN2*FLEN2)/2./WRAD2
      IF(ISEC.EQ.1)WRITE(6,2016)WRAD2,ZM2,FLEN2
      CR=(WRAD*WRAD+FLEN*FLEN)/2./WRAD
      READ(5,1000)XTR,AKT,AKL,XLP,XST,STR,PERR
      XXTR=XTR
      XAKT=AKT
      XAKL=AKL
      ISD=0.0
      IF(AKT.EQ.0.0)AKT=.9251
      IF(AKL.EQ.0.0)AKL=13.12
      IF(AKL.LT.1.6) ISD=1
      IF(XLP.LE.0.0)XLP=.04
      IF(XST.LE.0)XST=.2*WRAD
      J=2
      IE=1
      E1=.000001
      E2=E1
      DT=.04
C.....DEFINING COMMON QUANTITIES
      ICOUNT=0
      SHED=0.0
      IF(STR.NE.0)SHED=WRAD/STR/TAL
      U=1.
      N=5
      FVORT=0.0
      TOP=0.0
      DO 10 K=1,15
   10 XL(K)=0.0
C.....DETERMINE INITIAL INTEGRATION PARAMETERS
      CALL START(A,DD1,DT,E1,E2,XLP,XST)
C.....SET UP INTEGRATION
```

```
      CALL PROFILE(R,DR,X,DD1,1)                                        VORT  57
      Y(1)=E1*R*COS(E2)                                                 VORT  58
      Y(2)=E1*R*SIN(E2)                                                 VORT  59
      Y(3)=-Y(1)                                                        VORT  60
      Y(4)=Y(2)                                                         VORT  61
      Y(1)=Y(1)*(1.+PERR)                                               VORT  62
      Y(2)=Y(2)*(1.+PERR)                                               VORT  63
      Y(3)=Y(3)*(1.-PERR)                                               VORT  64
      Y(4)=Y(4)*(1.-PERR)                                               VORT  65
      Y(5)=THETI(DD1)                                                   VORT  66
      XS=X                                                              VORT  67
      Y(N+1)=X                                                          VORT  68
      Y(N+3)=-1.                                                        VORT  69
      READ(5,1005)M,NE,NGB,G,Y(N+2)                                     VORT  70
      MC=M                                                              VORT  71
      M=1                                                               VORT  72
      CALL REST(X,Y,J,G,L,NE,D,0,MC)                                    VORT  73
      CYM=0.0                                                           VORT  74
      CY =0                                                             VORT  75
      CDCN=SIN(A)*COS(A)*8.*R*Y(1)*XLP*(1.-R*R/(Y(1)*Y(1)+Y(2)*Y(2)))   VORT  76
     1/WRAD/WRAD                                                        VORT  77
      CDMN=CDCN*X/2./WRAD                                               VORT  78
      CDCL=2.*SIN(A)*COS(A)*R*R/WRAD/WRAD                               VORT  79
      X0=CR*CR-FLEN*FLEN                                                VORT  80
      X2=(X0+2.*FLEN*X-X*X)**.5                                         VORT  81
      X0=X0**.5                                                         VORT  82
      CDML=2.*SIN(A)*COS(A)*((WRAD-CR)*((X+FLEN)*X2/2.-FLEN/2.*X0-CR*CR/ VORT  83
     12.*(ASIN((X-FLEN)/CR)-ASIN(-FLEN/CR)))+X*X*(FLEN/2.-X/3.))/WRAD/WR VORT  84
     2AD/WRAD                                                           VORT  85
      TOP=0.0                                                           VORT  86
      FVORT=0.0                                                         VORT  87
   18 CONTINUE                                                          VORT  88
      CALL FNOL3(J,N,G,L,1,NE,X,Y,D,DERIV,TERM2,OUT,ERROR)              VORT  89
      M=1                                                               VORT  90
      CALL OUT(X,Y,D,ERROR,N,L,G)                                       VORT  91
      IF(X+.001.GE.TL)GO TO 20                                          VORT  92
C..... INTRODUCING FIRST NEW VORTEX                                      VORT  93
      N=7                                                               VORT  94
      IC=3                                                              VORT  95
      IF(Y(1)**2+Y(2)**2.GT.Y(3)**2+Y(4)**2)GO TO 25                    VORT  96
      WRITE(6,2003)                                                     VORT  97
      STOP                                                              VORT  98
   25 CONTINUE                                                          VORT  99
      Y(10)=Y(8)                                                        VORT 100
      Y(9)=Y(7)                                                         VORT 101
      Y(8)=Y(6)                                                         VORT 102
      Y(7)=Y(5)                                                         VORT 103
      Y(6)=Y(2)                                                         VORT 104
      Y(5)=Y(1)                                                         VORT 105
      XL(3)=XL(1)*(1.+PRTU)                                             VORT 106
   40 CALL REST(X,Y,J,G,L,NE,D,2,MC)                                    VORT 107
      TSL=X+SHED                                                        VORT 108
      M=1                                                               VORT 109
      CALL FNOL3(J,N,G,L,1,NE,X,Y,D,DERIV,TERM3,OUT,ERROR)              VORT 110
      M=1                                                               VORT 111
```

```
      CALL OUT(X,Y,D,ERROR,N,L,H)
      IF(X+.001.GE.TL)GO TO 20
C.....NEW VORTEX IS ADDED
      N=N+2
      IF(N.GT.31)GO TO 20
      Y(N+3)=Y(N+1)
      Y(N+2)=Y(N)
      Y(N+1)=Y(N-1)
      Y(N)=Y(N-2)
      IC=(N-1)/2
      IC2=IC-1
      DO 50 IN=1,IC2
      K=2*(IC-IN)
      Y(K+2)=Y(K)
      Y(K+1)=Y(K-1)
   50 XL(IC+1-IN)=XL(IC-IN)
      XL(3)=XL(3)*(1.+PRTU)
      ISTOP=1
      ICOUNT=0
      GO TO 40
   20 CNN=CDCL+CDCN
      CMM=CDMN+CDML
      CSP=CMM/CNN
      CYP=0.0
      IF(DRT.NE.0.0)CYP=CYM/CY
      WRITE(6,2004)
      WRITE(6,2005)CNN
      WRITE(6,2006)CMM
      WRITE(6,2007)CSP
      WRITE(6,2008)CY
      WRITE(6,2009)CYM
      WRITE(6,2010)CYP
   21 CONTINUE
      STOP
 1000 FORMAT(8F10.0)
 1001 FORMAT(6F10.0,I5)
 1005 FORMAT(3I5,2F10.0)
 2000 FORMAT(1H1,40X,16HANGLE OF ATTACK ,F5.2,2X,7HDEGREES)
 2001 FORMAT (1H0,46X,16HOGIVE DIMENSIONS/1H ,6X,14HMAXIMUM RADIUS,6X,
     113H OGIVE LENGTH,18X,16HZ MATCHING POINT,5X,11HBODY LENGTH/1H ,
     26X,F10.5,14X,F6.3,22X,F10.5,13X,F10.5)
 2003 FORMAT(27H0VORTEX IDENTITIES REVERSED)
 2004 FORMAT(1H0,40X,26H*****FINAL STATISTICS*****)
 2005 FORMAT(1H ,37X,32HNORMAL FORCE COEFFICIENT=CL+CN= ,F10.5)
 2006 FORMAT(1H ,35X,37HPITCHING MOMENT COEFFICIENT=CML+CMN= ,F10.5)
 2007 FORMAT(1H ,41X,23HCENTER OF NORMAL FORCE=,F10.5)
 2008 FORMAT(1H ,42X,22HYAW FORCE COEFFICIENT=,F10.5)
 2009 FORMAT(1H ,41X,23HYAW MOMENT COEFFICIENT=,F10.5)
 2010 FORMAT(1H ,43X,20HCENTER OF YAW FORCE=,F15.5)
 2016 FORMAT(1H0,46X,15HNOSE DIMENSIONS/1H ,28X,6HRADIUS,5X,  14HMATCHIN
     1G POINT,5X,6HLENGTH/1H ,35X,3(F12.7,3X))
      END
```

```
      SUBROUTINE REST(X,Y,J,G,L,NE,D,IT,M)
      COMMON/GARB/XL,R,DR,XC,TAL,FVORT
      COMMON/BG/N,DRT,PRAD,PRTU,TOP,XLP,PERR,S,SHED,AKT,AKL,XTR
      COMMON/GAMM/WRAD
      DIMENSION Y(1),D(1),XL(15),XLR(15),XC(15)
      COMPLEX XC
      COMMON/STA/A
      CONVR=57.2957795
      IC=(N-1)/2
      IF(IT.EQ.0)GO TO 10
      NE=NNE
      G=XG
      ANG=Y(N)
      IF((IC/2)*2.EQ.IC)ANG=3.1415926536-ANG
      P1=COS(ANG)*R
      P2=SIN(ANG)*R
      PAN=ABS((Y(6)-P2)/(Y(5)-P1))
      PAN=ATAN(PAN)
      IF(Y(5).LT.P1)PAN=3.1415926536-PAN
      Y(1)=P1+COS(PAN)*PRAD*R
      Y(2)=P2+SIN(PAN)*PRAD*R
      RETURN
   10 CONTINUE
      READ(5,1001)DRT,XG,PRAD,PRTU,NNE
      WRITE(6,2000)XLP,PERR,DRT,PRTU,PRAD,S,SHED,AKL,AKT,XTR
      PRTU=PRTU/100.
      WRITE(6,2005)G,M,NE,Y(N+2),NNE
      DRT=DRT*2.*WRAD
      RETURN
 1001 FORMAT(4F10.0,I5)
 2000 FORMAT(1H0,40X,25H*****FREE PARAMETERS*****/1H ,40X,24HINITIAL VOR
     1TEX STRENGTH ,F10.5/1H ,38X,28HINITIAL RADIAL PERTURBATION ,F10.5/
     21H ,30X,47HRADIAL ASYMMETRY AT WHICH FIRST VORTEX IS SHED ,F10.5/
     31H ,28X,50HPER CENT DECREASE IN CIRCULATION OF SHED VORTICES ,F10.
     45/1H ,25X,46HLOCATION FACTOR FOR NEWLY INTRODUCED VORTICES ,F10.5/
     51H ,18X,16HSTROUHAL NUMBER ,F10.5,2X,32HCORRESPONDING SHEDDING DIS
     6TANCE ,F10.5/1H ,12X,27HSEPARATION ANGLE CONSTANTS ,F10.5,2X,F10.5
     7,2X,20HPOINT OF TRANSITION ,F10.5)
 2005 FORMAT(1H0,42X,19HINTEGRATION OPTIONS/1H ,18HINITIAL STEP SIZE ,F1
     10.7,5X,15HPRINT FREQUENCY, I5,5X,12HERROR BOUND ,I5,2X,16HPRINT IN
     2CREMENT ,F10.7/1H ,42X,34HERROR BOUND AFTER VORTEX SHEDDING ,I5)
      END
```

```
      FUNCTION THETI(DELTA)
      COMMON/STA/AL
      COMMON/GAMM/WRAD,ZM,FLEN,CR,TL
      COMMON/TRAN/XTR,X,AKT,AKL,ISD
      CONVR=57.2957795
      IF(X/TL.LT.XTR)GO TO 11
      THETI=AKT
      RETURN
   11 CONTINUE
      IF(ISD.EQ.0)GO TO 12
      THETI=AKL
      RETURN
   12 CONTINUE
      THETI=(AKL+CONVR*DELTA)*(3.13-(.116*AL*CONVR-1.16)**.5)
      THETI=THETI/CONVR
      RETURN
   10 THETI=3.13*(AKL+CONVR*DELTA)
      THETI=THETI/CONVR
      RETURN
      END
```

```
      SUBROUTINE PROFILE(R,DR,Z,DEL,IC)                           PROFILE    2
      COMMON/GAMM/RO2,ZM2,XL2,CR2,TL,TSL,RO1,ZM1,XL1,CR1,OLAP     PROFILE    3
      IF(IC.EQ.1)GO TO 4                                          PROFILE    4
    6 CONTINUE                                                    PROFILE    5
      RO=RO2                                                      PROFILE    6
      CR=CR2                                                      PROFILE    7
      ZM=ZM2+OLAP                                                 PROFILE    8
      IF(Z.GT.ZM1)GO TO 3                                         PROFILE    9
      RO=RO1                                                      PROFILE   10
      CR=CR1                                                      PROFILE   11
      ZM=XL1                                                      PROFILE   12
      GO TO 3                                                     PROFILE   13
    4 SF=TAN(DEL)                                                 PROFILE   14
      IF(ZM1.EQ.0.0)GO TO 5                                       PROFILE   15
      Z=XL1-CR1*SF/((SF*SF+1.)**.5)                               PROFILE   16
      IF(Z.LT.ZM1)GO TO 6                                         PROFILE   17
    5 Z=ZM2+OLAP-CR2*SF/((SF*SF+1.)**.5)                          PROFILE   18
      IF(Z.LT.ZM1)Z=ZM1+.001                                      PROFILE   19
      GO TO 6                                                     PROFILE   20
    3 IF(Z.LT.ZM2)GO TO 20                                        PROFILE   21
      DES=CR*CR-(ZM-ZM2)**2                                       PROFILE   22
      R=RO-CR+DES**.5                                             PROFILE   23
      DR=0.0                                                      PROFILE   24
      IF(IC.EQ.1)Z=ZM2                                            PROFILE   25
      RETURN                                                      PROFILE   26
   20 DES=CR*CR-(ZM-Z)**2                                         PROFILE   27
      IF(DES.GE.0.0)GO TO 30                                      PROFILE   28
      WRITE(6,200)RO,ZM,Z,DEL,XL1,CR1                             PROFILE   29
      STOP                                                        PROFILE   30
   30 DES=DES**.5                                                 PROFILE   31
      R=RO-CR+DES                                                 PROFILE   32
      DR=(ZM-Z)/DES                                               PROFILE   33
      RETURN                                                      PROFILE   34
  200 FORMAT(1H ,25HPROBABLE INPUT DATA ERROR,6E16.8)             PROFILE   35
      END                                                         PROFILE   36
```

```
      SUBROUTINE START(AL,DD1,DT,E1,E2,XLMS,XST)
      COMMON/GAMM/WRAD,ZM,FLEN,CR,TL
      COMMON/TRAN/XTR,X,AKT,AKL,ISH
C.....INTERNAL FUNCTIONS
      XR(R1)=((R1**.5-1./(R1**.5))**2.)/4.
      XL(R1,T1,T0)=8.*(XR(R1)+(SIN((T1-T0)/2.))**2)*(XR(R1)
     1+(COS((T1+T0)/2.))**2) /COS(T1)/(R1-1./R1)
      EN1(D)=(AKL/CONVR+D)*XK2-ASIN(XK1*TAN(D))
      CONVR=57.2957795
C.....DETERMINE DELTA CRITICAL
      TAL=TAN(AL)
      IF(ISH.EQ.0)GO TO 3
      D=ATAN(TAL*SIN(AKL)/1.5)
      GO TO 10
    3 CONTINUE
      XK1=1.5/TAN(AL)
      XK2=3.13
      IF(AL.GT..17453)XK2=3.13-(.116*AL*CONVR-1.16)**.5
      D1=ATAN(1./XK1)
      IF((AKL+D1*CONVR)*XK2.LT.90.)GO TO 4
      WRITE(6,2004)
 2004 FORMAT(21H0NO STARTING SOLUTION)
      STOP
    4 CONTINUE
      DD1=D1/3.
      D=D1-DD1/2.
      DP=D
      IC=0
   30 ER1=EN1(D)
      IF(ABS(ER1).LT.E1)GO TO 10
      IC=IC+1
      IF(IC.NE.1)GO TO 20
      ER2=ER1
      DP=D
      D=D-DD1
      GO TO 30
   20 DH=D
      D=D-ER1*(DP-D)/(ER2-ER1)
      IF(D.GT.D1)D=(D1+DH)/2.
      DP=DH
      ER2=ER1
      GO TO 30
   10 CONTINUE
C.....TRIAL AND ERROR CALCUATION FOR R1
      CALL PROFILE(R,DR,X,D,1)
      IF(X.LT.0.0)X=0.0
      IF(X/TL.LT.XTR)GO TO 12
      D=ATAN(TAL*SIN(AKT)/1.5)
      CALL PROFILE(R,DR,X,D,1)
   12 IF(X.GT.XST)GO TO 31
   13 X=XST
      CALL PROFILE(R,DR,X,DEL,2)
      D=ATAN(DR)
   31 DDEG=D*CONVR
      D1=D
```

```
      TO=THETI(D1)
      T1=TO+.001
      IT=0
      IP2=1
      TP=TO+1.047198
      REX=SIN(TO)-TAN(TP)*COS(TO)
      TTP=TAN(TP)
   70 FE2=FE1
      R1=REX/(SIN(T1)-TTP*COS(T1))
      FE1=ABS(XL(R1,T1,TO))-XLMS
      IF(ABS(FE1).LT.E2) GO TO 90
      IT=IT+1
      IF(IT.NE.1) GO TO 100
      T2=T1
      T1=T1+DT
      GO TO 70
  100 TH=T1
      T1=T1-FE1*(T2-T1)/(FE2-FE1)
      IF(FE1*FE2.LT.0.0)IP2=0
      IF(IP2.EQ.1)T1=TH+DT
      T2=TH
      GO TO 70
   90 E1=R1
      IF(T1.GT.1.570796327)T1=3.141592654-T1
      E2=T1
      DD1=D1
      RETURN
      END
```

```
      SUBROUTINE FNOL3(J,NN,G,L,MPR,NE,X,Y,D,DERIV,TERM,OUTPUT,ERROR)   FNOL3
C 001 J=INTEGRATION METHOD CONTROL                                      FNOL3
C 002 NN=NUMBER OF SIMULTANEOUS DIFFERENTIAL EQUATIONS                  FNOL3
C 003 G=FIRST INTERVAL OF INTEGRATION                                   FNOL3
C 004 L=NUMBER OF Y$S GREATER THAN N TO BE PRINTED                      FNOL3
C 005 MPR=PRINT FREQUENCY                                               FNOL3
C 006 NE=CONTROL FOR INTERVAL OF INTEGRATION                            FNOL3
C 007 X=INDEPENDENT VARIABLE                                            FNOL3
C 008 Y=DEPENDENT VARIABLE                                              FNOL3
C 009 D=ARRAY CONTAINING DERIVATIVES                                    FNOL3
C 010 DERIV=SUBROUTINE IN WHICH DIFFERENTIAL EQUATIONS ARE FOUND        FNOL3
C 011 TERM=SUBROUTINE FOR TERMINATION CONDITION                         FNOL3
C 012 OUTPUT=SUBROUTINE FOR PRINTING OUTPUT                             FNOL3
C     NRET=TERM LOOP COUNTER                                            FNOL3
C     NPR=COUNT OF STEPS SINCE LAST PRINT                               FNOL3
C     PC=Y(N+1)=PRINT CONTROL OTHER THAN STEP COUNT                     FNOL3
C     JJ=J-2=0 FOR AM,-1 FOR RK,+1 FOR RK2                              FNOL3
C     MK=AM RK STEP COUNT                                               FNOL3
C     XD=DP FORM OF X                                                   FNOL3
C DOUBLE PRECISION CARD HAS BEEN REMOVED IN ORDER TO RUN ON 6400        FNOL3
C THIS DECK RUNS ON THE 7090 WITH OR WITHOUT DOUBLE PRECISION           FNOL3
C     DOUBLE PRECISION XD,YD,YP,YC,YK,H,HC,XS,XDS,HS,HN,HD24,HD6        FNOL3
      DIMENSION C(3),Y(183),YD(183),YP(183),YC(183),D(203),DM(183,4)    FNOL3
      DIMENSION DK(183,4),ERROR(183),YK(183)                            FNOL3
      DATA EP6,EP11,M4/1.E-6,1.E-11,-4/                                 FNOL3
      DATA (C(K),K=1,3)/2*.5,1./                                        FNOL3
      DATA HMAX5/1.E35/                                                 FNOL3
      NHTS=0                                                            FNOL3
      N=NN                                                              FNOL3
      JJ=J-2                                                            FNOL3
      H=G                                                               FNOL3
      HN=H                                                              FNOL3
      MK=1                                                              FNOL3
      NRET=M4                                                           FNOL3
      EC=Y(N+3)                                                         FNOL3
      JTEST=1                                                           FNOL3
      IF (JJ .LT. 0) JTEST=4                                            FNOL3
      IF(NE.EQ.0)GO TO 15                                               FNOL3
      EUP=10.**(-NE)                                                    FNOL3
      ELO=EUP*.001                                                      FNOL3
      EM=ELO*31.6227766                                                 FNOL3
   15 XD=X                                                              FNOL3
      DO 20 I=1,N                                                       FNOL3
      ERROR(I)=0.                                                       FNOL3
   20 YD(I)=Y(I)                                                        FNOL3
      CALL DERIV(X,Y,D)                                                 FNOL3
      CALL TERM (X,Y,D,F)                                               FNOL3
C     PRINT                                                             FNOL3
   50 CALL OUTPUT(X,Y,D,ERROR,N,L,H)                                    FNOL3
      IF (NRET) 65,60,55                                                FNOL3
   60 RETURN                                                            FNOL3
   55 WRITE (6,3000) HN                                                 FNOL3
 3000 FORMAT(108H1EXECUTION TERMINATED BECAUSE INTERVAL OF INTEGRATION L FNOL3
     1ESS THAN 1.0E -6 TIMES INDEPENDENT VARIABLE (X).  H =,1PE15.7)    FNOL3
      STOP                                                              FNOL3
```

```
   65 IF (JTEST .EQ. 5 .AND. H .NE. HN) GO TO 455
      NPR=0
      PC=Y(N+1)
  100 IF (JTEST .EQ. 5 .AND. H .NE. HN) GO TO 455
      IF (JJ .GE. 0) H=HN
      IF (MK .NE. 0 .OR. JJ .NE. 0) GO TO 300
C------THE ADAMS MOULTON METHOD
  200 HD24=H/24.
      JAM=0
      DO 210 I=1,N
      YPI=(55.*DM(I,1)+37.*DM(I,2))-(59.*DM(I,3)+9.*DM(I,4))
      YP(I)=YD(I)+HD24*YPI
      Y(I)=YP(I)
  210 CONTINUE
      X=XD+H
      CALL DERIV(X,Y,DM(1,4))
      DO 220 I=1,N
      YPI=(9.*DM(I,4)+19.*DM(I,1)+DM(I,2))-5.*DM(I,3)
      YC(I)=YD(I)+HD24*YPI
      ERROR(I)=(YP(I)-YC(I))/14.
C THIS ADDS IN A 2D CORRECTION
      YC(I)=YC(I)+ERROR(I)
  220 CONTINUE
      IF(NE.NE.0)GO TO 700
      GO TO 455
C------THE RUNGE KUTTA METHOD
  300 GO TO (301,309,308,309,303),JTEST
  301 DO 302 I=1,N
      YK(I)=YD(I)
  302 CONTINUE
      XDS=XD
      GO TO 309
  303 DO 304 I=1,N
      YK(I)=YC(I)
  304 CONTINUE
      XDS=XD+H
  308 HS=H
      H=2.*H
      GO TO 320
  309 X=XD
      JAM=1
      DO 310 I=1,N
      Y(I)=YD(I)
      DK(I,1)=D(I)
  310 CONTINUE
      IF (JTEST .LE. 2) CALL DERIV(X,Y,DK)
      IF (MK .GT. 1 .OR. JTEST .GT. 1) GO TO 320
      DO 315 I=1,N
      DM(I,4)=DK(I,1)
  315 CONTINUE
  320 DO 335 K=2,4
      HC=H*C(K-1)
      DO 330 I=1,N
      Y(I)=YD(I) + HC*DK(I,K-1)
  330 CONTINUE
```

```
      X=XD+HC
      CALL DERIV(X,Y,DK(1,K))
  335 CONTINUE
      HD6=H/6.
      DO 340 I=1,N
      YPI=DK(I,1)+DK(I,4)+2.*(DK(I,2)+DK(I,3))
      YC(I)=YD(I)+HD6*YPI
  340 CONTINUE
      GO TO (360,390,370,455,370),JTEST
  360 DO 365 I=1,N
      YP(I)=YC(I)
  365 CONTINUE
      JTEST=3
      GO TO 308
  370 DO 380 I=1,N
      YD(I)=YP(I)
      YP(I)=YC(I)
  380 CONTINUE
      H=HS
      XD=XD+H
      JTEST=2
      IF (MK .EQ. 1) GO TO 309
      GO TO 451
  390 DO 400 I=1,N
      ERROR(I)=(YC(I)-YP(I))/15.
      YC(I)=YC(I)+ERROR(I)
      YP(I)=YC(I)
  400 CONTINUE
      JTEST=5
      IF(NE.NE.0)GO TO 700
C------ACCEPT THE STEP SIZE
  450 IF (JAM .EQ. 0) GO TO 455
      IF (MK .EQ. 3 .AND. JJ .EQ. 0) GO TO 455
      IF (MK .NE. 1) GO TO 303
      IF (JTEST .EQ. 1) GO TO 455
  451 DO 452 I=1,N
      Y(I)=YD(I)
  452 CONTINUE
      GO TO 466
  455 DO 459 NQ=1,N
      YD(NQ)=YC(NQ)
      Y(NQ)=YD(NQ)
  459 CONTINUE
      IF (JJ .GE. 0) JTEST=1
      IF (MK .NE. 0 .OR. JJ .NE. 0 .OR. NRET .NE. M4) GO TO 465
      DO 460 I=1,N
      DM(I,4)=DM(I,2)
      DM(I,2)=DM(I,3)
      DM(I,3)=DM(I,1)
  460 CONTINUE
  465 XD=XD+H
  466 X=XD
      IF (MK .EQ. 3) MK=0
      CALL DERIV(X,Y,D)
      DO 470 I=1,N
```

```
      DM(I,MK+1)=D(I)
  470 CONTINUE
      FP=F
      CALL TERM (X,Y,D,F)
C------DO YOU TERMINATE
  500 IF (ABS(F) .LE. EP6) GO TO 800
      IF (FP .EQ. 0.) GO TO 510
      IF (NRET .NE. M4 .OR. F*FP .LT. EP11) GO TO 805
  510 XS=XD
      IF (MK .NE. 0 .AND. H .EQ. HN) MK=MK+1
C------DO YOU PRINT
  600 NPR=NPR+1
      IF (MPR .GT. 0 .AND. NPR .GE. MPR) GO TO 50
      IF (MPR .LE. 0 .AND. ABS(Y(N+1)-PC) .GE. Y(N+2)) GO TO 50
      GO TO 100
C------DETERMINING THE STEP SIZE
  700 HB = HMAX5
      DO 760 I = 1,N
      Z=ABS(ERROR(I))
      IF (YC(I) .EQ. 0.) GO TO 720
      ZZ= ABS(YC(I))
      IF (EC) 720,710,705
  705 IF (EC .GT. ZZ) ZZ=EC
  710 Z=Z/ZZ
  720 IF(Z.GT.ELO.AND.Z.LT.EUP) GOTO 750
      HB = AMIN1(HB,EM/(Z+EP11))
      GOTO760
  750 HB=AMIN1(HB,1.)
  760 CONTINUE
      IF(HB.EQ.1.) GOTO 450
      HN=H*HB**.2
      IF (MK .NE. 1) JTEST=1
      MK=1
      IF (HB.LT.1.) GOTO 770
      IF (ABS(HN) .GT. ABS(4.*H)) HN=4.*H
      NHTS=0
      GOTO 450
  770 HEPS=ABS(X*EP6) + EP11
      IF (ABS(HN) .LT. ABS(H/4.)) HN=H/4.
      IF (ABS(HN) .GT. HEPS) GO TO 790
      NHTS = NHTS + 1
      IF (NHTS.LT.10) GOTO 780
      JTEST=1
      NRET = 1
      GOTO 50
  780 HN=SIGN(HEPS,HN)
  790 IF (JAM .EQ. 0) GO TO 100
      DO 795 I=1,N
      YD(I)=YK(I)
  795 CONTINUE
      XD=XDS
      JTEST=1
      GO TO 100
C------THE TERMINATION LOOP
  800 NRET=0
```

```
      JTEST1=1                                                          FNOL3    222
  805 IF (NRET .NE. 0) GO TO 806                                        FNOL3    223
      H=XD-XS                                                           FNOL3    224
      GO TO 50                                                          FNOL3    225
  806 IF(F*FP.LT.0.) GOTO 810                                           FNOL3    226
      IF (F*FP2.LT.0.) GOTO 820                                         FNOL3    227
      GO TO 800                                                         FNOL3    228
  810 FP2 =FP                                                           FNOL3    229
      HP =H                                                             FNOL3    230
      GOTO 830                                                          FNOL3    231
  820 FP =FP2                                                           FNOL3    232
      HP =H + HP                                                        FNOL3    233
  830 NRET=NRET+1                                                       FNOL3    234
      H=HP*F/(FP-F)                                                     FNOL3    235
      JTEST=4                                                           FNOL3    236
      GOTO 300                                                          FNOL3    237
       END                                                              FNOL3    238
```

```
      SUBROUTINE TERM2(X,Y,D,F)
      DIMENSIONY(1),D(1)
      COMMON/GAMM/WRAD,ZM,FLEN,CR,TL
      COMMON/BG/N,DRT,PRAD,PRTU,TOP
      F=TL-X
      IF(DRT.EQ.0.0)RETURN
      R1=(Y(1)**2+Y(2)**2)**.5
      R2=(Y(3)**2+Y(4)**2)**.5
   15 IF(ABS(R1-R2).GT.DRT)F=0.0
      RETURN
      END
```

```
      SUBROUTINE TERM3(X,Y,D,F)
      COMMON/BG/N,DRT,PRAD,PRTU,TOP
      COMMON/GAMM/WRAD,ZM,FLEN,CR,TL,TSL
      DIMENSION Y(1),D(1)
      DELT=0.0
      CALL PROFILE(R,DR,X,DELT,2)
      R2=R*R
      IF(Y(1)**2+Y(2)**2.GT.R2.AND.Y(3)**2+Y(4)**2.GT.R2)GO TO 2
      TL=X
      WRITE(6,2000)
    2 XFIN=TSL
      IF(TL.LT.XFIN)XFIN=TL
      F=XFIN-X
      RETURN
 2000 FORMAT(51H0EXECUTION TERMINATED DUE TO NUMERICAL INSTABILITY.)
      END
```

```
      SUBROUTINE DERIV(X,Y,D)
      COMPLEXA,B,T,E,XF,G,XZ,XF1,XF2,XF3,DZOP,XJ,XJC,C1,C2,C3,C4,C5,
     1C6,K11,K12,K13,K14,K21,K22,K23,K24,K15,K16,K25,K26,DTH,DZO,TH2,
     2KN1,KN2,WN,XK,XKK,XWN,CIR,XC,L1,L2,X1,X2,XO,XOP,P,H,C7,K19,K29,XNP
      INTEGER ZO,ZOP,Z1,Z2,ZJ
      COMMON/GARB/XLR,R,DR,XC,TAL,FVORT
      COMMON/BG/N,DRT,PRAD,PRTU,TOP
      COMMON/VEL/U,IE
      DIMENSION Y(1),D(1),WN(15),DD(4,4),Q(4,1),XL(15),XC(15),XZ(2),
     1A(2,2),B(2),T(2,15),E(2,15),XF(2,15),G(2),P(2),H(2,2),XNP(15),
     3XLR(15)
      CALL PROFILE(R,DR,X,DELTA, 2)
      XK=CMPLX(0.0,1.0)
      XKK=XK*R
      IC=(N-1)/2
      DO 22 KQ=1,IC
   22 XL(KQ)=XLR(KQ)/R
C...OBTAIN THE STAGNATION POINTS
      THETA=Y(N)*(1.-TOP)
      S1=R*COS(THETA)
      S2=R*SIN(THETA)
      XZ(1)= CMPLX(S1,S2)
      S1=-S1
      XZ(2)=CMPLX(S1,S2)
      IF(IC.EQ.2.OR.IC.NE.2*(IC/2))GO TO 6
      DTH=XZ(1)
      XZ(1)=XZ(2)
      XZ(2)=DTH
    6 CONTINUE
C.....TRANSFORMS VORTEX POSITIONS TO COMPLEX COORDINATES
      DO 5 I=1,IC
    5 XC(I)=CMPLX(Y(2*I-1),Y(2*I))
C.....CALCULATE FUNCTIONAL VALUES
      DO 4 L=1,2
      X1=XZ(L)
      B(L)=(R*R/X1/X1+1.)/R+FVORT/X1
      G(L)=-2.*R/X1/X1/X1-FVORT/X1/X1
      P(L)=DR*(1./X1/X1-1./R/R)
      DO 4 K=1,IC
      XJ=XC(K)
      XJC=CONJG(XJ)
      XF1=1./(X1-XJ)-1./(X1-R*R/XJC)
      XF2=1./(X1-R*R/XJC)**2-1./(X1-XJ)**2
      XF3=-DR*2.*R/((X1-R*R/XJC)**2)/XJC
      XF(L,K)=(R/(X1-R*R/XJC)/XJC)**2
      E(L,K)=1./(X1-XJ)**2
      IF(K.GT.2)GO TO 3
      A(L,K)=XF1
      T(L,K)=XF2
      H(L,K)=XF3
      GO TO 4
    3 B(L)=B(L)+XL(K)*XF1
      G(L)=G(L)+XL(K)*XF2
      P(L)=P(L)+XL(K)*XF3
    4 CONTINUE
```

```
C.....CALCULATE THE TWO UNKNOWN CIRCULATIONS
      Z0=1
      Z0P=2
      Z1=1
      Z2=2
      A1=REAL(-B(Z0)*A(Z0P,Z2)+B(Z0P)*A(Z0,Z2))
      B1=REAL(-B(Z0P)*A(Z0,Z1)+B(Z0)*A(Z0P,Z1))
      C=REAL( A(Z0,Z1)*A(Z0P,Z2)-A(Z0,Z2)*A(Z0P,Z1))
      XL(1)=A1/C
      XL(2)=B1/C
      XLR(1)=XL(1)*R
      XLR(2)=XL(2)*R
      IF(U.LT.0)RETURN
C.....CALCULATE THE FLUID VELOCITY AT EACH VORTEX LOCATION
      DO 20 K=1,IC
      X1=XC(K)
      XWN=R*DR/X1/TAL-XK*(1.+R*R/X1/X1)-XK*FVORT/X1
      DO  10 L=1,IC
      XJ=XC(L)
      IF(L.NE.K)GO TO 8
      XNP(L)=XKK*XL(L)/(X1-R*R/CONJG(XJ))
      GO TO 10
    8 XNP(L)=-XKK*XL(L)*(1./(X1-XJ)-1./(X1-R*R/CONJG(XJ)))
   10 CONTINUE
      WN(K)=XWN+XNP(K)
      DO 15 MBS=1,IC
      IF(MBS.EQ.K)GO TO 15
      WN(K)=WN(K)+XNP(MBS)
   15 CONTINUE
   20 WN(K)=CONJG(WN(K))
C.....DETERMINE THE DERIVATIVE OF THETA
      DELTA=ATAN(DR)
      THETAI=THETI(DELTA)
      D(N)=(.7*TAL/R)*(THETAI-Y(N))
C.....CALCULATE DERIVATIVES FOR ALL FREE VORTICES
      IF(IC.LT.3)GO TO 40
      DO 30 IL=3,IC
      RWN=REAL(WN(IL))
      XIWN=AIMAG(WN(IL))
      D(2*IL)=XIWN*TAL
   30 D(2*IL-1)=RWN*TAL
   40 CONTINUE
C.....CALCULATE DD MATRIX FOR ATTACHED VORTICES
      X2=XC(2)
      X1=XC(1)
      X0=XZ(1)
      X0P=XZ(2)
      C1=-(A(Z0P,Z2)*E(Z0,Z1)-A(Z0,Z2)*E(Z0P,Z1))/C
      C2=-(A(Z0P,Z2)*XF(Z0,Z1)-A(Z0,Z2)*XF(Z0P,Z1))/C
      C3=-(A(Z0,Z1)*E(Z0P,Z2)-A(Z0P,Z1)*E(Z0,Z2))/C
      C4=-(A(Z0,Z1)*XF(Z0P,Z2)-A(Z0P,Z1)*XF(Z0,Z2))/C
      K11=C1*(X1-X0)+1.
      K12=C2*(X1-X0)
      K13=(C3-(B(Z0)*E(Z0P,Z2)-B(Z0P)*E(Z0,Z2))/A1)*(X1-X0)
      K14=(C4-(B(Z0)*XF(Z0P,Z2)-B(Z0P)*XF(Z0,Z2))/A1)*(X1-X0)
```

```
      K21=(C1-(B(Z0P)*E(Z0,Z1)-B(Z0)*E(Z0P,Z1))/B1)*(X2-X0P)
      K22=(C2-(B(Z0P)*XF(Z0,Z1)-B(Z0)*XF(Z0P,Z1))/B1)*(X2-X0P)
      K23=C3*(X2-X0P)+1.
      K24=C4*(X2-X0P)
      DD(1,1)=REAL(K11+K12)
      DD(1,2)=AIMAG(K12-K11)
      DD(1,3)=REAL(K13+K14)
      DD(1,4)=AIMAG(K14-K13)
      DD(2,1)=AIMAG(K11+K12)
      DD(2,2)=REAL(K11-K12)
      DD(2,3)=AIMAG(K13+K14)
      DD(2,4)=REAL(K13-K14)
      DD(3,1)=REAL(K21+K22)
      DD(3,2)=AIMAG(K22-K21)
      DD(3,3)=REAL(K23+K24)
      DD(3,4)=AIMAG(K24-K23)
      DD(4,1)=AIMAG(K21+K22)
      DD(4,2)=REAL(K21-K22)
      DD(4,3)=AIMAG(K23+K24)
      DD(4,4)=REAL(K23-K24)
C.....CALCULATE THE Q VECTORS
      C5=(-A(Z0P,Z2)*T(Z0,Z1)+A(Z0P,Z1)*T(Z0,Z2))/C
      C6=( A(Z0,Z1)*T(Z0P,Z2)-A(Z0,Z2)*T(Z0P,Z1))/C
      C7=(A(Z0P,Z1)*H(Z0,Z2)+A(Z0,Z2)*H(Z0P,Z1)-A(Z0P,Z2)*H(Z0,Z1)
     1-A(Z0,Z1)*H(Z0P,Z2))/C
      K15= (C5-(A(Z0P,Z2)*G(Z0)-B(Z0P)*T(Z0,Z2))/A1)*(X1-X0)
      K16=(C6+( T(Z0P,Z2)*B(Z0)-A(Z0,Z2)*G(Z0P))/A1)*(X1-X0)
      K19=(C7+(A(Z0,Z2)*P(Z0P)+B(Z0P)*H(Z0,Z2)-A(Z0P,Z2)*P(Z0)-B(Z0)*
     1H(Z0P,Z2))/A1)*(X1-X0)
      K25= (C5+( A(Z0P,Z1)*G(Z0)-T(Z0,Z1)*B(Z0P))/B1)*(X2-X0P)
      K26=(C6+( A(Z0,Z1)*G(Z0P)-B(Z0)*T(Z0P,Z1))/B1)*(X2-X0P)
      K29=(C7+(A(Z0P,Z1)*P(Z0)+B(Z0)*H(Z0P,Z1)-A(Z0,Z1)*P(Z0P)-B(Z0P)*
     1H(Z0,Z1))/B1)*(X2-X0P)
      DT2=D(N)*R*(1.-T0P)
      DTH=CMPLX(DR,DT2)
      TH2=CMPLX(0.0,THETA)
      DZ0=CEXP(TH2)*DTH
      DTH=CMPLX(-DR,DT2)
      DZ0P=-CEXP(-TH2)*DTH
      IF(IC.EQ.2.OR.IC.NE.2*(IC/2))GO TO 55
      TH2=DZ0
      DZ0=DZ0P
      DZ0P=TH2
   55 CONTINUE
      L1=-K15*DZ0-K16*DZ0P+TAL*WN(1)-DR*(X1-X0)/R-K19
      L2=-K25*DZ0-K26*DZ0P+TAL*WN(2)-DR*(X2-X0P)/R-K29
      IF(IC.LT.3)GO TO 50
      DO 60 M=3,IC
      DTH=CMPLX(D(2*M-1),D(2*M))
      TH2=CONJG(DTH)
      ZJ=M
      CIR=XL(M)
      KN1=(X1-X0)*(-A(Z0P,Z2)*E(Z0,ZJ)+A(Z0,Z2)*E(Z0P,ZJ))/A1*CIR
      KN2=(X1-X0)*(-A(Z0P,Z2)*XF(Z0,ZJ)+A(Z0,Z2)*XF(Z0P,ZJ))/A1*CIR
      L1=L1-KN1*DTH-KN2*TH2
```

```
      KN1=(-E(ZOP,ZJ)*A(ZO,Z1)+A(ZOP,Z1)*E(ZO,ZJ))*(X2-XOP)*CIR/B1
      KN2=(-XF(ZOP,ZJ)*A(ZO ,Z1)+XF(ZO,ZJ)*A(ZOP,Z1))*(X2-XOP)*CIR/B1
   60 L2=L2-DTH*KN1-TH2*KN2
   50 Q(1,1)=REAL(L1)
      Q(2,1)=AIMAG(L1)
      Q(3,1)=REAL(L2)
      Q(4,1)=AIMAG(L2)
      II=4
      IX=1
      CALL MATRIX(DD,II,II,Q,IX,DETERM,ID)
      D(1)=Q(1,1)
      D(2)=Q(2,1)
      D(3)=Q(3,1)
      D(4)=Q(4,1)
      RETURN
      END
```

```
      SUBROUTINE OUT(X,Y,D,ERROR,N,L,H)
      COMPLEX XC,F1
      DIMENSION XC(15),XL(15),D(1),ERROR(1),Y(1),XLR(15)
      COMMON/STA/A,NGB
      COMMON/XLIF/MC,M,CDMN,CDML,XS,CYM,CDCL1,CDCN1,CY1
      COMMON/GARB/XLR,R,DR,XC,TAL
      COMMON/VEL/U,IE
      COMMON/GAMM/RO,ZM,FLEN,CR,TL
      COMMON/BG/IBLANK,DRT
      CONVR=57.2957795
      IF(DRT.NE.0.0 )GO TO 8
      Y(1)=(Y(1)-Y(3))/2.
      Y(3)=-Y(1)
      Y(2)=(Y(2)+Y(4))/2.
      Y(4)=Y(2)
    8 CONTINUE
      U=-U
      CALL DERIV(X,Y,D)
      U=-U
C.....CALCULATE THE FORCE COEFFICIENTS
      CDCL=2.*SIN(A)*COS(A)*R*R/RO/RO
      F1=CMPLX(0.0,0.0)
      IC=(N-1)/2
      DO 22 KQ=1,IC
   22 XL(KQ)=XLR(KQ)/R
      DO 10 I=1,IC
   10 F1=XL(I)*(XC(I)-R*R/CONJG(XC(I)))+F1
      F1=4.*SIN(A)*COS(A)*F1*R/RO/RO
      CDCN=REAL(F1)
      CY=AIMAG(F1)
      CD=0.0
      IF(X.NE.XS)CD=(CDCN-CDCN1)/(X-XS)
      CD=CD*3.1416*R/2./SIN(A)/SIN(A)
C.....CALCULATE MOMENT COEFFICIENTS
      CDML=(X+XS)*(CDCL-CDCL1)/4./RO   +CDML
      CDMN=(XS+X)*(CDCN-CDCN1)/4./RO  +CDMN
      CYM=(X+XS)*(CY-CY1)/4./RO  +CYM
C.....REINITIALIZE FORCE COEFFICIENTS
      CDCL1=CDCL
      CDCN1=CDCN
      CY1=CY
      IF(X.EQ.XS)CIT=0
      XS=X
      M=M-1
      IF(X.EQ.TL)GO TO 16
      CIT=CIT+1
      IF(CIT.LT.NGB)GO TO 16
      IF(MC.EQ.0)GO TO 15
      IF(M.EQ.0)GO TO 16
      RETURN
   15 IF(M.EQ.0)GO TO 17
      IF(X-Y(N+1).LT.Y(N+2))RETURN
      Y(N+1)=X
      GO TO 17
   16 M=MC
```

```
   17 DDEG=CONVR*Y(N)                                                        OUT       57
      HPP=0.0                                                                OUT       58
      IF(ABS(H).LT.1.)HPP=H                                                  OUT       59
      WRITE(6,2000)X,R,DDEG,HPP                                              OUT       60
      WRITE(6,2004)                                                          OUT       61
      DO 20 KT=1,IC                                                          OUT       62
      K=1+IC-KT                                                              OUT       63
      IF(IC.EQ.2)K=KT                                                        OUT       64
      XR2=(Y(2*K-1)**2+Y(2*K)**2)**.5                                        OUT       65
      ANG2=CONVR*ATAN(Y(2*K-1)/Y(2*K))                                       OUT       66
      IF(Y(2*K).LT.0.0)ANG2=Y(2*K-1)/ABS(Y(2*K-1))*(ABS(ANG2)+90.0)          OUT       67
   20 WRITE(6,2001)KT,XL(K),XR2,ANG2,Y(2*K-1),Y(2*K)                         OUT       68
      WRITE(6,2002)CDCL,CDML,CDCN,CDMN,CD,CY,CYM                             OUT       69
      IF(IE.EQ.0)RETURN                                                      OUT       70
      WRITE(6,2003)(ERROR(II),II=1,N)                                        OUT       71
      RETURN                                                                 OUT       72
 2000 FORMAT(5H0X = ,F12.7,4X,4HR = ,F12.7,4X,9HTHETA0 = ,F10.5,4X,12HST    OUT       73
     1EP SIZE = ,E14.8)                                                      OUT       74
 2001 FORMAT(1H ,20X,I3,6X,5(F14.7,3X))                                     OUT       75
 2002 FORMAT(1H ,6X,2HCL,12X,4H CML,11X,2HCN,12X,3HCMN,11X,2HCD,12X,2HCY    OUT       76
     1,12X,3HCYM,/7F14.7)                                                    OUT       77
 2003 FORMAT( 8H ERRORS ,8E14.6)                                             OUT       78
 2004 FORMAT(1H ,15X,14HVORTEX NUMBER ,7X,3HLAM,13X,6HRADIUS,11X,5HANGLE    OUT       79
     1,13X,1HY,16X,1HZ)                                                      OUT       80
      END                                                                    OUT       81
```

```
      SUBROUTINE MATRIX(A,N1,I1,B,M1,DETERM,ID)
C     MATRIX INVERSION WITH ACCOMPANYING SOLUTION OF LINEAR EQUATIONS
C
C      TEST FOR LOST OF DIGITS DUE TO SUBTRACTION
C
      DIMENSION A(I1,I1),B(I1,M1),INDEX(50,3)
      EQUIVALENCE (IROW,JROW), (ICOLUM,JCOLUM), (AMAX, T, SWAP)
      DATA EPS4/1.E-7/
C
      ID=1
      M=M1
      N=N1
   10 DETERM=1.0
   15 DO 20 J=1,N
   20 INDEX(J,3) = 0
   30 DO 550 I=1,N
C
C     SEARCH FOR PIVOT ELEMENT
C
   40 AMAX=0.0
   45 DO 105 J=1,N
      IF (INDEX(J,3) .EQ. 1) GO TO 105
   60 DO 100 K=1,N
      IF(INDEX(K,3)-1) 80, 100, 100
   80 IF (AMAX .GE. ABS(A(J,K))) GO TO 100
   85 IROW=J
   90 ICOLUM=K
      AMAX =  ABS(A(J,K))
  100 CONTINUE
  105 CONTINUE
      INDEX(ICOLUM,3) = INDEX(ICOLUM,3) +1
  260 INDEX(I,1)=IROW
  270 INDEX(I,2)=ICOLUM
      IF(BMAX.EQ.AMAX)ID=2
C
C     INTERCHANGE ROWS TO PUT PIVOT ELEMENT ON DIAGONAL
C
  130 IF (IROW  .EQ. ICOLUM) GO TO 310
  140 DETERM=-DETERM
  150 DO 200 L=1,N
  160 SWAP=A(IROW,L)
  170 A(IROW,L)=A(ICOLUM,L)
  200 A(ICOLUM,L)=SWAP
      IF(M) 310, 310, 210
  210 DO 250 L=1, M
  220 SWAP=B(IROW,L)
  230 B(IROW,L)=B(ICOLUM,L)
  250 B(ICOLUM,L)=SWAP
C
C     DIVIDE PIVOT ROW BY PIVOT ELEMENT
C
  310 PIVOT   =A(ICOLUM,ICOLUM)
      DETERM=DETERM*PIVOT
  330 A(ICOLUM,ICOLUM)=1.0
  340 DO 352 L=1,N
```

```
      IF (PIVOT .NE. 0. )  GO TO 350
      A(ICOLUM,L)  = 0.
      GO TO 352
  350 A(ICOLUM,L)=A(ICOLUM,L)/PIVOT
  352 CONTINUE
  355 IF(M) 380, 380, 360
  360 DO 375 L=1,M
      IF (PIVOT .NE. 0. )  GO TO 370
      B(ICOLUM,L)  = 0.
      GO TO 375
  370 B(ICOLUM,L)=B(ICOLUM,L)/PIVOT
  375 CONTINUE
C
C     REDUCE NON-PIVOT ROWS
C
      BMAX=0.0
  380 DO 550 L1=1,N
  390 IF (L1 .EQ. ICOLUM) GO TO 550
  400 T=A(L1,ICOLUM)
  420 A(L1,ICOLUM)=0.0
  430 DO 450 L=1,N
      SUB =A(ICOLUM,L)*T
      A(L1,L)=A(L1,L)-SUB
C
C
      IF(INDEX(L1,3).EQ.1) GO TO 450
      IF(ABS(A(L1,L))-EPS4* ABS(SUB))449,449,450
  449 BMAX=AMAX1(BMAX,ABS(A(L1,L)))
  450 CONTINUE
  455 IF(M) 550, 550, 460
  460 DO 500 L=1,M
  500 B(L1,L)=B(L1,L)-B(ICOLUM,L)*T
  550 CONTINUE
C
C     INTERCHANGE COLUMNS
C
  600 DO 710 I=1,N
  610 L=N+1-I
  620 IF (INDEX(L,1) .EQ. INDEX(L,2)) GO TO 710
  630 JROW=INDEX(L,1)
  640 JCOLUM=INDEX(L,2)
  650 DO 705 K=1,N
  660 SWAP=A(K,JROW)
  670 A(K,JROW)=A(K,JCOLUM)
  700 A(K,JCOLUM)=SWAP
  705 CONTINUE
  710 CONTINUE
      DO 730 K = 1,N
      IF (INDEX(K,3) .NE. 1) GO TO 715
  730 CONTINUE
      RETURN
  715 ID=2
      RETURN
       END
```

```
                                   ANGLE OF ATTACK 45.00  DEGREES

                                           OGIVE DIMENSIONS
     MAXIMUM RADIUS        OGIVE LENGTH                      Z MATCHING POINT     BODY LENGTH
         .50000                3.100                              3.10000             11.00000

                                       *****FREE PARAMETERS*****
                                   INITIAL VORTEX STRENGTH      .04000
                                 INITIAL RADIAL PERTURBATION      .00600
                         RADIAL ASYMMETRY AT WHICH FIRST VORTEX IS SHED      .10000
                       PER CENT DECREASE IN CIRCULATION OF SHED VORTICES   -2.50000
                    LOCATION FACTOR FOR NEWLY INTRODUCED VORTICES      .07500
             STROUHAL NUMBER      .16660  CORRESPONDING SHEDDING DISTANCE    3.00120
       SEPARATION ANGLE CONSTANTS      .73300     -0.00000  POINT OF TRANSITION    1.00000

                                     INTEGRATION OPTIONS
 INITIAL STEP SIZE    .0002500     PRINT FREQUENCY   -0     ERROR BOUND     6  PRINT INCREMENT  1.0000000
                                     ERROR BOUND AFTER VORTEX SHEDDING      6

 X =      .1000000    R =      .0325289    THETAO =    41.99781    STEP SIZE =  .25000000E-03
                VORTEX NUMBER         LAM              RADIUS           ANGLE              Y                  Z
                      1             .0355897          .0331857       46.6493614        .0241315           .0227807
                      2            -.0578202          .0327899      -46.6493614       -.0238437           .0225090
      CL             CML            CN             CMN            CD             CY             CYM
   .0042325       .0002809       .0000144       .0000014      0.0000000       .0000029       .0000003
 ERRORS   0.             0.             0.             0.             0.

 X =     1.1030758    R =      .2956664    THETAO =    41.99781    STEP SIZE =  .21046273E-01
                VORTEX NUMBER         LAM              RADIUS           ANGLE              Y                  Z
                      1             .2438641          .3327822       39.0463583        .2096358           .2584508
                      2            -.2082865          .3244723      -40.5432500       -.2109141           .2465715
      CL             CML            CN             CMN            CD             CY             CYM
   .3496745       .2415966       .0430999       .0372341       .1302038       .0107881       .0094284
 ERRORS    .607359E-09    .218640E-09    .236340E-08   -.652509E-09   0.

 X =     2.1196964    R =      .4511470    THETAO =    41.99781    STEP SIZE =  .35862999E-01
                VORTEX NUMBER         LAM              RADIUS           ANGLE              Y                  Z
                      1             .4714942          .6214725       30.9960132        .3200449           .5327282
                      2            -.4356448          .5754213      -32.8963095       -.3125230           .4831553
      CL             CML            CN             CMN            CD             CY             CYM
   .8141343       .9785404       .4469488       .7358462       .9504091       .1361153       .2284237
 ERRORS   -.665432E-09   -.820530E-09    .471271E-10   -.646229E-09   0.

 X =     2.8623315    R =      .4971352    THETAO =    41.99781    STEP SIZE =  .25000000E-03
                VORTEX NUMBER         LAM              RADIUS           ANGLE              Y                  Z
                      1             .6638951          .8170361       26.8023124        .3684126           .7292599
                      2            -.6455558          .7118971      -27.9646625       -.3338277           .6287738
      CL             CML            CN             CMN            CD             CY             CYM
   .9885735      1.4009501      1.0517271      2.2520225      0.0000000       .3855470       .8595407
 ERRORS   -.105708E-09    .329976E-08   -.291649E-08   -.409414E-08   0.

 X =     2.8623315    R =      .4971352    THETAO =    41.99781    STEP SIZE =  .10000000E-02
                VORTEX NUMBER         LAM              RADIUS           ANGLE              Y                  Z
                      1             .6472977          .8170361       26.8023124        .3684126           .7292599
                      2            -.6421862          .7118971      -27.9646625       -.3338277           .6287738
                      3             .0022805          .5227481       44.9565092        .3693581           .3699192
      CL             CML            CN             CMN            CD             CY             CYM
   .9885735      1.4009501      1.0344401      2.2025413      0.0000000       .3598689       .7860415
 ERRORS   0.             0.             0.             0.             0.             0.             0.
```

```
X =     3.1358214    R =     .5000000    THETAO =    41.99781    STEP SIZE =  .17107098E-01
              VORTEX NUMBER         LAM              RADIUS           ANGLE              Y                Z
                      1           .6435889          .9293537       23.6852872         .3733331          .8510703
                      2          -.7280791          .7461542      -26.2962073        -.3305552          .6689390
                      3           .0139121          .5284685       46.1529236         .3811269          .3660892
      CL           CML          CN           CMN           CD           CY           CYM
   1.0000000     1.4345633    1.2155258    2.7449078     .9638301     .4855503    1.1628711
ERRORS     .166824E-07   .117700E-07  -.490723E-08   .449925E-08   .344445E-08   .805208E-08  0.

X =     4.1446835    R =     .5000000    THETAO =    41.99781    STEP SIZE =  .35007074E-01
              VORTEX NUMBER         LAM              RADIUS           ANGLE              Y                Z
                      1           .6435889         1.4027342       17.7113434         .4267421         1.3362464
                      2         -1.0237597          .8997440      -20.3545102        -.3129559          .8435625
                      3           .1757541          .5636118       39.5839052         .3591377          .4343713
      CL           CML          CN           CMN           CD           CY           CYM
   1.0000000     1.4345633    1.8985781    5.2548438    1.3165386     .6803161    1.8155487
ERRORS     .371962E-08   .239884E-11   .809811E-10  -.652020E-09  -.393803E-09  -.422120E-09  0.

X =     5.1549628    R =     .5000000    THETAO =    41.99781    STEP SIZE =  .29757162E-01
              VORTEX NUMBER         LAM              RADIUS           ANGLE              Y                Z
                      1           .6435889         1.9788370       16.2281326         .5530109         1.8999934
                      2         -1.2720087         1.2138898      -16.4435008        -.3436154         1.1642409
                      3           .3921419          .5724520       36.5638004         .3410197          .4597900
      CL           CML          CN           CMN           CD           CY           CYM
   1.0000000     1.4345633    2.9112933    9.9895735    1.8015862    -.1686913   -2.2403960
ERRORS    -.311141E-07  -.123495E-07   .649968E-10  -.286473E-09  -.973207E-12  -.383286E-10  0.

X =     5.8635320    R =     .5000000    THETAO =    41.99781    STEP SIZE = 0.
              VORTEX NUMBER         LAM              RADIUS           ANGLE              Y                Z
                      1           .6435889         2.4158047       15.6478473         .6516006         2.3262693
                      2         -1.4302811         1.5175554      -15.0338253        -.3936376         1.4656138
                      3           .5239926          .5833192       35.0541973         .3350300          .4775104
      CL           CML          CN           CMN           CD           CY           CYM
   1.0000000     1.4345633    3.7994491   14.8912346    0.0000000   -1.4771218   -9.4785667
ERRORS    -.165932E-06  -.758859E-07   .640592E-09   .155940E-08   .114145E-08   .486370E-09  0.

X =     5.8635320    R =     .5000000    THETAO =    41.99781    STEP SIZE =  .10000000E-02
              VORTEX NUMBER         LAM              RADIUS           ANGLE              Y                Z
                      1           .6435889         2.4158047       15.6478473         .6516006         2.3262693
                      2         -1.3945240         1.5175554      -15.0338253        -.3936376         1.4656138
                      3           .5145310          .5833192       35.0541973         .3350300          .4775104
                      4          -.0028980          .5263422      -45.0209574        -.3723162          .3720440
      CL           CML          CN           CMN           CD           CY           CYM
   1.0000000     1.4345633    3.7463173   14.5796946    0.0000000   -1.2954685   -8.4134367
ERRORS    0.            0.            0.            0.            0.            0.            0.            0.
ERRORS    0.

X =     6.1615320    R =     .5000000    THETAO =    41.99781    STEP SIZE =  .16000000E-01
              VORTEX NUMBER         LAM              RADIUS           ANGLE              Y                Z
                      1           .6435889         2.6042565       15.3967217         .6914326         2.5107913
                      2         -1.3945240         1.7091872      -13.9904236        -.4132126         1.6584861
                      3           .5714561          .5970385       33.7584075         .3317697          .4963707
                      4          -.0076643          .5335495      -46.3339277        -.3859569          .3683915
      CL           CML          CN           CMN           CD           CY           CYM
   1.0000000     1.4345633    4.0499953   16.4051674    1.5663684   -1.8966131  -12.0277866
ERRORS     .353227E-08   .589238E-09  -.121830E-09  -.504559E-10   .452755E-11   .363392E-11  -.873714E-12   .946037E-12
ERRORS    0.

X =     7.1721751    R =     .5000000    THETAO =    41.99781    STEP SIZE =  .32094397E-01
              VORTEX NUMBER         LAM              RADIUS           ANGLE              Y                Z
                      1           .6435889         3.2348758       14.4416539         .8067585         3.1326605
                      2         -1.3945240         2.4021354      -11.1526320        -.4646290         2.3567720
                      3           .8646256          .7177918       25.8484516         .3129517          .6459770
                      4          -.0825237          .5600676      -41.4797306        -.3709636          .4195971
      CL           CML          CN           CMN           CD           CY           CYM
   1.0000000     1.4345633    5.0887432   23.3413337    1.7434051   -3.5828642  -23.1921245
```

```
ERRORS    .132244E-08  -.211717E-08   .292732E-09  -.290729E-10  -.248214E-10   .382313E-10  -.172845E-10   .215497E-10
ERRORS   0.

X =     8.1991958    R =      .5000000    THETAO =     41.99781    STEP SIZE =  .32094397E-01
              VORTEX NUMBER        LAM              RADIUS          ANGLE             Y               Z
                    1            .6435889         3.8595730      13.1682765        .8792562       3.7580862
                    2          -1.3945240         3.1316880      -9.5957769       -.5220401       3.0878705
                    3           1.1935511         1.0327161      18.2391696        .3232239        .9808307
                    4           -.2689768          .5561387     -38.7058756       -.3477662        .4339919
      CL             CML             CN             CMN            CD             CY             CYM
   1.0000000      1.4345633      6.3164263     32.7899077     1.9881864     -3.7775881     -24.5257429
ERRORS    .731932E-09  -.986816E-10  -.325549E-09  -.216827E-09   .257688E-10   .622232E-11   .236255E-11  -.817124E-12
ERRORS   0.

X =     8.8647325    R =      .5000000    THETAO =     41.99781    STEP SIZE = 0.
              VORTEX NUMBER        LAM              RADIUS          ANGLE             Y               Z
                    1            .6435889         4.2580371      12.1574910        .8967408       4.1625396
                    2          -1.3945240         3.6060791      -9.1234539       -.5717880       3.5604585
                    3           1.3749567         1.3339893      15.6128605        .3590245       1.2847680
                    4           -.3515362          .5549913     -38.6311965       -.3464839        .4335485
      CL             CML             CN             CMN            CD             CY             CYM
   1.0000000      1.4345633      7.1938063     40.2793319     0.0000000     -2.9521614     -17.4474940
ERRORS    .888596E-06  -.352818E-06  -.744009E-09  -.187193E-08   .596501E-11  -.720727E-10  -.225967E-10  -.219927E-10
ERRORS   0.

X =     8.8647325    R =      .5000000    THETAO =     41.99781    STEP SIZE =  .10000000E-02
              VORTEX NUMBER        LAM              RADIUS          ANGLE             Y               Z
                    1            .6435889         4.2580371      12.1574910        .8967408       4.1625396
                    2          -1.3945240         3.6060791      -9.1234539       -.5717880       3.5604585
                    3           1.3405828         1.3339893      15.6128605        .3590245       1.2847680
                    4           -.3449832          .5549913     -38.6311965       -.3464839        .4335485
                    5            .0030946          .5254779      44.9261199        .3710896        .3720478
      CL             CML             CN             CMN            CD             CY             CYM
   1.0000000      1.4345633      7.1501010     39.8918962     0.0000000     -3.1014182     -18.7706156
ERRORS   0.            0.            0.            0.            0.            0.            0.            0.
ERRORS   0.            0.            0.

X =     9.2130058    R =      .5000000    THETAO =     41.99781    STEP SIZE =  .14707534E-01
              VORTEX NUMBER        LAM              RADIUS          ANGLE             Y               Z
                    1            .6435889         4.4654066      11.5864241        .8968582       4.3744144
                    2          -1.3945240         3.8539932      -8.9834568       -.6017983       3.8067181
                    3           1.3405828         1.5724424      13.6477708        .3710216       1.5280439
                    4           -.3858415          .5614540     -37.9124832       -.3449894        .4429592
                    5            .0106460          .5376864      46.1574387        .3878041        .3724441
      CL             CML             CN             CMN            CD             CY             CYM
   1.0000000      1.4345633      7.4810645     42.8818751     1.3880138     -2.5306527     -13.6101726
ERRORS   -.165317E-08   .131929E-08   .843059E-11  -.463477E-11  -.817403E-11   .558131E-11   .408816E-12  -.119777E-12
ERRORS    .639488E-13  -.178651E-12  0.

X =    10.2611996    R =      .5000000    THETAO =     41.99781    STEP SIZE =  .63391534E-01
              VORTEX NUMBER        LAM              RADIUS          ANGLE             Y               Z
                    1            .6435889         5.0895694       9.7266230        .8598694       5.0164072
                    2          -1.3945240         4.5943797      -8.8936108       -.7102921       4.5391420
                    3           1.3405828         2.3492428       9.1053566        .3717686       2.3196400
                    4           -.6270742          .6291921     -31.5159190       -.3289010        .5363831
                    5            .0965087          .6233788      40.7982071        .4073138        .4719074
      CL             CML             CN             CMN            CD             CY             CYM
   1.0000000      1.4345633      8.3707261     51.5497577     1.4464884      -.7860946      3.3568254
ERRORS   -.141296E-07  -.659408E-08  -.998941E-08   .161486E-07  -.408549E-09   .977546E-09   .201482E-09  -.208869E-09
ERRORS    .377907E-10  -.231874E-09  0.

X =    11.0000000    R =      .5000000    THETAO =     41.99851    STEP SIZE = 0.
              VORTEX NUMBER        LAM              RADIUS          ANGLE             Y               Z
                    1            .6435889         5.5301893       8.3632984        .8043622       5.4713797
                    2          -1.3945240         5.1088224      -8.9891053       -.7982364       5.0460762
                    3           1.3405828         2.9151405       7.0659801        .3585980       2.8930005
```

4	-.8784763	.7550590	-24.7394574	-.3159866	.6857598
5	.2409266	.6908357	36.0218935	.4062766	.5587426

CL	CML	CN	CMN	CD	CY	CYM
1.0000000	1.4345633	9.1400144	59.7364535	0.0000000	.0524773	12.2374875

ERRORS	.644419E-07	.419243E-06	.855520E-07	.533789E-06	.806359E-11	.303639E-11	.688279E-12	.253901E-11
ERRORS	.160275E-11	.120698E-11	.892321E-06					

*****FINAL STATISTICS*****

NORMAL FORCE COEFFICIENT=CL+CN= 10.14001

PITCHING MOMENT COEFFICIENT=CML+CMN= 61.17102

CENTER OF NORMAL FORCE= 6.03264

YAW FORCE COEFFICIENT= .05248

YAW MOMENT COEFFICIENT= 12.23749

CENTER OF YAW FORCE= 233.19566

APPENDIX C

EXPERIMENTAL INVESTIGATION

The experiments referred to in this report were carried out in the NOL Supersonic Tunnel No. 1. This facility is an open jet, blowdown tunnel, 16 inches square, and is capable of subsonic as well as supersonic speeds.

The test model had an overall fineness of 12, a nose fineness of 4 and a diameter of 1.1 inches. It was tested at the Mach numbers of 0.5, 0.7, 0.9 and 1.1, which corresponded to a Reynolds number variation of $2(10^5)$ to $5(10^5)$ based on the body diameter. The model was swept from 0 to 70 degrees angle of attack. Four runs were made at each Mach number with the nose roll orientation being varied 90 degrees from run to run. Select runs were made using a boundary-layer trip. This consisted of a grit strip 1/8-inch wide along the leeward meridian of the body. Since the wind tunnel is an open jet type, it was possible to use a subsonic nozzle throughout the tests without encountering problems with reflected shock waves.

Force measurements were made using a four-component strain-gage balance. This type of information was augmented by schlieren photographs which were taken at increments of five degrees in angle of attack. Oil-flow studies were made at each Mach number at angles of attack of 20, 35, 50 and 70 degrees.

Results from the force tests indicate that normal force increases slightly with increasing Mach number, while the yaw force decreased strongly under these conditions. The measured forces and moments agree well with the data taken by Pick (Ref. (20)) using the same model. Pick's results, though, only go up to an angle of attack of 45 degrees. The Strouhal number measured from the schlieren photographs appears to be lower than that measured by Pick, although there is considerable scatter in the data obtained in the present study. The boundary-layer trip significantly lowered the normal force and greatly reduced the yaw force at the lower Mach numbers.

In order for force measurements to be meaningful at low crossflow Mach numbers, it is necessary to know whether the boundary layer is laminar or turbulent. It is well known that for $M_c \lesssim 0.5$, the transition of the boundary is accompanied by a large decrease in normal force. This results from an increase in the crossflow separation angle. At larger crossflow Mach numbers the transition of the boundary layer no longer has a large effect on normal force (Ref. (3)).

In the tests conducted, the crossflow Reynolds number (Re $\sin\alpha$) were of the order of 10^5. Since transition is expected near this value, it is difficult to predict the state of the boundary layer. However, measurements of the crossflow separation angle taken from the oil-flow studies indicate that the boundary layer was laminar. This conclusion is supported by the reduction of force observed when the boundary-layer trip was used.

	Copies
Commander, Naval Ordnance Systems Command Headquarters Department of the Navy Washington, D. C. 20360 Chief Technical Analyst ORD 05121 ORD 035 ORD 03A ORD 9132	2
Commander, Naval Air Systems Command Headquarters Department of the Navy Washington, D. C. 20361 AIR 03B AIR 03C AIR 320 AIR 320C Dr. H. J. Mueller AIR 310 AIR 50174	2
Office of Naval Research Department of the Navy Washington, D. C. 20360 Mr. Morton Cooper ONR 430B 430C	2
Commander Naval Ship Research and Development Center Bethesda, Maryland 20034 Central Library Branch (5641) Aerodynamics Laboratory (5643)	
Commander, Naval Weapons Center China Lake, Calif. 93555 Technical Library (Code 753) Code 406 R. E. Meeker (Code 4063)	
Director, U.S. Naval Research Laboratory Washington, D. C. 20390 Library Code 6503	
NASA Langley Research Center Langley Station Hampton, Virginia 23365 Library Aeronautical & Space Mechanics Division Dennis Bushwell Ivan Beckwith	
NASA Lewis Research Center 21000 Brookpart Road Cleveland, Ohio 44135 Library 60-3 Chief, Wind Tunnel and Flight Division	
NASA George C. Marshall Space Flight Center Huntsville, Alabama 35812 Mr. T. Reed, R-AERO-AU Mr. W. K. Dahm, R-AERO-A	
NASA 600 Independence Avenue S.W. Washington, D. C. 20546 Dr. H. H. Kurzweg, Director of Research (Code RR)	
NASA P. O. Box 33 College Park, Md. 20740	

	Copies
Technical Library Office of Assistant Director (E&PS) Room 3E-1063, The Pentagon Washington, D. C. 20301 Stop 103	
Defense Documentation Center Cameron Station Alexandria, Virginia 22314	12
Commander (5632.2) Naval Missile Center Point Mugu, Calif. 93041 Technical Library	
Commanding Officer USA Aberdeen Research and Development Center Aberdeen Proving Ground Maryland 21005 STEAP-TL (Technical Library Division) AMXRD-XSE	
Commander, U.S. Naval Weapons Laboratory Dahlgren Virginia 22448 Library Thomas Clare (Code KB)	
Director, Stragetic Systems Project Office Department of the Navy Washington, D. C. 20390 NSP-2722	2
Commander, Armament Development and Test Center Eglin AFB, Florida 32542 DLOSL, Technical Library	
Commander Space and Missile Systems Organization Air Force Unit Post Office Los Angeles Air Force Station California 90045 SMTTM/LT C. Lee	
Headquarters, Arnold Enginneering Development Center Library/Documents Arnold Air Force Station Tennessee 37389 Library/Documents - Joe Ashley, Jr. R. W. Henzel, TD CAPT C. Tirres/DYR	
von Karman Gas Dynamics Facility ARO, Inc. Arnold Air Force Station Tennessee 37389 Mr. J. D. Whitfield, Chief Mr. C. J. Schueler	
Commanding Officer, Harry Diamond Laboratories Washington, D. C. 20438 Library, Room 211 Bldg. 92	
Commanding General U.S. Army Missile Command Redstone Arsenal Alabama 35809 AMSMI-RR Chief, Document Section AMSMI-RDK, Mr. R. A. Deep AMSMI-RDK, Mr. T. R. Street	

Copies

Department of the Army
Office of the Chief of
Research and Development
ABMDA, The Pentagon
Washington, D. C. 20350

Commanding Officer
Picatinny Arsenal
Dover, New Jersey 07801
Mr. A. A. Loeb
SMUPA-VC-3 SMUPA-TS-S

Commander (ADL)
Naval Air Development Center (Code 813)
Warminster
Pennsylvania 18974

Headquarters, Edgewood
Arsenal
Edgewood Arsenal
Maryland 21010
A. Flatau

U.S. Army Ballistic Missile Defense Agency
1100 Wilson Boulevard
Arlington, Virginia 22209
RDMD-NC
Dr. Sidney Alexander

The Johns Hopkins University
(C/NOw 7386)
Applied Physics Laboratory
8621 Georgia Avenue
Silver Spring, Maryland 20910
Document Library 2
Dr. F. Hill
Dr. L. L. Cronvich

Director, Defense Nuclear
Agency
Headquarters DASA
Washington, D. C. 20305
STSP (SPAS)

Commanding Officer
Naval Intelligence Support
Center
4301 Suitland Road
Washington, D. C. .20390

Department of Aeronautics
DFAN
USAF, Academy,
Colorado 80840
COL D. H. Daley
Prof. & Head

Chief of Naval Research
Arlington, Virginia 22217
ONR 100

Air Force Weapons Laboratory
Technical Library (SUL)
Kirtland Air Force Base
Albuquerque
New Mexico 87117
DYV
SRA

AERODYNAMICS DEPARTMENT
EXTERNAL DISTRIBUTION LIST (A2)

Copies

Aerospace Engineering
Program
University of Alabama
P. O. Box 2908
University of Alabama 35486
Prof. W. K. Rey, Chm.

AME Department
University of Arizona
Tucson, Arizona 85721
Dr. L. B. Scott

Polytechnic Institute of
Brooklyn
Graduate Center Library
Route 110, Farmingdale
Long Island, New York 11735
Dr. J. Polczynski

Polytechnic Institute of
Brooklyn
Spicer Library
333 Jay Street
Brooklyn, New York 11201
Reference Department

Ohio State University Libraries
2036 Neil Avenue
Columbus, Ohio 43210
Prof. J. D. Lee
Prof. G. L. Von Eschen
Aero-Civil Library

California Institute of
Technology
Pasadena
California 91109
Graduate Aeronautical
Laboratories Aero.
Librarian
Dr. H. Liepmann, Karman
Lab-301
Prof. L. Lees, Firestone
Flight Sciences Lab.
Dr. D. Coles, 306 Karman
Lab.
Dr. A. Roshko

University of California
Berkeley
California 94720
Dr. M. Holt, Div. of
Aeronautical Sciences
Research Coordinator
College of Engineering

GASDYNAMICS
University of California
Richmond Field Station
1301 South 46th Street
Richmond, California 94804
A. K. Oppenheim

Department of Aerospace
Engineering
University of Southern
California
University Park
Los Angeles
California 90007
Dr. John Laufer

University of California -
San Diego
Department of Aerospace and
Mechanical Engineering
Sciences
LaJolla, California 92037
Dr. P. A. Libby

Copies

Case Western Reserve
University
Division of Fluid, Thermal
and Aerospace Engineering
Cleveland, Ohio 44106
Dr. Eli Reshotko, Head

The Catholic University of
America
Washington, D.C. 20017
Dr. C. C. Chang
Dr. Paul K. Chang
Mechanical Engr. Dept.
Dr. M. J. Casarella
Mechanical Engr. Dept.

University of Cincinnati
Cincinnati, Ohio 45221
Department of Aerospace
Engineering
Dr. Arnold Polak

Department of Aerospace
Engineering Sciences
University of Colorado
Boulder, Colorado 80302

Cornell University
Graduate School of Aero.
Engineering
Ithaca, New York 14850
Prof W. R. Sears
Dr. S. F. Shen
Prof. F. K. Moore, Head
Thermal Engineering
Dept., 208 Upson Hall

University of Delaware
Mechanical and Aeronautical
Engineering Dept.
Newark, Delaware 19711
Dr. James E. Danberg

Georgia Institute of
Technology
225 North Avenue, N.W.
Atlanta, Georgia 30332
Dr. Arnold L. Ducoffe
Aerospace Engineering
Dept.

Technical Reports
Collection
Gordon McKay Library
Harvard University
Div. of Eng'g. and
Applied Physics
Pierce Hall
Oxford Street
Cambridge
Massachusetts 02138

Illinois Institute of
Technology
3300 South Federal
Chicago, Illinois 60616
Dr. M. V. Morkovin
Prof. A. A. Fejer
M.A.E. Dept.

University of Illinois
101 Transportation Bldg.
Urbana, Illinois 61801
Aeronautical and
Astronautical
Engineering Dept.

Iowa State University
Ames, Iowa 50010
Aerospace Engineering
Dept.

Copies

The Johns Hopkins University
Baltimore, Maryland 21218
Prof. S. Corrsin

University of Kentucky
Wenner-Gren Aero. Lab.
Lexington, Kentucky 40506
C. F. Knapp

Department of Aero. Engineering, ME 106
Louisianna State University
Baton Rouge
Louisiana 70803
Dr. P. H. Miller

University of Maryland
College Park
Maryland 20740
Prof. A. Wiley Sherwood
Department of Aerospace Engineering
Prof. Charles A. Shreeve
Department of Mechanical Engineering
Dr. S. I. Pai, Institute for Fluid Dynamics and Applied Mathematics
Dr. Redfield W. Allen
Department of Mechanical Engineering
Dr. W. L. Melnik
Department of Aerospace Engineering
Dr. John D. Anderson, Jr.
Department of Aerospace Engineering

Michigan State University Library
East Lansing
Michigan 48823
Documents Department

Massachusetts Institute of Technology
Cambridge
Massachusetts 02139
Mr. J. R. Martuccelli
Rm. 33-211
Prof. M. Finston
Prof. J. Baron, Dept. of Aero. and Astro.
Rm. 37-461
Prof. A. H. Shapiro
Head, Mech. Engr. Dept.
Aero. Engineering Library
Prof. Ronald F. Probestein
Dr. E. E. Covert
Aerophysics Laboratory

University of Michigan
Ann Arbor, Michigan 48104
Dr. A. Kuethe, Dept. of Aero. Engineering
Dr. O. Laporte, Dept of Physics
Dr. M. Sichel, Dept. of Aero. Engineering
Engineering Library
Aerospace Engineering Library

Serials and Documents Section
General Library
University of Michigan
Ann Arbor, Michigan 48104

Rensselaer Polytechnic Institute
Troy, New York 121181
Dept. of Aeronautical Engineering and Astronautics
Dr. Robert E. Duffy
Library

Copies

U.S. Naval Academy
Annapolis, Maryland 21402
Engineering Department
Aerospace Division

Library, Code 2124
U. S. Naval Postgraduate School
Monterey, California 93940
Technical Reports Section

New York University
University Heights
New York, New York 10453
Dr. Antonio Ferri
Director of Guggenheim Aerospace Laboratories
Prof. V. Zakkay
Engineering and Science Library

North Carolina State College
Raleigh
North Carolina 27607
Dr. R. W. Truitt, Head
Mech. and Aero. Engineering
Dr. H. A. Hassan, Dept. of Mech. and Aero. Engr.

D. H. Hill Library
North Carolina State University
P.O. Box 5007
Raleigh
North Carolina 27607

University of North Carolina
Chapel Hill
North Carolina 27514
Department of Aero. Engineering
Library, Documents Section
AFROTC Det 590

Northwestern University
Technological Institute
Evanston, Illinois 60201
Department of Mechanical Engineering
Library

Notre Dame University
South Bend, Indiana 46556
Dr. J. D. Nicolaides
Dept. of Aero Engineering
College of Engineering Library

Department of Aero-Astro Engineering
Ohio State University
2036 Neil Avenue
Columbus, Ohio 43210
Engineering Library
Prof. J. D. Lee
Prof. G. L. Von Eschen

Bevier Engineering Library
126 Benedum Hall
University of Pittsburgh
Pittsburgh, Pennsylvania 15261
U. S. A.

The Pennsylvania State University
University Park
Pennsylvania 18602
Dept. of Aero Engr.
Hammond Bldg.
Library, Documents Section

COPIES

Princeton University
James Forrestal Campus
Gas Dynamics Laboratory
Princeton
New Jersey 08540
Prof. S. Bogdonoff
Dr. I. E. Vas

Purdue University
School of Aeronautical and Engineering Sciences
Lafayette, Indiana 47907
Library
Dr. P. S. Lykoudis, Dept. of Aero. Engineering

General Electric Company
AEG Technical Information Center N-32
Cincinnati
Ohio 45215
James J. Brady

Department of Mechanical Industrial and Aerospace Engineering
Rutgers - The State University
New Brunswick
New Jersey 08903
Dr. R. H. Page

Stanford University
Stanford
California 94305
Librarian, Dept. of Aeronautics and Astronautics

Stevens Institute of Technology
Hoboken, New Jersey 07030
Mechanical Engineering Department Library

The University of Texas at Austin
Applied Research Laboratories
P.O. Box 8029
Austin, Texas 78712
Director

University of Toledo
2801 W. Bancroft
Toledo, Ohio 43606
Dept. of Aero Engineering
Dept. of Mech Engineering

University of Virginia
School of Engineering and Applied Science
Charlottesville
Virginia 22901
Dr. I. D. Jacobson
Dr. G. Matthews

University of Washington
Seattle
Washington 98105
Engineering Library
Dept. of Aeronautics and Astronautics
Prof. R. E. Street, Dept. of Aero. and Astro.
Prof. A. Hertzberg, Aero. and Astro., Guggeheim Hall

COPIES

Federal Reports Center
462 Mechanical Engineering Bldg.
1513 University Avenue
Madison, Wisconsin 53706
S. Reilly
J. S. Murphy

Los Alamos Scientific Laboratory
P.O. Box 1663
Los Alamos
New Mexico 87544
Report Library

University of Maryland
Baltimore County (UMBC)
5401 Wilkens Avenue
Baltimore, Maryland 21228
Dr. R. C. Roberts
Mathematics Department

Oklahoma State University
Office of Engineering Research
Stillwater, Oklahoma 74074
Dr. V. S. Haneman, Jr.

Institute for Defense Analyses
400 Army-Navy Drive
Arlington, Virginia 22202
Classified Library

Kaman Sciences - Library
Box 7463
Colorado Springs
Colorado 80933
J. Newbury

Kaman Science Corporation
Avidyne Division
83 Second Avenue
Burlington
Massachusetts 01803
Dr. J. R. Ruetenik

North American Rockwell Corporation
International Airport
Los Angeles
California 90009
LAD Library, Dept. 299

North American Rockwell Corporation
Engineering Data Services
4300 E. Fifth Avenue
Columbus, Ohio 43216

M. T. T. Lincoln Laboratory
P.O. Box 73
Lexington
Massachusetts 02173
Library A-082

The RAND Corporation
1700 Main Street
Santa Monica
California 90406
Library - D

Copies

The Boeing Company Kent Library
P.O. Box 3707
Seattle
Washington 98124
87-67 E.C. VOGT (AD)

United Aircraft Corporation
Research Laboratories
East Hartford
Connecticut 06108
Dr. William M. Foley

United Aircraft Corporation
400 Main Street
East Hartford
Connecticut 06108
Library

Hughes Aircraft Company
Centinela and Teale Streets
Culver City
California 90230
Co. Tech. Doc. Ctr.
MS 6/E110

Lockheed Missiles and Space Company
Dept. 55-20, Building 102
1111 Lockheed Way
Sunnyvale
California 94088
Maurice Tucker

Lockheed Missiles and Space Company
P.O. Box 504
Sunnyvale
California 94086
Mr. G. M. Laden, Dept. 81-25, Bldg. 154
Mr. Murl Culp

Lockheed Missiles and Space Company
3251 Hanover Street
Palo Alto, California 94304
Technical Information Center

Lockheed-California Company
Burbank, California 91503
Central Library, Dept. 84-40, Bldg. 170
PLT. B-1

Vice President and Chief Scientist
Dept. 03-10
Lockheed Aircraft Corporation
P.O. Box 551
Burbank, California 91503

Martin Marietta Corporation
P.O. Box 988
Baltimore
Maryland 21203
Science-Technology Library (Mail No. 398)

Martin Company
3211 Trade Winds Trail
Orlando, Florida 32805
Mr. H. J. Diebolt

General Dynamics
P.O. Box 748
Fort Worth, Texas 76101
Research Library 2246
George Kaler, Mail Zone 2880
R. A. Stevens, Mail Zone 2887

Copies

Cornell Aeronautical Laboratory, Inc.
4455 Genesee Street
Buffalo, New York 14221
Library

Air University Library
(SE) 63-578
Maxwell Air Force Base
Alabama 36112

McDonnell Company
P.O. Box 516
St. Louis, Missouri 63166
R. D. Detrich, Dept. 218
Bldg. 101M

McDonnell-Douglas Astronautics Corporation
Space Systems Center
5301 Bolsa Avenue
Huntington Beach
California 92647
Technical Library A3-339
A2-260 Library
Dr. J. S. Murphy, A-830
Mr. W. H. Branch, Director
L. Cassel, A3-830

Fairchild Hiller
Republic Aviation Division
Farmingdale
New York 11735
Engineering Library

Hercules Incorporated
Allegany Ballistics Laboratory
P.O. Box 210
Cumberland
Maryland 21502
Library

General Electric Company
Research and Development Lab. (Comb. Bldg.)
Schenectady
New York 12301
Dr. H. T. Nagamatsu

Mississippi State University
Department of Aerophysics and Aerospace Engineering
P.O. Drawer AP
State College
Mississippi 39762
Dr. Sean C. Roberts

General Electric Company
Missile and Space Division
P.O. Box 8555
Philadelphia
Pennsylvania 19101
MSD Library
Larry Chasen, Mgr.
Dr. J. D. Stewart, Mgr. Research and Engineering

West Virginia University
Morgantown
West Virginia 26506
Library

General Electric Company
Re-Entry and Environmental Systems Division
P.O. Box 8555
Philadelphia, Pennsylvania 19101
Dr. S. M. Scala
Dr. H. Lew
D. Florence
A. Martellucci
M. Brunner
D. Nestler
J. Pettus
P. Cline

Copies

AVCO-Everett Research
Laboratory
2385 Revere Beach Parkway
Everett
Massachusetts 02149
Library
Dr. George Sutton

LTV Aerospace Corporation
Vought Aeronautics Division
P.O. Box 5907
Dallas, Texas 75222
Unit 2-51131 (Library)

LTV Aerospace Corporation
Missiles and Space Division
P.O. Box 5907
Dallas, Texas 75222
MSD-T-Library (2-50381)

Northrop Norair
3901 West Broadway
Hawthorne
California 90250
Tech. Info. 3343-32

Philco-Ford Corporation
Aeroneutronic Division
Newport Beach
California 92660
Dr. A. Demetriades

Grumman Aircraft
Engineering Corporation
Bethpage, Long Island
New York 11714
Mr. R. A. Scheuing
Mr. H. B. Hopkins
Mr. H. R. Reed

Marquardt Aircraft
Corporation
16555 Saticoy Street
Van Nuys, California 91409
Library

ARDE Associates
P.O. Box 286
580 Winters Avenue
Paramus, New Jersey 07652
Librarian

Aerophysics Company
3500 Connecticut Ave., N.W.
Washington, D.C. 20003
Mr. G. D. Boehler

Aeronautical Research
Associates of Princeton
50 Washington Road
Princeton
New Jersey 08540
Dr. C. duP. Donaldson

General Research Corporation
5383 Hollister Avenue
P.O. Box 3587
Santa Barbara
California 93105
Technical Information
Office

Sandia Corporation
Box 5800
Albuquerque
New Mexico 87115
Mr. K. Goin, Div. 5642
Mr. A. M. Torneby
Org. 3141
Mr. W. H. Curry, 5625

General Applied Science
Laboratories Inc.
Merrick and Stewart
Avenues
Westbury, Long Island
New York 11590
Dr. F. Lane
Dr. Ray Edelman

Copies

General Electric Company
P.O. Box 2500
Daytona Beach
Florida 32015
Charles Day Rm. 1430

TWR Systems Group
1 Space Park
Redondo Beach
California 90278
Technical Library-
Document Acquisitions

Stanford Research Institute
333 Ravenswood Avenue
Menlo Park
California 94025
Dr. G. Abrahamson

Hughes Aircraft Company
P.O. Box 3310
Fullerton
California 92634
R. H. Sterling, 600-E201

Westinghouse Electric
Corporation
Astronuclear Laboratory
P.O. Box 10864
Pittsburgh
Pennsylvania 15236
Library

University of Tennesse
Space Institute
Tullahoma
Tennessee 37388
Prof. J. T. Wu

General Dynamics
Convair Aerospace Division
Research Library
P. O. Box 80986
San Diego
California 92138
U. J. Sweeney, Chief Librarian

CONVAIR Division of
General Dynamics
P.O. Box 1128
San Diego
California 92112
Dr. Jan Raat
Aeroballistics Dept.
Mail Zone 583-00

AVCO Missiles Systems
Division
201 Lowell Street
Wilmington
Massachusetts 01887
E. E. H. Schurmann
J. Otis

Chrysler Corporation
Space Division
P.O. Box 29200
New Orleans,Louisiana 70129
Edgar A. Rawls
G. T. Boyd, Dept. 2781

General Dynamics
Pomona Division
Pomona, California 91766
Division Library, Mail
Zone 6-20

General Electric Company
Room 3034
3198 Chesnut Street
Philadelphia
Pennsylvania 19101
W. Daskin

Copies Copies

Raytheon Company
Missile Systems Division
Hartwell Road
Bedford
Massachusetts 01730
D. P. Forsmo

TRW Systems Group
Space Park Drive
Houston, Texas 77058
M. W. Sweeney, Jr.

Marine Bioscience
Laboratory
527 Las Alturas Road
Santa Barbara
California 93103
Dr. A. C. Charters

University of California -
Los Angeles
Department of Mechanics
and Structures
Los Angeles
California 90024
Prof. J. D. Cole

University of Wyoming
University Station
P.O. Box 3295
Laramie, Wyoming 82070
Prof. J. Matheny, Head
Dept. Mech. Eng.

Applied Mechanics Review
Southwest Research Institute
8500 Culebra Road
San Antonio, Texas 78228

American Institute of
Aeronautics and
Astronautics
1290 Sixth Avenue
New York, New York 10019
J. Newbauer

Technical Information
Service
American Institute of
Aeronautics and
Astronautics
750 Third Avenue
New York, New York 10017
Miss P. Marshall

Faculty of Aeronautical
Systems
University of West Florida
Pensacola, Florida 32504
Dr. R. Fledderman

Space Research Corporation
Chittenden Bank Building
North Troy, Vermont 05859
Library
J. A. Finkel

Aerophysics Company
3500 Connecticut Avenue, N.W.
Washington, D.C. 20003